

# Quantum Transport Theory of Strongly Correlated Matter

Assa Auerbach and Sauri Bhattacharyya

<sup>a</sup>Physics Department Technion 32000 Haifa Israel.

---

## Abstract

This report reviews recent progress in computing Kubo formulas for general interacting Hamiltonians. The aim is to calculate electric and thermal magneto-conductivities in strong scattering regimes where Boltzmann equation and Hall conductivity proxies exceed their validity. Three primary approaches are explained.

1. Degeneracy-projected polarization formulas for Hall-type conductivities, which substantially reduce the number of calculated current matrix elements. These expressions generalize the Berry curvature integral formulas to imperfect lattices.
2. Continued fraction representation of dynamical longitudinal conductivities. The calculations produce a set of thermodynamic averages, which can be controllably extrapolated using their mathematical relations to low and high frequency conductivity asymptotics.
3. Hall-type coefficients summation formulas, which are constructed from thermodynamic averages.

The thermodynamic formulas are derived in the operator Hilbert space formalism, which avoids the opacity and high computational cost of the Hamiltonian eigenspectrum. The coefficients can be obtained by well established imaginary-time Monte Carlo sampling, high temperature expansion, traces of operator products, and variational wavefunctions at low temperatures.

We demonstrate the power of approaches 1–3 by their application to well known models of lattice electrons and bosons. The calculations clarify the far-reaching influence of strong local interactions on the metallic transport near Mott insulators. Future directions for these approaches are discussed.

---

arXiv:2406.02677v2 [cond-mat.str-el] 29 Aug 2024

## Contents

|            |   |           |
|------------|---|-----------|
| <b>I</b>   | <b>Introduction</b>   | <b>6</b>  |
| 1          | Why calculate conductivities?   | 6         |
| 2          | Lingering issues clarified  | 6         |
| 2.1        | Are DC Hall conductivities <i>on-shell</i> or <i>off-shell</i> expressions?                                 | 6         |
| 2.2        | What is the origin of magnetization subtractions in $\alpha_{xy}$ and $\kappa_{xy}$ ? Must we compute them? | 7         |
| 2.3        | Can DC dissipative transport coefficients be expressed in terms of static thermodynamic coefficients?       | 7         |
| 2.4        | What are the effects of a Mott insulator phase on the longitudinal and Hall transport of a nearby metal?    | 7         |
| 3          | Organization of the report  | 7         |
| <b>II</b>  | <b>Brief history of weak scattering</b>   | <b>8</b>  |
| 4          | Drude theory  | 9         |
| 5          | Boltzmann equation  | 9         |
| 5.1        | Example: The square lattice   | 10        |
| 5.2        | Conductivity relations at low temperatures  | 11        |
| 6          | Memory Function Formalism   | 11        |
| 7          | Limits of weak scattering approaches  | 12        |
| <b>III</b> | <b>Kubo Formulas</b>  | <b>13</b> |
| 8          | Polarizations and Currents  | 13        |
| 9          | Examples: Hamiltonians and polarizations  | 13        |
| 10         | Kubo formulas in Lehmann Representation   | 16        |
| 10.1       | Non-interacting conductivities  | 16        |
| 11         | The Tricky DC limit   | 17        |
| 12         | Onsager relations   | 18        |
| 13         | Hall conductivity proxies   | 18        |
| 13.1       | Chern number  | 18        |
| 13.2       | Streda formula  | 20        |
| 14         | Kubo formulas in operator Hilbert space   | 20        |

|           |  |           |
|-----------|--|-----------|
| 14.1      | Equilibrium Susceptibilities . . . . .                                   | 21        |
| 14.2      | The Liouvillian and its inverse . . . . .                                | 21        |
| 14.3      | Dynamical linear response functions . . . . .                            | 22        |
| 14.4      | Electric and Thermal conductivities . . . . .                            | 23        |
| <b>IV</b> | <b>DPP Hall conductivities</b>   | <b>24</b> |
| <b>15</b> | <b>Derivation of DPP formulas</b>  | <b>24</b> |
| 15.1      | The Magnetization terms . . . . .  | 25        |
| <b>16</b> | <b>DPP formulas for non-interacting Hamiltonians</b>                     | <b>26</b> |
| <b>17</b> | <b>Berry curvature integrals</b>   | <b>26</b> |
| <b>18</b> | <b>DPP formula for confined Landau levels</b>                            | <b>29</b> |
| <b>19</b> | <b>DPP Hall conductivity in a disordered metal</b>                       | <b>30</b> |
| <b>20</b> | <b>Physical consequences of DPP formulas</b>                             | <b>31</b> |
| <b>V</b>  | <b>Continued fractions of longitudinal conductivities</b>                | <b>32</b> |
| <b>21</b> | <b>Moments expansion</b>   | <b>32</b> |
| 21.1      | Krylov bases . . . . .   | 33        |
| 21.2      | The continued fraction representation . . . . .                          | 35        |
| <b>22</b> | <b>From moments to recurrences</b>                                       | <b>35</b> |
| 22.1      | Single Mode Spectra . . . . .  | 36        |
| <b>23</b> | <b>From recurrences to conductivities</b>                                | <b>37</b> |
| 23.1      | Freud's high order asymptotics . . . . .                                 | 37        |
| 23.2      | Termination functions . . . . .  | 39        |
| 23.3      | Low frequency behavior . . . . .   | 39        |
| 23.4      | Addition of spectral functions with different frequency scales . . . . . | 41        |
| 23.5      | Variational Extrapolation of Recurrences . . . . .                       | 42        |
| <b>VI</b> | <b>Thermodynamic formulas of Hall coefficients</b>                       | <b>44</b> |
| <b>24</b> | <b>Magnetic Field Expansion of Hall-type Conductivity</b>                | <b>44</b> |
| <b>25</b> | <b>Hall Coefficient</b>  | <b>46</b> |
| 25.1      | Weak scattering limit . . . . .  | 47        |
| <b>26</b> | <b>Modified Nernst Coefficient</b>                                       | <b>47</b> |

|  |           |
|--|-----------|
| <b>27 Thermal Hall coefficient</b>   | <b>48</b> |
| <b>28 Calculating the correction terms</b>   | <b>48</b> |
| <b>29 Optimization of thermodynamic approaches</b>   | <b>49</b> |
| 29.1 The Separability problem . . . . .  | 49        |
| 29.2 Renormalized Hamiltonians at low temperatures . . . . .                                 | 50        |
| <br>   |           |
| <b>VII Numerical algorithms for thermodynamic coefficients</b>                               | <b>51</b> |
| <br>   |           |
| <b>30 High temperature series</b>  | <b>52</b> |
| 30.1 Linked clusters theorem . . . . .   | 52        |
| <br>   |           |
| <b>31 Stochastic algorithms</b>  | <b>53</b> |
| 31.1 Determinant Quantum Monte Carlo . . . . .   | 53        |
| 31.2 Directed Loop Algorithm . . . . .   | 55        |
| <br>   |           |
| <b>VIII Strongly Correlated Electrons</b>  | <b>58</b> |
| <br>   |           |
| <b>32 The Hubbard Model</b>  | <b>58</b> |
| <br>   |           |
| <b>33 The t-J Model</b>  | <b>58</b> |
| 33.1 Linear Resistivity slope . . . . .  | 59        |
| 33.2 Hall map for large $U/t$ . . . . .  | 61        |
| 33.3 Hall coefficient corrections . . . . .  | 62        |
| 33.4 Numerical calculation Krylov operators and hypermagnetization matrix elements . . . . . | 63        |
| <br>   |           |
| <b>34 Discussion</b>   | <b>64</b> |
| <br>   |           |
| <b>IX Strongly Correlated Bosons</b>   | <b>65</b> |
| <br>   |           |
| <b>35 The Bose Hubbard model</b>   | <b>65</b> |
| 35.1 Weak interactions . . . . .   | 66        |
| 35.2 Strong interaction . . . . .  | 66        |
| <br>   |           |
| <b>36 Hard Core Bosons on the square lattice</b>   | <b>68</b> |
| 36.1 Superconducting phase . . . . .   | 68        |
| 36.2 Metallic phase: longitudinal conductivity . . . . .                                     | 70        |
| 36.3 Metallic phase: Hall coefficient . . . . .  | 72        |
| 36.4 Hall coefficient corrections . . . . .  | 74        |
| <br>   |           |
| <b>37 Discussion</b>   | <b>75</b> |

|  |           |
|--|-----------|
| <b>X Summary and Future Directions</b> | <b>76</b> |
| <b>38 Acknowledgements</b>             | <b>76</b> |

## Part I

# Introduction

### 1. Why calculate conductivities?

Theorists commonly describe phases of matter by their order parameters, since they can be calculated by tried and tested algorithms of equilibrium statistical mechanics. These “*thermodynamic methods*” include stochastic series expansions [1], worm algorithm of Quantum Monte-Carlo simulations [2, 3], and variational methods such as density matrix renormalization group [4, 5], projected entangled-pair states [6] and tensor networks [7].

Experimentalists on the other hand, commonly probe phases of matter by transport measurements. For example: Hall coefficients can characterize the current-carriers’ density (near band extrema). Temperature dependent resistivity may herald the onset of superconductivity or charge localization. Quantized Hall conductivity is associated with topologically ordered ground states.

Electric, thermo-electric and thermal transport coefficients,  $\sigma$ ,  $\alpha$ ,  $\bar{\alpha}$  and  $\kappa$ , are defined by linear response equations,

$$\begin{aligned}\mathbf{j} &= \sigma \cdot (\mathbf{E} - \nabla\mu/e) + \alpha \cdot (-\nabla T) \quad , \\ \mathbf{j}_Q &= T\bar{\alpha} \cdot (\mathbf{E} - \nabla\mu/e) + \kappa \cdot (-\nabla T) \quad .\end{aligned}\tag{1}$$

$\mathbf{j}$  and  $\mathbf{j}_Q$  are the electric and thermal currents respectively.  $\mathbf{E} - \nabla\mu/e$  and  $\nabla T$  are the electrochemical field and temperature gradient respectively. In Eq. (1), the wavevector  $\mathbf{q}$  and frequency  $\omega$  dependence of all variables are suppressed.

For systems described by weakly scattered Bloch-band quasiparticles, the Boltzmann equation [8, 9] and diagrammatic perturbation theory [10] are adequate. For incompressible quantum Hall phases [11] and topological insulators [12], proxies such as the Chern number [13, 14] and Streda formula [15] yield the Hall conductivity.

However, for strongly correlated gapless systems which exhibit “bad metal” phenomenology [16], quasiparticle descriptions may fail. The only Hamiltonian-based alternative to weak scattering approaches is the computation of the Kubo formulas [17]. However, dynamical Kubo formulas may be forbiddingly difficult. Exact diagonalizations entail exponentially large memory costs, and analytic continuation of Quantum Monte Carlo data to real frequencies is ill-posed at low frequencies [18]. Simplifications of Kubo formulas which apply to gapless phases are in dire need.

This Report reviews recent advances which sidestep some of the Kubo formula difficulties, and render conductivity calculations in the presence of strong interactions more accessible.

### 2. Lingering issues clarified

Before delving into details, we list certain questions which have permeated the common lore of transport theory, and are resolved in this Report.

#### 2.1. Are DC Hall conductivities on-shell or off-shell expressions?

In the Lehmann (eigenstates) representation of Kubo formulas, *on-shell* expressions involve current matrix elements  $j_{nm}^\alpha$  between quasi-degenerate states (i.e. whose energies’ separation  $E_n - E_m$  vanishes in the large volume limit). On-shell expressions are implemented by taking

$$\lim_{\varepsilon \rightarrow 0} \lim_{\mathbf{q} \rightarrow 0} \lim_{\mathcal{V} \rightarrow \infty} \text{Im} \frac{1}{E_n(\mathcal{V}) - E_m(\mathcal{V}) - i\varepsilon} \rightarrow \pi \lim_{\mathbf{q} \rightarrow 0} \lim_{\mathcal{V} \rightarrow \infty} \delta(E_n(\mathcal{V}) - E_m(\mathcal{V})) \quad .\tag{2}$$

Real longitudinal conductivities turn out to be on-shell expressions.

In contrast, Hall-type (antisymmetric transverse) conductivities, involve sums over the *real* part of energy denominators, i.e.

$$\text{Re} \frac{1}{E_n - E_m - i\varepsilon} = \frac{E_n - E_m}{(E_n - E_m)^2 + \varepsilon^2} \quad .\tag{3}$$

By blithely setting  $\varepsilon \rightarrow 0$ , and neglecting  $O(\varepsilon^2)$  terms, one may be wrongly led to believe that “Hall conductivities are off-shell expressions”, i.e. that they include  $J_{nm}^\alpha$  which connect between well separated energies in the large volume limit.

This statement is misleading. As shown below by the degeneracy projected polarization (DPP) formulas in Part IV, on open boundary conditions (OBC), terms of order  $\varepsilon^2$  in (3) are *essentially important* in the DC limit! In fact, Hall-type conductivities with OBC are *purely on-shell expressions*. Physically, this implies that at low temperatures, the Hall current is carried by low energy gapless excitations, which may be located in the bulk or at the system’s edges.

Off-shell Kubo formulas have been used in the literature, most notably by Thouless *et al.* [13] in their seminal derivation of the quantized Hall conductance of perfectly periodic lattices. However, they are only valid in limited cases such as a gapped ground state with periodic boundary conditions (PBC), as discussed in Section 13.

## 2.2. What is the origin of magnetization subtractions in $\alpha_{xy}$ and $\kappa_{xy}$ ? Must we compute them?

The infamous magnetization corrections for  $\alpha_{xy}$  and  $\kappa_{xy}$  [19, 20] (which inconveniently diverge at zero temperature) are an artifact of introducing a static “gravitational field”  $\psi_{\omega=0}$  in lieu of the temperature gradient  $-\nabla T$ , which is a *non-equilibrium* statistical force. The static  $\psi$  produces superfluous magnetization currents which must be subtracted from the Kubo formula in the DC limit [19, 20]. However, magnetization subtractions can be eliminated using the DPP formulas for  $\alpha_{xy}$  and  $\kappa_{xy}$  as shown in subsection 15.1. The magnetization terms also fall out of the Hall coefficient summation formulas of Part VI.

## 2.3. Can DC dissipative transport coefficients be expressed in terms of static thermodynamic coefficients?

At first thought, one may suspect that expressions involving on-shell scattering rates (i.e. Fermi’s golden rule), may not be applicable to calculations of static thermodynamic averages.

On the other hand, it has long been realized that some dynamical conductivities may be computed by continued fraction representations [21, 22], which are constructed from the conductivity moments which are a set of thermodynamic averages. The price to pay is a necessary *extrapolation* of the calculated moments up to infinite order. While this may turn out to be a daunting task, extrapolation is occasionally facilitated by appealing to mathematical relations, which are reviewed in Section 23. These relations connect between high order moments and high frequency limits of the dynamical conductivity.

In a different approach, Part VI derives thermodynamic summation formulas for the low magnetic field Hall-type coefficients. Truncation of this sum may sometimes be justified by calculating leading order corrections, as demonstrated in the model examples of Part VIII and Part IX.

## 2.4. What are the effects of a Mott insulator phase on the longitudinal and Hall transport of a nearby metal?

Strong local interactions effects give rise to the Mott insulator and extend deep into the nearby metallic phase. The effects include large high temperature linear resistivity slopes, and Hall coefficient sign reversal and divergence at low doping of the Mott insulator. These effects are captured by thermodynamic Kubo formula calculations of the two dimensional t-J model and Hard Core Bosons model, in Part VIII and Part IX respectively.

## 3. Organization of the report

In Part II, we present a brief review of Drude, Boltzmann, and memory functional transport theories which apply to Hamiltonians of weakly scattered quasiparticles. In Parts III-VI, we lay the mathematical basis for approaches applicable to strongly interacting Hamiltonians. First, in Part III, the Kubo formula with its proper DC order of limits is defined. The reversal of that order of limits in Chern number and Streda formula proxies is discussed.

New approaches are derived, starting from Part IV, where the DPP formulas for DC Hall type conductivities are presented. The DPP formulas reduce to Berry curvature integrals in the disorder-free limit. Part V derives the continued

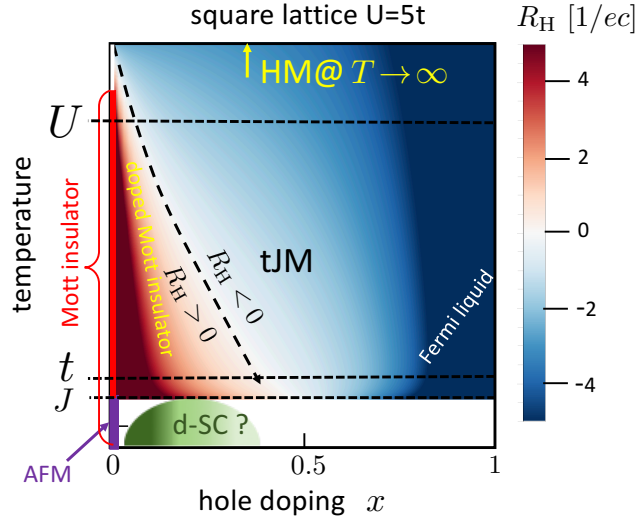


Figure 1: Hall coefficient map for the strongly interacting Hubbard model on the square lattice. The Hall coefficient was calculated [23] using the thermodynamic summation formula reviewed in Part VI. The model and its parameters are defined in Part VIII. The anomalous (reddish-brown) region near the Mott insulator is a consequence of the strong local electron-electron interactions which affect the current commutation relations and produce the sign reversal and divergence. At low temperatures (beyond the present analysis), we mark the region of antiferromagnetic (AFM) order, and a hypothetical region of  $d$ -wave superconductivity (d-SC) [4, 24, 25].

fraction conductivities from the moments expansion, and presents viable extrapolation schemes. Part VI derives the Hall coefficient summation formulas.

Part VIII demonstrates recent application [23] of the continued fraction conductivity and Hall coefficient summation formula to strongly interacting electrons near a Mott insulator, as modelled by the two dimensional Hubbard and t-J Hamiltonians. The resulting Hall coefficient map is depicted in Fig. 1. Part IX demonstrates the application of the same formulas to obtain the resistivity and Hall coefficient of strongly interacting lattice bosons.

Part X summarizes the Report. A discussion of strategies for optimizing the thermodynamic approaches is given. Future applications and directions of research are proposed.

## Part II

# Brief history of weak scattering

Perturbative calculations of Kubo formulas for DC conductivities of metals suffer from the singular effect of scattering. At leading order in impurity concentration an infinite resummation of diagrams is needed to obtain a finite longitudinal conductivity at finite impurity concentration [10].

Older (and simpler) alternatives for the weak scattering regimes are to apply the Drude and Boltzmann approaches. In this Report, unless otherwise specified, we use units of  $\hbar = k_B = 1$ .



#### 4. Drude theory

Drude theory [26] is particularly useful for lightly doped semiconductors. It is based on a Fermi gas of electrons of mass  $m^*$  and charge  $e$  whose kinetic energy is described by the single particle dispersion,

$$\epsilon_{\mathbf{k}} = \frac{\mathbf{k}^2}{2m^*} . \quad (4)$$

Collisions with disorder and other electrons are introduced by a scattering time  $\tau$ . Solving for the single electron equation of motion in a time dependent field, the dynamical longitudinal conductivity is

$$\sigma_{xx}^{\text{Drude}}(\omega) = \frac{ne^2}{m^*} \frac{\tau}{1 + (\omega\tau)^2} . \quad (5)$$

where  $e$  is the electron charge. The DC conductivities in a uniform magnetic field  $\mathbf{B} = B\hat{\mathbf{z}}$  are

$$\begin{aligned} \sigma_{xx}^{\text{dc}} &= \frac{ne^2}{m^*} \frac{\tau}{1 + (\omega_c\tau)^2} , \\ \sigma_{xy}^{\text{dc}} &= \frac{ne^2}{m^*} \frac{\omega_c\tau^2}{1 + (\omega_c\tau)^2} , \end{aligned} \quad (6)$$

where  $\omega_c = \frac{eB}{m^*c}$  is the cyclotron frequency, and  $c$  is the speed of light. The zero field Hall coefficient is defined as,

$$R_{\text{H}}^{\text{Drude}} \equiv - \lim_{B \rightarrow 0} \frac{\rho_{xy}(B)}{B} = \frac{1}{\sigma_{xx}^{\text{dc}}(0)} \left. \frac{d\sigma_{xy}^{\text{dc}}}{dB} \right|_{B=0} = \frac{1}{nec} . \quad (7)$$

Thus,  $R_{\text{H}}^{\text{Drude}}$  is proportional to the inverse charge density. We note that  $R_{\text{H}}^{\text{Drude}}$ , in contrast to  $\sigma_{xy}$ , is independent of dynamical parameters  $m^*$  and  $\tau$ . Later, in Part VI, the expression of the Hall coefficient in terms of thermodynamic coefficients is shown to be a general feature of non-separable Hamiltonians.

#### 5. Boltzmann equation

The single band Boltzmann equation (BE) [8, 9, 27] for the quasiparticle distribution function deviation  $\delta f_{\mathbf{k},r}$  is based on small deviations from the Fermi-Dirac distribution  $f_0(\epsilon_{\mathbf{k}} - \mu)$ , where  $\epsilon_{\mathbf{k}}$  is the non-interacting Bloch band dispersion,  $\mathbf{k}$  is a wavevector within the Brillouin zone (BZ), and  $\mu$  is the chemical potential. In the presence of an externally imposed electrochemical field  $\mathbf{E} - \frac{1}{e}\nabla\mu$  and temperature gradient  $-\nabla T$ , the BE is,

$$\frac{\partial \delta f}{\partial t} + \dot{\mathbf{k}} \cdot \frac{\partial \delta f}{\partial \mathbf{k}} + \dot{\mathbf{x}}_{\mathbf{k}} \cdot \left[ -\nabla\mu - \frac{\epsilon_{\mathbf{k}} - \mu}{T} \nabla T \right] \left( \frac{\partial f_{\mathbf{k}}^0}{\partial \epsilon} \right) = \mathcal{I}_{\mathbf{k}}^1[\delta f] . \quad (8)$$

where the semiclassical equations of motion are,

$$\begin{aligned} \dot{\mathbf{x}}_{\mathbf{k}} &= \nabla_{\mathbf{k}} \epsilon_{\mathbf{k}} - \dot{\mathbf{k}} \times \boldsymbol{\Omega}_{\mathbf{k}} , \\ \dot{\mathbf{k}} &= e\mathbf{E} - \frac{e}{c} \dot{\mathbf{r}}_{\mathbf{k}} \times \mathbf{B} . \end{aligned} \quad (9)$$

The band and spin indices are suppressed. The band Berry curvature  $\boldsymbol{\Omega}_{\mathbf{k}}$ , which modifies the velocity [27, 28] is given by,

$$\boldsymbol{\Omega}_{\mathbf{k}} \equiv i \langle \nabla_{\mathbf{k}} u_{\mathbf{k}} | \times | \nabla_{\mathbf{k}} u_{\mathbf{k}} \rangle , \quad (10)$$

where  $|u_{\mathbf{k}}\rangle$  is the periodic part of the Bloch state.  $\mathcal{I}_{\mathbf{k}}^1$  is the collision integral which is commonly simplified by the relaxation time approximation,

$$\mathcal{I}_{\mathbf{k}}^1[f] = -\frac{\delta f_{\mathbf{k}}}{\tau_{\mathbf{k}}} . \quad (11)$$

Weak electron-electron and electron-phonon interactions can be incorporated into BE by renormalizing the  $\mathbf{v}_{\mathbf{k}}$ , and contributing to the quasiparticle scattering rate  $1/\tau_{\mathbf{k}}$ .

In the absence of time-reversal symmetry breaking in the equilibrium density matrix, the electric and thermal currents are given respectively by

$$\begin{aligned}\mathbf{j} &= \sum_{\mathbf{k} \in \text{BZ}} \mathbf{v}_{\mathbf{k}} \delta f_{\mathbf{k}} \quad , \\ \mathbf{j}_Q &= \sum_{\mathbf{k} \in \text{BZ}} (\epsilon_{\mathbf{k}} - \mu) \mathbf{v}_{\mathbf{k}} \delta f_{\mathbf{k}} \quad ,\end{aligned}\tag{12}$$

where BZ is the Brillouin zone. Using the solution of Eq. (8) in (12), for  $C_4$  symmetric bands, yields BE expression for the DC longitudinal and Hall conductivities,

$$\begin{aligned}\sigma_{xx}^{\text{dc}} &= \frac{e^2}{c\mathcal{V}} \sum_{\mathbf{k}} \left( -\frac{\partial f}{\partial \epsilon} \right) (v_{\mathbf{k}}^x)^2 \tau_{\mathbf{k}} \quad , \\ \sigma_{xy}^{\text{dc}} &= \frac{e^3 B}{c\mathcal{V}} \sum_{\mathbf{k} \in \text{BZ}} \left( -\frac{\partial f_{\mathbf{k}}^0}{\partial \epsilon} \right) v_{\mathbf{k}}^y \tau_{\mathbf{k}} \left( v_{\mathbf{k}}^y \frac{\partial}{\partial k_x} - v_{\mathbf{k}}^x \frac{\partial}{\partial k_y} \right) (v_{\mathbf{k}}^x \tau_{\mathbf{k}}) \quad .\end{aligned}\tag{13}$$

For an isotropic (energy dependent) scattering time  $\tau_{\mathbf{k}} = \tau(\epsilon_{\mathbf{k}})$ , one obtains simplified expressions at low temperatures relative to the Fermi energy  $\epsilon_F$ ,

$$\begin{aligned}\sigma_{xx}^{\text{dc}} &= \tau(\epsilon_F) \chi_{\text{csr}} \quad , \\ \sigma_{xy}^{\text{dc}} &= \tau^2(\epsilon_F) \frac{e^3}{c\mathcal{V}} \sum_{\mathbf{k} \in \text{BZ}} \left( -\frac{\partial f_{\mathbf{k}}^0}{\partial \epsilon} \right) \left( v_{\mathbf{k}}^y \left( v_{\mathbf{k}}^y \frac{\partial}{\partial k_x} - v_{\mathbf{k}}^x \frac{\partial}{\partial k_y} \right) v_{\mathbf{k}}^x \right) \quad ,\end{aligned}\tag{14}$$

where the conductivity sum rule (CSR) is,

$$\chi_{\text{csr}} = \frac{e^2}{\mathcal{V}} \sum_{\mathbf{k} \in \text{BZ}} \left( -\frac{\partial f_{\mathbf{k}}^0}{\partial \epsilon} \right) (v_{\mathbf{k}}^x)^2 \quad .\tag{15}$$

The Hall coefficient acquires a scattering time independent expression [9],

$$R_{\text{H}}^{\text{Boltz}} = \frac{e^3}{c\chi_{\text{csr}}^2 \mathcal{V}} \sum_{\mathbf{k}} \left( -\frac{\partial f_{\mathbf{k}}^0}{\partial \epsilon} \right) \left( v_{\mathbf{k}}^y \left( v_{\mathbf{k}}^y \frac{\partial}{\partial k_x} - v_{\mathbf{k}}^x \frac{\partial}{\partial k_y} \right) v_{\mathbf{k}}^x \right) \quad .\tag{16}$$

Eq. (16) generalizes Drude's result (7) to non-spherical Fermi surfaces.

### 5.1. Example: The square lattice

The square lattice (SL) tight binding model is,

$$H^{\text{SL}} = - \sum_{\langle ij \rangle, s=\uparrow, \downarrow} t_{ij} (c_{is}^\dagger c_{js} + c_{js}^\dagger c_{is}) \quad ,\tag{17}$$

where  $c_{is}^\dagger$  creates an electron on site  $i$  with spin  $s$ .  $\langle ij \rangle$  are nearest neighbor bonds on the square lattice (SL), and electron occupation per site is  $n_{is} = c_{is}^\dagger c_{is}$ .

The Hall coefficients given by Eq. (16) and related band structure contours are depicted in Fig. 2 for nearest neighbor (nn) and next nearest neighbor (nnn) model.

The most important prediction of Boltzmann theory is that the Hall coefficient is everywhere continuous and diverges only toward the full and empty band limits.

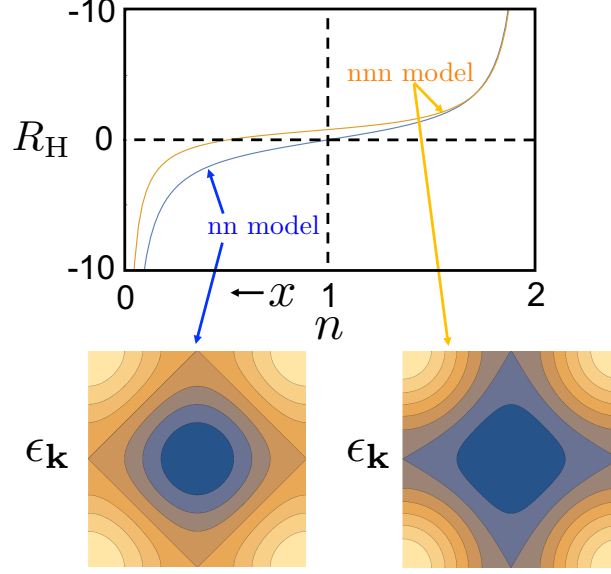


Figure 2: Hall coefficient  $R_H$ , as given by Boltzmann equation of the weakly scattered ( $U = 0$ ) square lattice, given by Eq. (16) at  $T = 0$ .  $n$  is the electron filling, and  $x$  is the hole doping concentration customarily used in describing cuprate superconductors. The nearest neighbor (nn) model has particle-hole antisymmetry about  $n = 1$ . Next nearest neighbor (nnn) hopping moves the Hall sign reversal toward lower electron density.

### 5.2. Conductivity relations at low temperatures

For  $C_4$  symmetric bands, the isotropic lifetime leads to simple relations between for the longitudinal electric, thermoelectric and thermal conductivities, which can be expanded at low temperatures as

$$\begin{aligned}
 \sigma_{xx}^{\text{dc}}(T) &= \sigma_{xx}^{\text{dc}}(0) \left( 1 + \frac{\pi^2 (k_B T)^2}{8 \mu^2} + \dots \right) \\
 \alpha_{xx}^{\text{dc}}(T) &= \frac{\sigma_{xx}^{\text{dc}}(0) \pi^2 (k_B T)^2}{e^2 2 \mu} + \dots \\
 \kappa_{xx}^{\text{dc}}(T) &= \frac{\sigma_{xx}^{\text{dc}}(0) \pi^2}{e^2 3} (k_B T)^2 + \dots
 \end{aligned} \tag{18}$$

As  $T \rightarrow 0$ , one obtains the Wiedemann-Franz law

$$\frac{\kappa}{\sigma T} = \frac{\pi^2}{3} (k_B/e)^2 = 2.45 \times 10^{-8} \text{V}^2 \text{K}^{-2} \quad . \tag{19}$$

## 6. Memory Function Formalism

The Memory Function (MF) formalism [29, 30, 31] is closely related to the Operator Hilbert Space (OHS) formulation of dynamical response functions as described in Section 14.

A primary goal of the MF was to obtain the dynamical response of a set of “slow operators” which nearly commute with the Hamiltonian, by integrating out all the “fast operators” to obtain a self energy, called ‘memory matrix’  $M(z)$ . Götze-Wölfle [32] have applied the MF to evaluate the longitudinal conductivity in a weakly scattered parabolic band of effective mass  $m^*$ ,

$$\sigma_{xx}(\omega) = \frac{ne^2}{m^*} \text{Re} \frac{i}{z - M(z)/\frac{ne^2}{m^*}} \quad , \tag{20}$$

where  $M(z)$  is the current-current correlation function. They consider a white noise random potential  $V$ , whose ensemble average is

$$\langle V_{\mathbf{q}} V_{-\mathbf{q}'} \rangle_{\text{dis}} = w^2 \delta_{\mathbf{q}, -\mathbf{q}'} \quad , \quad (21)$$

and its commutator with the current is

$$[j^x, V_{\mathbf{q}}] = -i \frac{\hbar}{m} q_x V_{\mathbf{q}} \quad . \quad (22)$$

At low temperatures, MF recovers Drude result (5),

$$\sigma_{xx} = \frac{ne^2\tau}{m^*} \quad . \quad (23)$$

The MF scattering rate agrees with Fermi's golden rule,

$$\frac{\hbar}{\tau} = \pi \mathcal{N}(\epsilon_F) w^2 \quad , \quad (24)$$

where  $\mathcal{N}(\epsilon_F)$  is the density of electron states at the Fermi energy.

More generally, the MF separation of timescales can facilitate obtaining the low temperature and frequency conductivities by renormalization of the dynamical response functions onto the low energy Hilbert space.

In Part V, the memory function  $M(z)$  can be related to the first order termination function  $\Delta_1^2 G_{11}^>(z)$  in the continued fraction of the longitudinal conductivity.

## 7. Limits of weak scattering approaches

BE describes transport by quasiparticles in the conduction band, with velocity  $\mathbf{v}_{\mathbf{k}}$  at wavevector  $\mathbf{k}$  near the Fermi surface. For elastic scattering in dimensions one and two, BE is invalidated by wavefunction localization [33, 34, 35, 36]. The collision integral of Eq. (8) describes incoherent scattering processes which do not lead to localization.

The validity of BE depends on the existence of well defined quasiparticles. Inelastic scattering broadens the quasiparticle energies and wavevectors by  $1/\tau$  and  $2\pi/l$ . The BE therefore requires

$$\epsilon_F \tau \gg 1 \quad , \quad k_F l \gg 1 \quad . \quad (25)$$

The criteria (25) have been related by Ioffe and Regel (IR) [37] to experimental values of the resistivity. Using the simplified Drude theory of a parabolic band,  $\epsilon_F = \hbar^2 k_F^2 / 2m^*$ , and  $n = k_F^3 / 3\pi^2$ , and by (5), one obtains an upper bound on value of resistivity which can be explained by Boltzmann equation,

$$\rho_{xx} = \frac{m^*}{ne^2\tau} = \frac{3\lambda_F}{2} \frac{\hbar}{e^2} \frac{1}{k_F l} \leq \rho_{xx}^{\text{IR}}|_{k_F l=1} \quad . \quad (26)$$

For typical cubic metals with  $\lambda_F \sim 1\text{nm}$ , the IR limit is  $\rho_{xx}^{\text{IR}} \simeq 40\mu\Omega \text{ cm}$ .

In metals,  $\rho_{xx}$  usually increases with temperature due to enhanced inelastic scattering. Many metals (see review in [38]) exhibit resistivity saturation at the values not far above the IR limit.

However, resistivity in certain strongly correlated metals exceeds this limit as temperature is raised, which has been dubbed ‘‘bad metal’’ behavior [16]. Boltzmann equation fails to account for this regime.

In semimetals and semiconductors with a small interband gap  $\Delta_{\text{ib}}$ , interband matrix elements of the current must be included when

$$\Delta_{\text{ib}} \tau < 1 \quad . \quad (27)$$

This leads to a multi-band BE, which involves coupled equations for intra-band and inter-band distribution functions [39, 40, 41]. The equations are in general unwieldy. In the presence of disorder and electron-phonon scattering, a microscopic knowledge of inter-band temperature dependent scattering rates, and inter-band current matrix elements, is required.

## Part III

# Kubo Formulas

### 8. Polarizations and Currents

Kubo's formulation [17] of dynamical linear response, provides a rigorous approach to calculating conductivities of a microscopic model Hamiltonian  $H_0$  which is supported on a finite  $d$ -dimensional volume  $\mathcal{V}$ .

The underlying assumption of Kubo's linear response theory is that local equilibrium is established throughout the sample. In other words, the currents' equilibration length and time scales are much shorter than those of the driving fields.

Following Luttinger [19, 42, 43], it is also assumed that the same electric and thermal currents which are driven by slowly varying *statistical* forces, such as  $-\nabla\mu$  and  $-\nabla T$ , can be induced by *mechanical* electric and "gravitational" forces,  $\mathbf{E}$  and  $\psi$  respectively, which couple linearly to the Hamiltonian,

$$H(t) = H_0 - \Theta(t) \int \frac{d^d q}{(2\pi)^d} \left( \mathbf{P}_q \mathbf{E}_{-q}(t) + \frac{1}{T} \mathbf{Q}_q \psi_{-q}(t) \right) . \quad (28)$$

The polarizations which couple to the external force fields are,

$$\begin{aligned} \text{Electric polarization :} \quad \mathbf{P}_q &= e \int_{\mathcal{V}} d^d x e^{-iq\mathbf{x}} \mathbf{x} n(\mathbf{x}) , \\ \text{Thermal polarization :} \quad \mathbf{Q}_q &= \int_{\mathcal{V}} d^d x e^{-iq\mathbf{x}} \mathbf{x} (h(\mathbf{x}) - \mu n(\mathbf{x})) . \end{aligned} \quad (29)$$

$n(\mathbf{x})$  is particle density and  $h(\mathbf{x})$  is a local decomposition of the Hamiltonian which satisfies,

$$H_0 = \int d^d x h(\mathbf{x}) . \quad (30)$$

The Kubo formulas for conductivities require knowledge of  $H_0$  and its polarization operators of Eq. (29). The electric and thermal currents are derived by Heisenberg's equations,

$$\begin{aligned} \mathbf{j}_q &= i [H_0, \mathbf{P}_q] , \\ (\mathbf{j}_Q)_q &= i [H_0, \mathbf{Q}_q] . \end{aligned} \quad (31)$$

We note that the polarizations (29) depend on the choice of coordinate  $\mathbf{x}$ . However, any finite shift in the origin  $\mathbf{x} \rightarrow \mathbf{x} + \mathbf{a}$  drops out of the commutators in Eqs. (31). For PBC, uniform polarizations can be defined as a  $\mathbf{q} \rightarrow 0$  limit after taking volume to infinity, as shown later in Eqs. (59).

### 9. Examples: Hamiltonians and polarizations

The explicit forms of polarizations are shown for five generic models of many particle systems.

1. The Hamiltonian of  $N_p$  interacting Schrödinger particles (bosons or fermions) in first quantization notation is,

$$H_0^{\text{particles}} = \sum_{i=1}^{N_p} \frac{\mathbf{P}_i^2}{2m} + \sum_i V(\mathbf{x}_i) + \sum_{i<j} U(\mathbf{x}_i - \mathbf{x}_j) , \quad (32)$$

where  $[\mathbf{x}_i^\alpha, \mathbf{p}_j^\beta] = i\hbar\delta_{ij}\delta_{\alpha\beta}$ . The polarizations are given by,

$$\begin{aligned} P_{\mathbf{q}}^\alpha &= -|e| \sum_{i=1}^{N_p} \mathbf{x}_i^\alpha e^{-i\mathbf{q}\cdot\mathbf{x}_i} \quad , \\ Q_{\mathbf{q}}^\alpha &= \sum_{i=1}^{N_p} \frac{1}{2} \left\{ x_i^\alpha e^{-i\mathbf{q}\cdot\mathbf{x}_i}, \frac{\mathbf{p}_i^2}{2m} \right\} + \sum_i x_i^\alpha e^{-i\mathbf{q}\cdot\mathbf{x}_i} \left( V(\mathbf{x}_i) + \sum_{i<j} U(\mathbf{x}_i - \mathbf{x}_j) \right) \quad . \end{aligned} \quad (33)$$

2. Particles on a lattice  $L$  with electric charge  $e^*$ , local occupation  $n_i$ , and hermitian two-site interaction terms:

$$\begin{aligned} H_0^{\text{lattice}} &= \sum_{ij \in L} O_{ij} \quad , \\ P_{\mathbf{q}}^\alpha &= -|e^*| \sum_{i \in L} e^{-i\mathbf{q}\cdot\mathbf{x}_i} x_i^\alpha n_i \quad , \\ Q_{\mathbf{q}}^\alpha &= \sum_{i \in L} e^{-i\mathbf{q}\cdot\mathbf{x}_i} x_i^\alpha \left( \left( \sum_{j \in L} O_{ij} \right) - \mu n_i \right) \quad . \end{aligned} \quad (34)$$

3. General non-interacting (NI) normal Hamiltonians in second quantized form as

$$H^{\text{NI}} = \sum_l \epsilon_l a_l^\dagger a_l \quad , \quad [a_l, a_{l'}^\dagger]_{\pm} = \delta_{ll'} \quad . \quad (35)$$

where  $a_l^\dagger$  creates a particle of charge  $e^*$  in single-particle eigenstate  $|l\rangle$  with energy  $\epsilon_l$ .  $[\bullet, \bullet]_{\pm}$  denotes an anticommutator (commutator) for fermions (bosons).

The polarizations are given by the bilinear forms,

$$\begin{aligned} P_{\mathbf{q}}^\alpha &= ie^* \frac{\partial}{\partial q^\alpha} \sum_{l'l'} \langle l|e^{-i\mathbf{q}\cdot\mathbf{x}}|l'\rangle a_l^\dagger a_{l'} \quad , \\ Q_{\mathbf{q}}^\alpha &= i \frac{\partial}{\partial q^\alpha} \sum_{l'l'} \frac{\epsilon_l + \epsilon_{l'} - 2\mu}{2} \langle l|e^{-i\mathbf{q}\cdot\mathbf{x}}|l'\rangle a_l^\dagger a_{l'} \quad . \end{aligned} \quad (36)$$

4. Non-interacting normal Hamiltonians of bosons or fermions with  $M$  basis states  $\{|\mathbf{R}, i\rangle\}$  per unit cell at lattice site  $\mathbf{R} \in L$ :

$$\langle \mathbf{R}, i | \mathbf{R}', i' \rangle = \delta_{\mathbf{R}, \mathbf{R}'} \delta_{i, i'} \quad . \quad (37)$$

In a periodic crystal (PC), the Hamiltonian is given by

$$H^{\text{PC}} = \sum_{\mathbf{k} \in \text{BZ}} \sum_{ij=1}^M (h_{ij}(\mathbf{k}) - \mu \delta_{ij}) a_{\mathbf{k}, i}^\dagger a_{\mathbf{k}, j} \quad . \quad (38)$$

$a_{\mathbf{k}, i}^\dagger |0\rangle = |\mathbf{k}, i\rangle$  creates a fermion (boson) state of wavevector  $\mathbf{k} \in \text{BZ}$  of lattice  $L$ , and basis state  $i$ . After taking  $\mathcal{V} \rightarrow \infty$ , the polarization operators of Eq. (36) may be represented by continuous derivatives with respect to  $\mathbf{q}$ ,

$$\begin{aligned} P_{\mathbf{q}}^\alpha &= e \sum_{\mathbf{k}ij} a_{\mathbf{k}, i}^\dagger (i\nabla_{\mathbf{q}}^\alpha a_{\mathbf{k}+\mathbf{q}, j}) \quad , \\ Q_{\mathbf{q}}^\alpha &= \sum_{\mathbf{k}ij} a_{\mathbf{k}, i}^\dagger \left\{ \left( \frac{h_{ij}(\mathbf{k}) + h_{ij}(\mathbf{k} + \mathbf{q})}{2} - \mu \delta_{ij} \right), i\nabla_{\mathbf{q}}^\alpha \right\} a_{\mathbf{k}+\mathbf{q}, j} \quad . \end{aligned} \quad (39)$$

5. Coupled Harmonic Oscillators (CHO) Eq. can describe collective bosonic modes such as phonons [44] and magnons [45] in an insulator. A general CHO Hamiltonian which linearly couples to an external orbital magnetic field is,

$$H^{\text{CHO}} = \frac{1}{2} \sum_i \frac{p_i^2}{m_i} + \frac{1}{2} \sum_{i,j} u_{ij} D_{ij} u_j + \sum_{\alpha=x,y,z} B^\alpha \cdot \sum_{i,j} p_i M_{ij}^\alpha u_j \quad , \quad (40)$$

where  $i \rightarrow \mathbf{x}_i$ ,  $s(i)$  denotes both site and polarization indices, where and  $[u_i, p_j] = i\delta_{ij}$  are canonically conjugated coordinates.  $m_i$  and  $D_{ij}$  are local mass and force constants.  $H^{\text{CHO}}$  can include lattice imperfections, impurities with different masses  $m_i$ , and boundaries. The magnetic field  $\mathbf{B}$  breaks time reversal symmetry by coupling between  $u_i$  and  $p_j$  as represented by a magnetization matrix  $\mathbf{M}$ . The thermal polarization is,

$$Q_q^\alpha = \sum_{i=1}^N e^{iq \cdot \mathbf{x}_i} x_i^\alpha \left( \frac{p_i^2}{2m_i} + \frac{1}{2} u_i \sum_j D_{ij} u_j + \frac{1}{2} p_i \sum_j \sum_{\alpha=x,y,z} B^\alpha \cdot \sum_j M_{i,j}^\alpha u_j \right) . \quad (41)$$

The thermal current is obtained by Eq. (31). Using second quantized operators,

$$a_i = \frac{1}{\sqrt{2}} (u_i + ip_i), \quad a_i^\dagger = \frac{1}{\sqrt{2}} (u_i - ip_i), \quad [a_i, a_j^\dagger] = \delta_{ij} \quad , \quad (42)$$

the Hamiltonian is written in a duplicated Bogoliubov form,

$$H^{\text{CHO}} = \frac{1}{2} \sum_{ij=1}^N (a_i^\dagger, a_i) H_{ij} \begin{pmatrix} a_j \\ a_j^\dagger \end{pmatrix} \equiv \frac{1}{2} \sum_{ij} (a_i^\dagger, a_i) \begin{pmatrix} H_{ij}^N & H_{ij}^A \\ (H_{ij}^A)^* & (H_{ij}^N)^* \end{pmatrix} \begin{pmatrix} a_j \\ a_j^\dagger \end{pmatrix} + \text{const} \quad , \quad (43)$$

where the constant comes from the ordering the operators  $a, a^\dagger$ . The duplicated form allows us to choose  $H^N$  to be hermitian, and  $H^A$  to be a symmetric matrix.

$H^{\text{CHO}}$  can be diagonalized by a Bogoliubov transformation<sup>1</sup> defined by a symplectic matrix  $S_{in}$  of size  $2N \times 2N$ ,

$$\begin{pmatrix} a_i \\ a_i^\dagger \end{pmatrix} = \sum_{n=1}^N S_{in} \begin{pmatrix} b_n \\ b_n^\dagger \end{pmatrix} = \sum_{n=1}^N \begin{pmatrix} U_{in} & V_{in}^* \\ V_{in} & U_{in}^* \end{pmatrix} \begin{pmatrix} b_n \\ b_n^\dagger \end{pmatrix} \quad , \quad (44)$$

where  $[b_n, b_{n'}^\dagger] = \delta_{nn'}$ , since

$$S^\dagger JS = S JS^\dagger = J, \quad J \equiv \begin{pmatrix} \mathbb{1}_N & 0 \\ 0 & -\mathbb{1}_N \end{pmatrix} \quad (45)$$

and  $\mathbb{1}_N$  is a unit matrix of size  $N$ . Using  $S$ ,

$$H^{\text{CHO}} = \frac{1}{2} \sum_{ij} (b_n^\dagger, b_n) \begin{pmatrix} \varepsilon_n & 0 \\ 0 & \varepsilon_n \end{pmatrix} \begin{pmatrix} b_n \\ b_n^\dagger \end{pmatrix} . \quad (46)$$

Using the relation  $S^{-1} = JS^\dagger J$ ,  $S$  is determined from  $H^{\text{CHO}}$  by the equations,

$$\begin{aligned} S^\dagger HS &= \begin{pmatrix} \varepsilon & 0 \\ 0 & \varepsilon \end{pmatrix} \\ \Rightarrow HS &= (S^\dagger)^{-1} \begin{pmatrix} \varepsilon & 0 \\ 0 & \varepsilon \end{pmatrix} = JSJ \begin{pmatrix} \varepsilon & 0 \\ 0 & \varepsilon \end{pmatrix} \\ JHS &= S \begin{pmatrix} \varepsilon & 0 \\ 0 & -\varepsilon \end{pmatrix} . \end{aligned} \quad (47)$$

$U, V$  are readily obtained numerically by computing the *right eigenvectors* of the (non hermitian) matrix  $JH$ , and retaining those which belong to the positive spectrum  $\varepsilon_n > 0$ . (Existence of complex eigenvalues is possible: they reflect an instability of the harmonic Hamiltonian). The upper left block yields the eigenvalue equation, for  $n = 1, \dots, N$ :

$$\begin{aligned} \sum_{j=1}^N H_{ij}^N U_{jn} + H_{ij}^A V_{jn} &= U_{in} \varepsilon_n \\ \sum_{j=1}^N -(H_{ij}^A)^* V_{jn} - (H_{ij}^N)^* U_{jn} &= V_{in} \varepsilon_n \quad , \end{aligned} \quad (48)$$

<sup>1</sup>We thank Dan Arovav for sharing with us his impeccable notes

where the eigenvectors  $(U_{in}, V_{in})$  must be normalized as,

$$\forall n \in [1, \dots, N] : \sum_{i=1}^N (|U_{in}|^2 + |V_{in}|^2) = 1 \quad . \quad (49)$$

Using Eqs. (42) and (44),  $(p_i, u_i)$  are transformed into the eigenmode representation  $b_n^\dagger, b_n$ , the thermal polarization (41) is given by,

$$\mathbf{Q}_q = \frac{1}{2} \sum_{n,n'=1}^N (b_n^\dagger, b_n) \begin{pmatrix} \mathbf{Q}_q^N & \mathbf{Q}_q^A \\ (\mathbf{Q}_q^A)^* & (\mathbf{Q}_q^N)^* \end{pmatrix} \begin{pmatrix} b_{n'} \\ b_{n'}^\dagger \end{pmatrix} \quad . \quad (50)$$

## 10. Kubo formulas in Lehmann Representation

Henceforth we use unified notations

$$\begin{aligned} (\mathbf{P}, \mathbf{Q}) &\rightarrow (\mathbf{P}_1, \mathbf{P}_2) \\ (\mathbf{j}, \mathbf{j}_Q) &\rightarrow (\mathbf{J}_1, \mathbf{J}_2) \quad . \end{aligned} \quad (51)$$

In the Lehmann (eigenstate) representation, the currents' response functions are given by the sums,

$$\begin{aligned} L_{ij}^{\alpha\beta}(\mathbf{q}, \omega + i\varepsilon) &= -\frac{i}{\mathcal{V}} \sum_{mn} \frac{\rho_m - \rho_n}{E_n - E_m} \left( \frac{\langle n|(J_i^\alpha)_{-\mathbf{q}}|m\rangle \langle n|(J_j^\beta)_{\mathbf{q}}|m\rangle}{E_n - E_m - \omega - i\varepsilon} \right) \\ &= \frac{1}{\mathcal{V}} \sum_{mn} \frac{\rho_m - \rho_n}{E_n - E_m} \operatorname{Im} \left( \frac{\langle n|(J_i^\alpha)_{-\mathbf{q}}|m\rangle \langle n|(J_j^\beta)_{\mathbf{q}}|m\rangle}{E_n - E_m - \omega - i\varepsilon} \right) \\ &\quad - \frac{i}{\mathcal{V}} \sum_{mn} \frac{\rho_m - \rho_n}{E_n - E_m} \operatorname{Re} \left( \frac{\langle n|(J_i^\alpha)_{-\mathbf{q}}|m\rangle \langle n|(J_j^\beta)_{\mathbf{q}}|m\rangle}{E_n - E_m - \omega - i\varepsilon} \right) \quad . \end{aligned} \quad (52)$$

where  $E_m$  and  $|m\rangle$  are the eigenenergies and eigenstates of  $H_0$ , with  $\rho_m = e^{-\beta E_m} / Z$  as Boltzmann's weights.  $\alpha, \beta \in (x, y, z)$  are the Cartesian components of the currents.

The complex uniform ( $\mathbf{q} = 0$ ) dynamical conductivities which correspond to the transport equations (1), are calculable by the Kubo formulas,

$$\begin{aligned} \text{electric conductivity :} \quad \sigma_{\alpha\beta}(\omega) &= \lim_{\mathbf{q} \rightarrow 0} \lim_{\mathcal{V} \rightarrow \infty} \operatorname{Re} L_{11}^{\alpha\beta}(\mathbf{q}, \omega + i\varepsilon) \quad , \\ \text{thermoelectric conductivities :} \quad \alpha_{\alpha\beta}(\omega) &= \frac{1}{T} \lim_{\mathbf{q} \rightarrow 0} \lim_{\mathcal{V} \rightarrow \infty} \operatorname{Re} L_{12}^{\alpha\beta}(\mathbf{q}, \omega + i\varepsilon) \quad , \\ &\quad \bar{\alpha}_{\alpha\beta}(\omega) = \frac{1}{T} \lim_{\mathbf{q} \rightarrow 0} \lim_{\mathcal{V} \rightarrow \infty} \operatorname{Re} L_{21}^{\mathbf{q}, \alpha\beta}(\omega + i\varepsilon) \quad , \\ \text{thermal conductivity :} \quad \kappa_{\alpha\beta}(\omega) &= \frac{1}{T} \lim_{\mathbf{q} \rightarrow 0} \lim_{\mathcal{V} \rightarrow \infty} \operatorname{Re} L_{22}^{\alpha\beta}(\mathbf{q}, \omega + i\varepsilon) \quad . \end{aligned} \quad (53)$$

Straightforward computation of Eqs. (52) for general many-body Hamiltonians is generally a daunting task. Exact diagonalizations (ED) of  $H_0$  may increase exponentially with  $\mathcal{V}$  even for a single eigenstate and eigenenergy. The difficulty is compounded by the apparent necessity to compute many current matrix elements.

### 10.1. Non-interacting conductivities

ED is of course more manageable for non-interacting bosons and fermions. For the single particle Hamiltonian (35) and polarizations Eq. (36), using Eq. (31), the current matrix elements are,

$$\begin{aligned} \langle l|j_{\mathbf{q}}^\alpha|l'\rangle &= ie(\epsilon_l - \epsilon_{l'}) \langle l|x^\alpha e^{i\mathbf{q}\cdot\mathbf{x}}|l'\rangle \quad , \\ \langle l|(j_Q)_{\mathbf{q}}^\alpha|l'\rangle &= i(\epsilon_l - \epsilon_{l'}) \frac{(\epsilon_l + \epsilon_{l'} - 2\mu)}{2} \langle l|x^\alpha e^{i\mathbf{q}\cdot\mathbf{x}}|l'\rangle \quad . \end{aligned} \quad (54)$$



The Kubo formulas reduce to sums over single particle eigenstates,

$$L_{ij}^{\alpha\beta}(\mathbf{q}, \omega + i\varepsilon) = -i \frac{1}{\mathcal{V}} \sum_{l'l''} \frac{n(\epsilon_{l'}) - n(\epsilon_l)}{\epsilon_l - \epsilon_{l'}} \left( \frac{\langle l | (J_i^\alpha)_{-\mathbf{q}} | l' \rangle \langle l' | (J_j^\beta)_{\mathbf{q}} | l \rangle}{\epsilon_l - \epsilon_{l'} - \omega - i\varepsilon} \right) , \quad (55)$$

where

$$n(\epsilon) = \frac{1}{e^{\beta(\epsilon - \mu)} \pm 1} , \quad (56)$$

for fermions (bosons) with a plus (minus) sign.

## 11. The Tricky DC limit

DC transport coefficients require taking the orders of limits carefully. Since for any time independent Hamiltonian on a finite volume ( $\mathcal{V} < \infty$ ) the density matrix is in equilibrium. By definition, it cannot support any dissipative (entropy generating) steady-state transport currents. As argued by Luttinger [42], the DC steady state (which he called ‘‘rapid case’’) can be achieved if the driving force satisfies  $|\omega + i\varepsilon| > |\mathbf{q}|^2$ , as both  $\omega + i\varepsilon, |\mathbf{q}|$  are taken to zero, after we have taken  $\mathcal{V} \rightarrow \infty$  to eliminate finite size gaps in the continuous thermodynamic spectrum.

For thermal transport, the statistical field  $-\nabla T$  is replaced by Luttinger’s frequency dependent ‘‘gravitational’’ field  $\psi(\omega)$  [42]. The legality of this substitution has been widely accepted [19, 43], although its rigorous conditions are still debated <sup>2</sup>.

In taking the DC limit, one must contend with the (superfluous) effects of the static gravitational field  $\psi_{\omega=0}$ . This force field may create an equilibrium circulating ‘‘magnetization current’’ in any finite system, which is not part of the transport current [19]. It contributes to  $L_{ij}^{\alpha\beta}(\omega + i\varepsilon = 0)$  part of the Kubo formula which must be subtracted out *before* taking the DC limit.

In summary, the proper DC order of limits is given by

$$(L_{ij}^{\alpha\beta})^{\text{dc}} = \lim_{\omega+i\varepsilon \rightarrow i0^+} \lim_{\mathbf{q} \rightarrow 0} \lim_{\mathcal{V} \rightarrow \infty} \text{Re} \left( L_{ij}(\mathbf{q}, \omega + i\varepsilon, \mathcal{V}) - L_{ij}(\mathbf{q}, 0, \mathcal{V}) \right) . \quad (57)$$

The causal decay of the real-time response function ensures that  $L_{ij}(z)$  is analytic in the upper half plane ( $\text{Im}(z) > 0$ ). Therefore the limit  $\omega + i\varepsilon \rightarrow 0$  can be taken by a-priori setting  $\omega = 0$ , and sending  $\varepsilon \rightarrow 0^+$  *after* sending  $\mathcal{V} \rightarrow \infty$ .

On finite volume, we can distinguish between OBC and PBC. For OBC, the uniform limit  $\lim_{\mathbf{q} \rightarrow 0} (\mathbf{P}_i)_{\mathbf{q}}$  can be taken continuously, since the driving field is not required to be periodic between the boundaries. The DC limit is then simplified further to,

$$(L_{ij}^{\alpha\beta})^{\text{dc, OBC}} = \lim_{\varepsilon \rightarrow i0^+} \lim_{\mathcal{V} \rightarrow \infty} \text{Re} \left( L_{ij}(0, i\varepsilon, \mathcal{V}) - L_{ij}(0, 0, \mathcal{V}) \right) , \quad (58)$$

where the uniform polarizations are given by Eqs. (29) by setting  $\mathbf{q} = 0$  on any finite volume. In practice, as demonstrated in Part IV, Eq. (58) can be implemented by computing  $L_{ij}(i\varepsilon(\mathcal{V}), \mathcal{V})$  on an increasing sequence of volumes  $\{\mathcal{V}_i\}$ , by choosing the  $\varepsilon(\mathcal{V}_i)$  to be larger than the finite-size eigenenergy gaps in the Kubo formula.

On finite PBC lattices, the force fields must be continuous, and therefore their wavevectors  $\mathbf{q}$  are discretized. Therefore, in contrast to OBC, the order of limits on PBC must be taken by Eq. (57). Furthermore, since the uniform polarization cannot be taken continuously on  $\mathcal{V} < \infty$ , the limit is taken after  $\mathcal{V} \rightarrow \infty$ , i.e.

$$\begin{aligned} \mathbf{P}_{\mathbf{q}=0}^\alpha &= i\varepsilon \lim_{\mathbf{q} \rightarrow 0} \lim_{\mathcal{V} \rightarrow \infty} \frac{1}{q^\alpha} \int_{\mathcal{V}} d^d x e^{-i\mathbf{q}\cdot\mathbf{x}} n(\mathbf{x}) , \\ \mathbf{Q}_{\mathbf{q}=0}^\alpha &= i \lim_{\mathbf{q} \rightarrow 0} \lim_{\mathcal{V} \rightarrow \infty} \frac{1}{q^\alpha} \int_{\mathcal{V}} d^d x e^{-i\mathbf{q}\cdot\mathbf{x}} (h(\mathbf{x}) - \mu n(\mathbf{x})) . \end{aligned} \quad (59)$$

An alternative to using the uniform polarization, the uniform *electric* current on a finite volume PBC can be defined as the derivative of the free energy with respect to an enclosed Aharonov-Bohm flux, see Eq. (68). No such definition exists for the thermal current.

<sup>2</sup>Challenges to the equality of the current response to ‘‘mechanical forces’’ and ‘‘statistical forces’’ have been made by e.g. Ref [46].

## 12. Onsager relations

In the absence of spontaneous time reversal (TR) symmetry breaking, TR transformation of Kubo formulas for  $L_{ij}$  involves reversal of the external magnetic field and transposition of the two currents. The conductivities satisfy Onsager's reciprocal relations [47, 48],

$$L_{ij}^{\alpha\beta}(\mathbf{B}) = L_{ji}^{\beta\alpha}(-\mathbf{B}) \quad . \quad (60)$$

As a consequence, the longitudinal conductivities  $L_{ii}^{\alpha\alpha}$  are even functions of magnetic field  $\mathbf{B}$ . For  $\mathbf{B} \parallel \hat{\mathbf{z}}$ , the transverse conductivities can be written as,

$$L^{xy,\pm} = \frac{1}{2} (L^{xy} \pm L^{yx}) \quad , \quad (61)$$

$L^{xy,-}$  are the *Hall conductivities* which, by Eq. (60), are antisymmetric with respect to reversal of magnetic field:

$$\begin{aligned} \sigma_{xy,-}(\mathbf{B}) &= -\sigma_{xy,-}(-\mathbf{B}) \quad , \\ \kappa_{xy,-}(\mathbf{B}) &= -\kappa_{xy,-}(-\mathbf{B}) \quad . \end{aligned} \quad (62)$$

Eqs. (62) allow experimenters to measure the Hall conductivities in a four-probe bar geometry, by reversing the applied magnetic field.

For general crystals,  $\alpha_{xy,-} \neq \bar{\alpha}_{xy,-}$ . However, if the Hamiltonian has C4 rotation symmetry about the  $z$ -axis, and C2 symmetry about the  $x$ -axis, by Eq. (60) it is easy to verify that

$$\alpha_{xy}(\mathbf{B}) \underbrace{=}_{C_4} \bar{\alpha}_{xy}(\mathbf{B}) \quad . \quad (63)$$

and that all symmetric transverse conductivities vanish,

$$\sigma_{xy,+} = \alpha_{xy,+} = \bar{\alpha}_{xy,+} = \kappa_{xy,+} \underbrace{=}_{C_4} 0 \quad . \quad (64)$$

## 13. Hall conductivity proxies

For general Hamiltonians, the Kubo formula (52) for the DC Hall conductivity  $\sigma_{xy}^{\text{dc}}$  is computationally challenging. Hence, two simpler proxy formulas for  $\sigma_{xy}^{\text{dc}}$  have been very popular: (i) The Chern conductivity  $\sigma_{xy}^{\text{Chern}}$  and (ii) the Streda conductivity  $\sigma_{xy}^{\text{Streda}}$ . We emphasize that these proxies are only valid under restricted conditions, since they reverse the DC order of limits prescribed by Eq. (57).

### 13.1. Chern number

One considers a Hamiltonian

$$H = H_0(\mathbf{B}, \theta^x, \theta^y) \quad , \quad (65)$$

which describes particles with charge  $e$  placed on the surface of a torus of area  $\mathcal{V} = L_x \times L_y$ , with PBC. A uniform magnetic field  $\mathbf{B}$  penetrates the surface, and two Aharonov-Bohm fluxes  $\Phi^\alpha$ ,  $\alpha = x, y$  are threaded through the  $x$  and  $y$  holes of the torus, as depicted in Fig. 3. The fluxes are parametrized by,

$$\Phi^\alpha = \frac{\Phi_0}{2\pi} \theta^\alpha \quad , \quad \theta_\alpha \in [0, 2\pi] \quad , \quad (66)$$

where  $\Phi_0 = hc/e$  is the flux quantum.

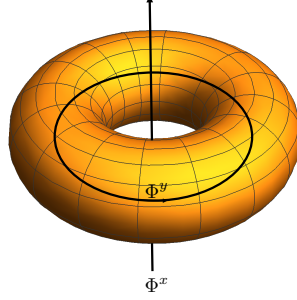


Figure 3: The Gauged Torus setup for a Chern number calculation. The charged system is placed on the surface of the torus, which is penetrated by a uniform magnetic field. Two Aharonov-Bohm fluxes  $\Phi^x, \Phi^y$  which thread the holes of the torus serve as adiabatic parameters of the ground state wavefunction  $\Psi_0$ .

The Chern number of the ground state  $|\Psi_0\rangle$  defined by an integral over the Berry curvature with respect to the angles  $\theta_x, \theta_y$ :

$$\begin{aligned} C_{xy} &= \frac{1}{\pi} \int_0^{2\pi} \int_0^{2\pi} d\theta_x d\theta_y \operatorname{Im} \left\langle \frac{\partial}{\partial \theta_x} \Psi_0 \left| \frac{\partial}{\partial \theta_y} \Psi_0 \right. \right\rangle = \frac{1}{2\pi} \oint d\theta \cdot \operatorname{Im} \langle \Psi_0 | \nabla_\theta \Psi_0 \rangle \\ &= \text{Chern number (integer)} \quad . \end{aligned} \quad (67)$$

The Chern number is a topological integer which characterizes a gapped Quantum Hall ground state  $|\Psi_0\rangle$ .

First order perturbation of the ground state w.r.t. the interaction

$$H' = -\frac{\hbar}{e} \sum_{\alpha} j_0^{\alpha} \frac{\theta^{\alpha}}{L_{\alpha}} \quad (68)$$

yields,

$$\frac{\partial}{\partial \theta_{\alpha}} |\Psi_0\rangle = \frac{\hbar}{e L_{\alpha}} \sum_{m \neq 0} |\Psi_m\rangle \frac{\langle \Psi_m | j_0^{\alpha} | \Psi_0 \rangle}{E_m - E_0} \quad . \quad (69)$$

Thus the Chern number can be related to the finite volume, zero frequency  $\mathbf{q} = 0$  Kubo formula for  $\sigma_{xy}$  as given by the real part of Eq. (52):

$$\begin{aligned} \sigma_{xy}^{\text{Kubo}}(\mathbf{q} = 0, i\varepsilon = 0, \mathcal{V})_{\theta_x, \theta_y} &= \frac{\hbar}{\mathcal{V}} \sum_{0m} \frac{\langle \Psi_0 | j_0^x | \Psi_m \rangle \langle \Psi_m | j_0^y | \Psi_0 \rangle - \langle \Psi_0 | j_0^y | \Psi_m \rangle \langle \Psi_m | j_0^x | \Psi_0 \rangle}{(E_m - E_0)^2} \\ &= \frac{2e^2}{\hbar} \operatorname{Im} \left\langle \frac{\partial}{\partial \theta_x} \Psi_0 \left| \frac{\partial}{\partial \theta_y} \Psi_0 \right. \right\rangle \quad . \end{aligned} \quad (70)$$

Thus,

$$\sigma_{xy}^{\text{Chern}} \equiv \frac{1}{(2\pi)^2} \int_0^{2\pi} d\theta_x \int_0^{2\pi} d\theta_y \sigma_{xy}^{\text{Kubo}}(\mathbf{q} = 0, i\varepsilon = 0, \mathcal{V})_{\theta_x, \theta_y} = \frac{e^2}{\hbar} C_{xy} \quad . \quad (71)$$

In other words, the flux-averaged Kubo formula yields an integer times  $e^2/h$ . The variation of the integrand  $\sigma_{xy}^{\text{Kubo}}$ , with flux parameters  $\theta_x, \theta_y \in [0, 2\pi)$  is expected to vanish in the large volume limit. The double integral  $\int \int \frac{d\theta_x d\theta_y}{(2\pi)^2}$  can be replaced by  $\sigma_{xy}(0, \mathcal{V})$  at  $\theta_x = \theta_y = 0$ .

Historically, the topological relation between  $\sigma^{\text{Chem}}$  and the Chern number was initially discovered by Thouless, Kohmoto, Nightingale, and den Nijs, (TKNN) [13], for filled bands of non interacting, disorder-free electrons on a torus, penetrated by a unit-cell-commensurate magnetic field.

The Chern proxy formula (67) for interacting Hamiltonians was independently derived by adiabatic transport theory by Niu, Thouless and Wu [49] and by Avron and Seiler [14]. The one plaquette Chern number formulation by Kudo *et al.* [50] provides a useful simplification of the computation of  $\sigma_{xy}^{\text{Chem}}$  in the large volume limit.

However, we must caution that  $\sigma_{xy}^{\text{Chem}}$  *reverses* the proper DC order of limits prescribed by Eq. (57). Therefore the validity of this proxy is limited to the following conditions:

1. For the adiabatic theorem to apply [14], a finite gap  $\Delta > 0$  between the ground state and all excitations must exist in the infinite volume limit.
2. The longitudinal conductivity must vanish  $\sigma_{xx} = 0$ . This can be ensured only at zero temperature if there are no gapless current carrying excitations and no inelastic scattering processes.
3. If disorder is present it should be weak enough to prevent gapless current-carrying states from percolating through the bulk of the sample.

That said, we emphasize that  $\sigma_{xy}^{\text{Chem}}$  has been instrumental in mathematical and experimental characterization of Quantum Hall and topological insulator phases [12, 51].

### 13.2. Streda formula

The Streda formula proxy for  $\sigma_{xy}$  is obtained by reversing the DC order of limits of Eq. 57. In Ref. [52] it is shown that,

$$\begin{aligned}\sigma_{xy}^{\text{Streda}} &= \lim_{\mathbf{q} \rightarrow 0} \lim_{\mathcal{V} \rightarrow \infty} \lim_{i\varepsilon \rightarrow 0^+} \sigma_{xy}(\mathbf{q}, i\varepsilon) \\ &= c \lim_{\mathbf{q} \rightarrow 0} \lim_{\mathcal{V} \rightarrow \infty} (\rho_{\mathbf{q}} | M_{\mathbf{q}}^z ) = c \left. \frac{\partial \rho}{\partial B} \right|_{\mu, T} = c \left. \frac{\partial m^z}{\partial \mu} \right|_{B, T},\end{aligned}\quad (72)$$

where  $m^z$  is the  $z$ -magnetization and  $\rho$  is the charge density. The last equation follows from a Maxwell relation. The Streda formula is often used to characterize quantum Hall phases and topological insulators by scanning compressibility measurements [53].

In general the Streda order of limits does not commute with the DC order of limits (57), and therefore

$$\sigma_{xy}^{\text{Streda}} = \lim_{\mathbf{q} \rightarrow 0} \lim_{\mathcal{V} \rightarrow \infty} \lim_{\omega \rightarrow 0} \sigma_{xy}(\mathbf{q}, \omega) \neq \lim_{\omega \rightarrow 0} \lim_{\mathbf{q} \rightarrow 0} \lim_{\mathcal{V} \rightarrow \infty} \sigma_{xy}(\mathbf{q}, \omega) = \sigma_{xy}^{\text{dc}}. \quad (73)$$

The conditions which may permit the use Streda's proxy is that the ground state is bulk-incompressible, and that the Hall angle is large, i.e.  $\sigma_{xy}/\sigma_{xx} \gg 1$ . Such conditions occur when there is a gap  $\Delta > 0$  for excitations above the ground state, and the temperature is lower than this gap. A weaker condition is a pseudogap, where the density of charge excitations vanishes rapidly enough at low energies to allow reversal of the  $\omega, \mathbf{q} \rightarrow 0$  order of limits in the Kubo formula.

## 14. Kubo formulas in operator Hilbert space

The Kubo formulas of Eq. (52) may be formulated as matrix elements in OHS. This formalism avoids the Lehmann representation, and proves to be convenient for further mathematical manipulation. Below, we shall use the OHS formalism to derive the DPP formulas in Part IV, the continued fractions in Section 21, and the Hall coefficient summation formulas in Part VI. We start with the formulation of susceptibilities as inner product in OHS. We then proceed to formulate dynamical response functions in OHS.

### 14.1. Equilibrium Susceptibilities

Given a static Hamiltonian and free energy,

$$H = H_0 - h_A A - h_B B, \quad F = -T \log \text{Tr} e^{-\beta H} \quad . \quad (74)$$

A thermodynamic expectation value is given by,

$$\begin{aligned} \langle A \rangle &\equiv - \left. \frac{\partial F}{\partial h_A} \right|_{h_A=h_B=0} \\ &= \text{Tr}(\rho_0 A) \quad , \end{aligned} \quad (75)$$

where Boltzmann weights are  $\rho = e^{-\beta H_0} / \text{Tr} e^{-\beta H_0}$ . Static susceptibilities with respect to  $A$  and  $B$  are,

$$\begin{aligned} \chi_{AB} &= - \left. \frac{\partial^2 F[h_A, h_B]}{\partial h_A \partial h_B} \right|_{h_A=h_B=0} \\ &= \int_0^\beta d\tau \langle A(\tau) B \rangle + \beta \langle A^{\text{diag}} B^{\text{diag}} \rangle - \beta \langle A \rangle \langle B \rangle \\ &= \sum_{m,n} \frac{\rho_m - \rho_n}{E_n - E_m} \langle n|A|m \rangle \langle m|B|n \rangle + \beta \langle A^{\text{diag}} B^{\text{diag}} \rangle - \beta \langle A \rangle \langle B \rangle \quad . \end{aligned} \quad (76)$$

where  $O^{\text{diag}} = \sum_n |n \rangle \langle n| O |n \rangle \langle n|$ . In the second line  $B(\tau) \equiv e^{\tau H_0} B e^{-\beta H_0}$ . The last line of (76) is written in the Lehmann representation of  $H_0$ . The vector space of linear operators  $A \rightarrow |A \rangle$  which act within the Schrodinger Hilbert space of the Hamiltonian  $H_0$ , is an OHS containing hyperstates  $|A \rangle$ , and closed under linear superpositions. Henceforth we consider general operators  $A^{\text{diag}} = B^{\text{diag}} = 0$ , whose susceptibility is

$$\begin{aligned} \chi_{AB} &= \sum_{nm} W_{nm} A_{nm}^* B_{nm} \equiv (A|B) \quad , \\ W_{nm} &\equiv \frac{\rho_m - \rho_n}{E_n - E_m} \geq 0 \quad . \end{aligned} \quad (77)$$

$(A|B)$  defines the Bogoliubov-Mori (BM) inner product, [29] which depends on  $H_0$  (with its boundary conditions) and inverse temperature  $\beta$ . It obeys the Hilbert space conditions of (i) a positive norm, (ii) hermiticity and (iii) linearity,

$$\begin{aligned} \text{(i)} \quad &(A|A) \geq 0 \quad , \\ \text{(ii)} \quad &(A|B) = (B|A)^* \quad , \\ \text{(iii)} \quad &(A|aB + bC) = a(A|B) + b(A|C), \quad \forall a, b \in \mathbb{C} \quad . \end{aligned} \quad (78)$$

All operators which commute with  $H_0$  are identified with the null hyperstate of zero norm.

### 14.2. The Liouvillian and its inverse

In OHS, the Liouvillian hyperoperator  $\mathcal{L}$ , which generates the time evolution of hyperstates, is defined by,

$$\mathcal{L}|A \rangle = i[H_0, A] \quad , \quad (79)$$

where  $A$  is any operator in the Hilbert space of  $H_0$ .

**Lemma 1.** *The Liouvillian is a hermitian hyperoperator in OHS,*

*Proof.*

$$\begin{aligned} (A|\mathcal{L}|B) &= \sum_{nm} \frac{\rho_m - \rho_n}{E_n - E_m} A_{nm}^* (E_m - E_n) B_{mn} = - \sum_{nm} (\rho_m - \rho_n) A_{nm}^* B_{mn} \\ &= \left( \sum_{nm} (\rho_n - \rho_m) \frac{E_m - E_n}{E_m - E_n} B_{mn}^* A_{mn} \right)^* = (B|\mathcal{L}|A)^* \\ &\Rightarrow \mathcal{L} = \mathcal{L}^\dagger \quad \square \end{aligned} \quad (80)$$

where the summation indices are relabelled  $mn \rightarrow nm$  in the last equation.  $\square$

$\mathcal{L}$  is therefore diagonalizable. Its eigenoperators are  $|n\rangle\langle m|$  with real eigenvalues  $E_n - E_m$ . It is the generator of time evolution in the OHS, since

$$|A(t)\rangle = |e^{iH_0 t} A e^{-iH_0 t}\rangle = e^{i\mathcal{L}t}|A\rangle \quad . \quad (81)$$

The inverse Liouvillian  $\left(\frac{1}{\mathcal{L}}\right)'_{\varepsilon}$  does not exist if the kernel of  $\mathcal{L}$  is non zero. Hence we define it with an imaginary infinitesimal  $\varepsilon$  prescription,

$$\left(\frac{1}{\mathcal{L} - i\varepsilon}\right)_{\varepsilon} \equiv \left(\frac{1}{\mathcal{L}}\right)'_{\varepsilon} + i\left(\frac{1}{\mathcal{L}}\right)''_{\varepsilon} \quad , \quad (82)$$

where the real part of the inverse is the hyperoperator

$$\left(\frac{1}{\mathcal{L}}\right)'_{\varepsilon} \equiv \frac{\mathcal{L}}{\mathcal{L}^2 + \varepsilon^2} \quad , \quad (83)$$

and the imaginary part is

$$\left(\frac{1}{\mathcal{L}}\right)''_{\varepsilon} \equiv \frac{\varepsilon}{\mathcal{L}^2 + \varepsilon^2} = \pi\delta_{\varepsilon}(\mathcal{L}) \quad . \quad (84)$$

The weight of the inner product, Eq. (77) can be expressed as

$$W_{nm} = \lim_{\varepsilon \rightarrow 0} \sum_{nm} \operatorname{Re} \left( \frac{\rho_m - \rho_n}{E_n - E_m + i\varepsilon} \right) \quad . \quad (85)$$

Using Eq. (83) we can write BM inner product in a representation independent form,

$$\begin{aligned} (A|B) &= -\lim_{\varepsilon \rightarrow 0} \operatorname{Tr} \left[ \rho, \left(\frac{1}{\mathcal{L}}\right)'_{\varepsilon} A^{\dagger} \right] B \\ &= -\lim_{\varepsilon \rightarrow 0} \operatorname{Tr} \rho \left[ \left(\frac{1}{\mathcal{L}}\right)'_{\varepsilon} A^{\dagger}, B \right] \quad . \end{aligned} \quad (86)$$

The advantage of Eq. (86) over Eq. (77) will be made clear during the mathematical manipulations of the Kubo formulas performed in the following Sections.

### 14.3. Dynamical linear response functions

Dynamical response functions are obtained in linear response by adding to the Hamiltonian  $H_0$  a weak time-dependent field  $h_B(t)$  coupled to an operator  $B$ . The field is turned at  $t \geq 0$ ,

$$H(t) = H_0 - \Theta(t) h_B(t) B \quad . \quad (87)$$

At  $t > 0$  the expectation value of an observable  $A^{\dagger}$  is

$$\langle A^{\dagger} \rangle(t) = \operatorname{Tr} \rho(\beta) U^{\dagger}(t) A^{\dagger} U([h_B], t) = \int_0^t dt' R_{AB}(t, t') h_B(t') + \mathcal{O}(h_B^2) \quad , \quad (88)$$

where the density matrix  $\rho = \frac{1}{Z} e^{-\beta H_0}$  and the evolution operator  $U$  satisfies  $i\dot{U} = H(t)U$ . Expanding  $U$  to linear order in  $h_B$  yields,

$$R_{AB}(t - t') = -i \operatorname{Tr} \rho \left[ A^{\dagger}(t - t'), B \right] \Theta(t - t') \quad , \quad (89)$$

where  $A(t) = e^{iH_0 t} A e^{-iH_0 t}$ , and using  $[\rho, H_0] = 0$  to obtain  $R_{AB}(t, t') = R_{AB}(t - t')$ . The transform of (89) into the upper complex plane defines the complex response function,

$$\begin{aligned} R_{AB}(z) &= \int_0^{\infty} e^{-izt} R_{AB}(t) dt = \sum_{mn} \frac{\rho_m - \rho_n}{E_n - E_m - z} \langle n|A^{\dagger}|m\rangle \langle m|B|n\rangle \\ &= \left( A \left| \frac{\mathcal{L}}{\mathcal{L} - z} \right| B \right) \quad , \quad \operatorname{Im}(z) > 0 \quad . \end{aligned} \quad (90)$$

#### 14.4. Electric and Thermal conductivities

The Kubo formulas of Eq. (52) are matrix elements in OHS,

$$L_{ij}^{\alpha\beta}(\mathbf{q}, \omega + i\varepsilon) = \frac{1}{\mathcal{V}} R_{J_i^\alpha, J_j^\beta}(\omega + i\varepsilon) = -\frac{i}{\mathcal{V}} \left( (J_i^\alpha)_{\mathbf{q}} \left| \frac{1}{\mathcal{L} - \omega - i\varepsilon} \right| (J_j^\beta)_{\mathbf{q}} \right) . \quad (91)$$

The values of  $\omega, i\varepsilon, \mathbf{q}, \mathcal{V}$  are all finite. The DC limit must to be taken carefully as required by Eq. (57).

## Part IV

# DPP Hall conductivities

### 15. Derivation of DPP formulas

For simplicity the magnetic field is chosen along the  $z$  axis and  $C_4$  symmetry is assumed in the  $XY$  plane. According to Eq. (57), the DC Hall-type conductivities are given by,

$$\text{Re}(L_{ij}^{xy})^{\text{dc}} = \lim_{\varepsilon \rightarrow 0} \lim_{\mathbf{q} \rightarrow 0} \lim_{\mathcal{V} \rightarrow \infty} \left( \text{Re} L_{ij}^{xy}(\varepsilon, \mathcal{V}) - \text{Re} L_{ij}^{xy}(0, \mathcal{V}) \right) \quad . \quad (92)$$

As mentioned before, the second term cancels the spurious magnetization currents which are created by the static component of the ‘‘gravitational’’ field  $\psi(\omega = 0)$ . In OHS notation,

$$\text{Re} L_{ij}^{xy}(\varepsilon, \mathcal{V}) \equiv \frac{1}{\mathcal{V}} \text{Im} \left( J_i^x \left| \left( \frac{1}{\mathcal{L}} \right)' \right| J_j^y \right) + \frac{1}{\mathcal{V}} \text{Re} \left( J_i^x \left| \left( \frac{1}{\mathcal{L}} \right)'' \right| J_j^y \right) \xrightarrow{0} \quad (C_4) \quad . \quad (93)$$

where  $\mathbf{q}$ -dependence of the currents is implicit. Under  $\pi/2$  rotation in the plane  $\text{Re} L_{ij}^{xy}(\varepsilon, \mathcal{V}) = -\text{Re} L_{ij}^{yx}(\varepsilon, \mathcal{V})$ , and since the second term is symmetric under  $x \leftrightarrow y$ , it vanishes. In the Lehmann representation,

$$\text{Re} L_{ij}^{xy}(\varepsilon, \mathcal{V}) = \frac{1}{\mathcal{V}} \sum_{mn} \frac{\rho_m - \rho_n}{E_n - E_m} \text{Im} \left( \langle n | J_i^x | m \rangle \langle m | J_j^y | n \rangle \right) \left( \frac{E_m - E_n}{(E_m - E_n)^2 + \varepsilon^2} \right) \quad . \quad (94)$$

At first glance, one might be tempted to discard  $\mathcal{O}(\varepsilon^2)$  contributions in the denominator of Eq. (94). On OBC, this would be a gross error! As shown below, the DC limit is dominated by eigenstates with  $|E_n - E_m| \leq \varepsilon$ .

Using the identity (86),

$$\text{Re} L_{ij}^{xy}(\varepsilon, \mathcal{V}) = -\frac{1}{\mathcal{V}} \text{Im} \text{Tr} \rho \left[ \left( \frac{1}{\mathcal{L}} \right)'_{\varepsilon'} J_i^x, \left( \frac{1}{\mathcal{L}} \right)'_{\varepsilon} J_j^y \right] \quad . \quad (95)$$

To remain consistent with  $C_4$  symmetry, on finite volumes we identify  $\varepsilon' = \varepsilon$ , while keeping the DC order of limits in Eq. (92). By Eq. (31),

$$\left( \frac{1}{\mathcal{L}} \right)'_{\varepsilon} J_j^{\alpha} = i(1 - \Theta_{\varepsilon}) P_j^{\alpha} \equiv i(P_j^{\alpha} - (\tilde{P}_j^{\alpha})_{\varepsilon}) \quad , \quad \alpha = x, y \quad . \quad (96)$$

$\Theta_{\varepsilon}$  is a Lorentzian degeneracy projector,

$$\Theta_{\varepsilon} = \frac{\varepsilon^2}{\mathcal{L}^2 + \varepsilon^2} \quad (97)$$

and  $(\tilde{P}_j^{\alpha})_{\varepsilon} \equiv \Theta_{\varepsilon} P_j^{\alpha}$  are DPP’s (*degeneracy projected polarizations*), whose matrix elements in the Lehmann representation are restricted (at small  $\varepsilon$ ) to connect quasi-degenerate eigenstates,

$$\langle n | (\tilde{P}_i^{\alpha})_{\varepsilon} | m \rangle = \langle n | P_i^{\alpha} | m \rangle \frac{\varepsilon^2}{|E_n - E_m|^2 + \varepsilon^2} \quad . \quad (98)$$

Eq. (95) can be written as

$$\text{Re} L_{ij}^{xy}(\varepsilon, \mathcal{V}) = \frac{1}{\mathcal{V}} \text{Im} \text{Tr} \rho \left[ P_i^x - (\tilde{P}_i^x)_{\varepsilon}, P_j^y - (\tilde{P}_j^y)_{\varepsilon} \right] \quad . \quad (99)$$

Expansion of the terms in (99) we obtain a sum of four terms,

$$\text{Re} L_{ij}^{xy}(\varepsilon, \mathcal{V}) = \text{Re} L_{ij}^{xy}(\varepsilon = 0, \mathcal{V}) - L_b(\varepsilon) - L_c(\varepsilon) + L_d(\varepsilon) \quad . \quad (100)$$

The first term, which is independent of  $\varepsilon$  and  $\varepsilon'$  is called a magnetization term,

$$\text{Re} L_{ij}^{xy}(\varepsilon = 0, \mathcal{V}) \equiv \frac{1}{\mathcal{V}} \text{Im} \text{Tr} \rho \left[ P_i^x, P_j^y \right] \quad . \quad (101)$$



The physical content of magnetization terms is discussed in Section 15.1. The magnetization term precisely cancels the second term in Eq. (92), and therefore does not need to be calculated for the Hall-type conductivity.

The remaining three terms are related to each other,

$$\begin{aligned}
L_b(\varepsilon) &= \frac{1}{\mathcal{V}} \text{Im Tr } \rho \left[ P_i^x, (\tilde{P}_j^y)_\varepsilon \right] = \frac{1}{\mathcal{V}} \text{Im} \sum_n \rho_n \sum_m \langle n | P_i^x | m \rangle \langle m | P_j^y | n \rangle \left( \frac{\varepsilon^2}{(E_n - E_m)^2 + \varepsilon^2} \right) , \\
L_c(\varepsilon) &= \frac{1}{\mathcal{V}} \text{Im Tr } \rho \left[ (\tilde{P}_i^x)_\varepsilon, P_j^y \right] = \frac{1}{\mathcal{V}} \text{Im} \sum_n \rho_n \sum_m \langle n | P_i^x | m \rangle \langle m | P_j^y | n \rangle \left( \frac{(\varepsilon')^2}{(E_n - E_m)^2 + (\varepsilon')^2} \right) , \\
L_d(\varepsilon) &= \frac{1}{\mathcal{V}} \text{Im Tr } \rho \left[ (\tilde{P}_i^x)_{\varepsilon'}, (\tilde{P}_j^y)_\varepsilon \right] = \frac{1}{\mathcal{V}} \text{Im} \sum_n \rho_n \sum_m \langle n | P_i^x | m \rangle \langle m | P_j^y | n \rangle \left( \frac{\varepsilon^2}{(E_n - E_m)^2 + \varepsilon^2} \right)^2 . \quad (102)
\end{aligned}$$

$L_b$  and  $L_c$  contain one DPP, and therefore a Lorentzian factor,  $\varepsilon^2 / ((E_n - E_m)^2 + \varepsilon^2)$ .  $L_d$  contains a Lorentzian square  $(\varepsilon^2 / ((E_n - E_m)^2 + \varepsilon^2))^2$ . The Lorentzian factor and its square can be effectively replaced for small  $\varepsilon$  by box projectors  $\Theta(\pi\varepsilon/2 - |E_n - E_m|)$  and  $\Theta(\pi\varepsilon/4 - |E_n - E_m|)$ , respectively. Since we are taking  $\varepsilon \rightarrow 0$ , (after  $\mathcal{V} \rightarrow \infty$ ), the three terms have the same DC limit,

$$\lim_{\varepsilon \rightarrow 0} L_b(\varepsilon) = \lim_{\varepsilon \rightarrow 0} L_c(\varepsilon) = \lim_{\varepsilon \rightarrow 0} L_d(\varepsilon) . \quad (103)$$

Thus, summing up Eq. (100) the DC Hall conductivities are given by the DPP formulas,

$$\begin{aligned}
\sigma_{xy}^{\text{dc}} &= - \lim_{\varepsilon \rightarrow 0} \lim_{\mathbf{q} \rightarrow 0} \lim_{\mathcal{V} \rightarrow \infty} \frac{1}{\hbar \mathcal{V}} \text{Im Tr } \rho \left[ (\tilde{P}^x)_\varepsilon, (\tilde{P}^y)_\varepsilon \right] , \\
\alpha_{xy}^{\text{dc}} &= - \lim_{\varepsilon \rightarrow 0} \lim_{\mathbf{q} \rightarrow 0} \lim_{\mathcal{V} \rightarrow \infty} \frac{1}{\hbar \mathcal{V} k_B T} \text{Im Tr } \rho \left[ (\tilde{P}^x)_\varepsilon, (\tilde{Q}^y)_\varepsilon \right] , \\
\kappa_{xy}^{\text{dc}} &= - \lim_{\varepsilon \rightarrow 0} \lim_{\mathbf{q} \rightarrow 0} \lim_{\mathcal{V} \rightarrow \infty} \frac{1}{\hbar \mathcal{V} k_B T} \text{Im Tr } \rho \left[ (\tilde{Q}^x)_\varepsilon, (\tilde{Q}^y)_\varepsilon \right] . \quad (104)
\end{aligned}$$

Here we have restored the dimensionful dependence on  $\hbar$  and  $k_B$  for practical applications.

### 15.1. The Magnetization terms

The terms  $L_{ij}^{\text{xy}}(\varepsilon = 0, \mathcal{V})$  in Eq. (101) cancel against their counterterms in Eq. (92). For electric Hall conductivity  $\sigma_{xy}$ , the magnetization term vanishes since the two polarizations commute:  $[P^x, P^y] = 0$ . The thermoelectric and thermal Hall magnetization terms do not vanish. For Schrödinger particles governed by  $H^{\text{particles}}$ , the polarization commutators can be readily calculated to yield,

$$\begin{aligned}
\lim_{\mathbf{q} \rightarrow 0} \lim_{\mathcal{V} \rightarrow \infty} L_{12}^{\text{xy}} &= \lim_{\mathbf{q} \rightarrow 0} \lim_{\mathcal{V} \rightarrow \infty} \frac{1}{\mathcal{V}} \text{Im} \langle \frac{[P^x, Q^y] + [Q^x, P^y]}{2} \rangle = - \lim_{\mathcal{V} \rightarrow \infty} \frac{1}{\mathcal{V}} \langle \sum_{i=1}^{N_p} \mathbf{x}_i \times \mathbf{j}(\mathbf{x}_i) \cdot \hat{\mathbf{z}} \rangle = -c \langle m^z \rangle , \\
\lim_{\mathbf{q} \rightarrow 0} \lim_{\mathcal{V} \rightarrow \infty} L_{22} &= \lim_{\mathbf{q} \rightarrow 0} \lim_{\mathcal{V} \rightarrow \infty} \frac{1}{\mathcal{V}} \text{Im} \langle [Q^x, Q^y] \rangle = - \lim_{\mathcal{V} \rightarrow \infty} \frac{1}{\mathcal{V}} \langle \sum_{i=1}^{N_p} \mathbf{r}_i \times \mathbf{j}_Q(\mathbf{x}_i) \cdot \hat{\mathbf{z}} \rangle = -2 \langle m_Q^z \rangle , \quad (105)
\end{aligned}$$

which agrees with Ref. [19, 20].  $m^z$  and  $m_Q^z$  are the  $z$ -direction electric and thermal magnetization densities respectively.

The magnetization subtractions create considerable headache when computing the Kubo formulas from Eq. (52). Since  $L_{ij}$  are weighted by  $\frac{1}{T}$  in Eqs. (53), any separate approximations of the two terms in Eq. (92) could result in an error which embarrassingly diverges at low temperature. (Heat conductivities should actually vanish at low temperatures by the third law of thermodynamics). Elimination of these subtractions from the DPP formulas (104) provides an essential simplification.

## 16. DPP formulas for non-interacting Hamiltonians

For a normal Hamiltonian of non-interacting fermions or bosons, Eq. (35), the DPP formula is

$$\begin{aligned} L_{ij}^{xy} &= -\lim_{\varepsilon \rightarrow 0} \lim_{\mathbf{q} \rightarrow 0} \lim_{\mathcal{V} \rightarrow \infty} \frac{1}{\mathcal{V}} \text{Im} \sum_l n(\varepsilon_l) \langle l | [\tilde{P}_i^x, \tilde{P}_j^y] | l \rangle \\ &= -\lim_{\varepsilon \rightarrow 0} \lim_{\mathbf{q} \rightarrow 0} \lim_{\mathcal{V} \rightarrow \infty} \sum_{l'l'} (n(\varepsilon_l) - n(\varepsilon_{l'})) \text{Im} \langle l | \tilde{P}_i^x | l' \rangle \langle l' | \tilde{P}_j^y | l \rangle . \end{aligned} \quad (106)$$

where the polarizations  $P_i^x, P_j^y$  are defined in (36), and their DPP's are given by

$$\langle l | \tilde{P}_i^\alpha | l' \rangle = \langle l | P_i^\alpha | l' \rangle \frac{\varepsilon^2}{\varepsilon^2 + (\varepsilon_l - \varepsilon_{l'})^2} . \quad (107)$$

At low temperatures, the factor  $n(\varepsilon_l) - n(\varepsilon_{l'})$  ensures the sum is dominated by excitation energies at less than of order  $T$  from the chemical potential.

For a bosonic Hamiltonian of coupled harmonic oscillators (40), the thermal polarization is generally an anomalous bilinear form given by Eq. (50). The anomalous matrix blocks  $Q_{A,\mathbf{q}}^\alpha, (Q_{A,\mathbf{q}}^\alpha)^*$  involve creation or annihilation of two positive energy states, such that  $\varepsilon_l + \varepsilon_{l'} > 0$ . Thus, there are no anomalous contributions to the DPP<sup>3</sup>. Thus we are left with the normal parts of the polarizations,

$$\langle l | \tilde{Q}_i^\alpha | l' \rangle = \sum_{l''} \left( \frac{\varepsilon^2}{\varepsilon^2 + (\varepsilon_l^{\text{diag}} - \varepsilon_{l''}^{\text{diag}})^2} \right) (Q_{N;\mathbf{q}}^\alpha)_{ll''} . \quad (108)$$

## 17. Berry curvature integrals

Hall-type conductivities for non-interacting periodic crystal Hamiltonians  $H^{\text{PC}}$ , defined in Eq. (38), can be expressed as Berry curvature integrals over BZ, where the band Berry curvature is defined in Eq. (10).

The relations between Berry curvature integrals and Hall conductivity [28], Transverse thermoelectric conductivity [54] and thermal Hall conductivity [20, 55], have been previously derived from semiclassical dynamics and also directly from the Kubo formula of perfectly periodic lattices (55).

Here we provide a somewhat simpler derivation (in our view) starting from the single-particle DPP formulas for periodic lattices.  $U_{li}(\mathbf{k})$  is a unitary matrix which diagonalizes  $h_{ij}(\mathbf{k})$  in  $H^{\text{PC}}$ , and defines the eigenmode operators,

$$b_{\mathbf{k}l}^\dagger = \sum_{i=1}^M U_{li}(\mathbf{k}) a_{\mathbf{k}i}^\dagger \quad l = 1, \dots, M \quad , \quad (109)$$

such that,

$$H^{\text{PC}} = \sum_{\mathbf{k} \in \text{BZ}} \sum_{l=1}^M (\varepsilon_{\mathbf{k}l} - \mu) b_{\mathbf{k}l}^\dagger b_{\mathbf{k}l} . \quad (110)$$

The uniform polarizations can be defined by sending  $\mathbf{q} \rightarrow 0$  after  $\mathcal{V} \rightarrow \infty$  in Eq. (39), (see Eq. (59):

$$\begin{aligned} P^\alpha &= e \sum_{\mathbf{k}ij} a_{\mathbf{k}i}^\dagger (i\nabla_{\mathbf{k}}^\alpha) a_{\mathbf{k}j} \quad , \\ Q^\alpha &= \frac{1}{2} \sum_{\mathbf{k}ij} a_{\mathbf{k}i}^\dagger \left\{ (h_{ij}(\mathbf{k}) - \mu\delta_{ij}), (i\nabla_{\mathbf{k}}^\alpha) \right\} a_{\mathbf{k}j} \quad . \end{aligned} \quad (111)$$

<sup>3</sup>Unlike their contribution to the magnetization terms. It is good to know that anomalous terms are projected out, since their commutator would lead to diverging contributions to the low temperature limit of  $\kappa_{xy}$ .

The DPP operators are constrained to act only within the same band  $l$ . Using Eq. (109), the electric DPP's are given by

$$\langle \mathbf{k}l | \tilde{P}_\varepsilon^\alpha | \mathbf{k}'l \rangle = e \frac{\varepsilon^2}{\varepsilon^2 + (\epsilon_{\mathbf{k}l} - \epsilon_{\mathbf{k}'l})^2} \left\{ \overbrace{\sum_i U_{li}^\dagger(\mathbf{k}) \left( i \nabla_{\mathbf{k}}^\alpha U_{il}(\mathbf{k}) \right)}^{A_l^\alpha(\mathbf{k})} + i \nabla_{\mathbf{k}'}^\alpha \right\} . \quad (112)$$

The vector function  $\mathbf{A}_l(\mathbf{k})$  is the *Berry gauge field* [56] of eigenmode  $|\mathbf{k}, l\rangle$ ,

$$\mathbf{A}_l(\mathbf{k}) \equiv i \sum_{j=1}^M U_{lj}(\mathbf{k}) \nabla_{\mathbf{k}}^\alpha U_{jl}^\dagger(\mathbf{k}) . \quad (113)$$

Similarly, the thermal DPP's are

$$\langle \mathbf{k}l | \tilde{Q}_\varepsilon^\alpha | \mathbf{k}'l \rangle = \frac{\varepsilon^2}{\varepsilon^2 + (\epsilon_{\mathbf{k}l} - \epsilon_{\mathbf{k}'l})^2} \left( (\epsilon_{\mathbf{k}l} - \mu) \left( i \nabla_{\mathbf{k}'}^\alpha + A_l^\alpha(\mathbf{k}) \right) + \frac{i}{2} v_{\mathbf{k}l}^\alpha \right) , \quad (114)$$

where  $\mathbf{v}_{\mathbf{k}l} = \nabla_{\mathbf{k}} \epsilon_{\mathbf{k}l}$ . Note that on a finite volume,  $\mathbf{k}$  are discrete with intervals of  $\delta \mathbf{k} = 2\pi/\mathcal{V}^{\frac{1}{d}}$ . The DC limit is obtained by keeping  $\varepsilon > \delta \mathbf{k}$ , as  $\mathcal{V} \rightarrow \infty$ . The differentiability of  $\epsilon_{\mathbf{k}l}$  and  $U_{il}(\mathbf{k})$  allows us to set  $\mathbf{k}' \rightarrow \mathbf{k}$  in Eqs. (112) and (114), which involve a relative correction of  $\mathcal{O}(\varepsilon)$ .

By (112) the commutator

$$\begin{aligned} \langle \mathbf{k}, l | [\tilde{P}_\varepsilon^x, \tilde{P}_\varepsilon^y] | \mathbf{k}, l \rangle &= i \nabla_{\mathbf{k}} \times \mathbf{A}_l(\mathbf{k}) \cdot \hat{\mathbf{z}} + \mathcal{O}(\varepsilon^2) \\ &= i \Omega^z(\mathbf{k}, l) , \end{aligned} \quad (115)$$

where we discarded  $[\partial_{k_x}, \partial_{k_y}] = 0$  when acting on differentiable wavefunctions.  $\Omega^z(\mathbf{k}, l)$  defines the Berry curvature field in the  $\hat{\mathbf{z}}$  direction of eigenmode  $l$ .

By Eq. (104) the intrinsic Hall conductivity recovers the result of Chang and Niu [28],

$$\sigma_{xy}^{\text{dc}} = - \lim_{\varepsilon \rightarrow 0} \sum_l \int \frac{d^d k}{(2\pi)^d} n(\epsilon_{\mathbf{k}l}) \Omega_{\mathbf{k}l}^z . \quad (116)$$

This expression has been used to describe the anomalous Hall effect in ferromagnets [57]. Additional effects of impurities have been introduced semiclassically [58].

The thermal Hall DPP's have a slightly more complicated commutator,

$$\begin{aligned} \langle \mathbf{k}l | [\tilde{Q}_\varepsilon^x, \tilde{Q}_\varepsilon^y] | \mathbf{k}l \rangle &= i \langle \mathbf{k}l | \left( \epsilon_{\mathbf{k}l}^2 \nabla_{\mathbf{k}} \times \mathbf{A}_l(\mathbf{k}) + \epsilon_{\mathbf{k}l} \mathbf{v}_{\mathbf{k}l} \times \mathbf{A}_{\mathbf{k}l} + \epsilon_{\mathbf{k}l} \mathbf{v}_{\mathbf{k}l} \times \nabla \right) | \mathbf{k}l \rangle + \frac{i}{2} \epsilon_{\mathbf{k}l} \nabla \times \mathbf{v}_{\mathbf{k}l} + \mathcal{O}(\varepsilon) \\ &= i \epsilon_{\mathbf{k}l}^2 \nabla_{\mathbf{k}} \times \mathbf{A} + 2 \epsilon_{\mathbf{k}l} \mathbf{v}_{\mathbf{k}l} \times \mathbf{A}_{\mathbf{k}l} + \mathcal{O}(\varepsilon) . \end{aligned} \quad (117)$$

where  $i \nabla_{\mathbf{k}} \times \mathbf{v}_{\mathbf{k}l} = 0$ .

For convenience we define energy resolved conductivities by,

$$\begin{aligned} \tilde{\sigma}_{xy}(\varepsilon) &= - \frac{1}{\mathcal{V}} \sum_{\mathbf{k}l} \delta(\varepsilon - \epsilon_{\mathbf{k}l}) \Omega_{\mathbf{k}l}^z , \\ \tilde{\Sigma}_{xy}(\varepsilon) &= - \frac{1}{\mathcal{V}} \sum_{\mathbf{k}l} \delta(\varepsilon - \epsilon_{\mathbf{k}l}) (\nabla_{\mathbf{k}} \epsilon_{\mathbf{k}l}) \times \mathbf{A}_{\mathbf{k}l} \cdot \hat{\mathbf{z}} . \end{aligned} \quad (118)$$

In three dimensions, for fixed  $k_z$ , the  $\delta$  function restricts the wavevectors to a circle on sphere of energy  $\varepsilon$ , such that

$$\sum_{\mathbf{k}_\perp l} \delta(\varepsilon - \epsilon_{\mathbf{k}l}) = \frac{1}{(2\pi)^2} \oint_{s \in \partial\{\epsilon_{k_z, \mathbf{k}_\perp l} \leq \varepsilon\}} \frac{ds}{|\nabla_{\mathbf{k}_\perp} \epsilon_{\mathbf{k}l}|} . \quad (119)$$

Thus, we use Stokes theorem to relate  $\tilde{\Sigma}_{xy}$  to  $\sigma_{xy}$  by,

$$\begin{aligned}
\tilde{\Sigma}_{xy}(\epsilon) &= \frac{1}{(2\pi)^3} \sum_l \int dk_z \oint_{\partial\{\mathbf{s} \in \epsilon_{k_z, \mathbf{k}_\perp} \leq \epsilon\}} d\mathbf{s} \cdot \mathbf{A}_l^z \\
&= \sum_l \int \frac{d^3k}{(2\pi)^3} \Theta(\epsilon - \epsilon_{\mathbf{k}l}) \Omega_l^z(\mathbf{k}) \\
&= \int_{-\infty}^{\epsilon} d\epsilon' \tilde{\sigma}_{xy}(\epsilon') .
\end{aligned} \tag{120}$$

Thus, we arrive at the expression previously derived by Qin, Niu and Shi [20],

$$\begin{aligned}
\kappa_{xy}^{\text{dc}} &= \lim_{\epsilon \rightarrow 0} \lim_{\mathbf{q} \rightarrow 0} \lim_{\mathcal{V} \rightarrow \infty} \frac{1}{T} \int_{-\infty}^{\infty} d\epsilon n(\epsilon) \left( \epsilon^2 \tilde{\sigma}_{xy} + 2\epsilon \int_0^{\epsilon} d\epsilon' \tilde{\sigma}_{xy}(\epsilon') \right) \\
&= \frac{1}{T} \int_{-\infty}^{\infty} d\epsilon \left( -\frac{\partial n}{\partial \epsilon} \right) \epsilon^2 \tilde{\Sigma}_{xy}(\epsilon) .
\end{aligned} \tag{121}$$

Similarly, the DPP formula for the thermoelectric conductivity of a clean  $C_4$ -symmetric metallic band of electrons with charge  $e < 0$ , is given by

$$\alpha_{xy}^{\text{dc}} = -\lim_{\epsilon \rightarrow 0} \lim_{\mathbf{q} \rightarrow 0} \lim_{\mathcal{V} \rightarrow \infty} \frac{1}{2\mathcal{V}T} \sum_{\mathbf{k}l} n(\epsilon_{\mathbf{k}l}) \left( [\tilde{P}_{\mathbf{k}l}^x, \tilde{Q}_{\mathbf{k}l}^y] + [\tilde{Q}_{\mathbf{k}l}^x, \tilde{P}_{\mathbf{k}l}^y] \right) . \tag{122}$$

Using (115) and defining,

$$\begin{aligned}
\tilde{\sigma}_{xy}(\epsilon) &= -\frac{1}{\mathcal{V}} \sum_{\mathbf{k}l} \delta(\epsilon - \epsilon_{\mathbf{k}l}) \Omega_{\mathbf{k}l}^z \\
\tilde{\Sigma}_{xy}(\epsilon) &= \int_{-\infty}^{\epsilon} d\epsilon' \tilde{\sigma}_{xy}(\epsilon') ,
\end{aligned} \tag{123}$$

one can express,

$$\alpha_{xy}^{\text{dc}} = \frac{1}{eT} \int_{-\infty}^{\infty} d\epsilon \left( -\frac{\partial n}{\partial \epsilon} \right) \epsilon \tilde{\Sigma}_{xy}(\epsilon) . \tag{124}$$

For low temperatures Eqs. (121) and (124) for metals reduce to the relations,

$$\begin{aligned}
\kappa_{xy}^{\text{dc}} &\simeq \frac{\pi^2 k_B^2 T}{3e} \tilde{\sigma}_{xy}(\epsilon_F) , \\
\alpha_{xy}^{\text{dc}} &\simeq \frac{\pi^2 k_B^2 T}{3e} \frac{d\tilde{\sigma}_{xy}}{d\epsilon_F} .
\end{aligned} \tag{125}$$

these relations extend Mott relations [59] between electric and thermoelectric conductivities to bandstructures with Berry curvatures [54].

Introducing the effects of disorder in the anomalous Hall effect has been a major challenge in the field. The main difficulty is to extend the semiclassical analysis to include effects of short range scattering [58, 60, 61, 62]. The general non-interacting DPP formulas (106) can feasibly study effects of disorder numerically.

### 18. DPP formula for confined Landau levels

We consider an electron in a uniform magnetic field  $\mathbf{B}$ , with vector potential  $\mathbf{A}$ ,  $\nabla \times \mathbf{A} = B\hat{z}$ . In first quantized notation, the Landau operators are,

$$\Pi^\alpha \equiv p^\alpha - \frac{e}{c} A^\alpha \quad . \quad (126)$$

The Landau level (LL) raising and lowering operators are respectively,

$$a = \frac{l_B^2}{\hbar} (\Pi^x + i\Pi^y) \quad , \quad a^\dagger = \frac{l_B^2}{\hbar} (\Pi^x - i\Pi^y) \quad . \quad (127)$$

where  $[a, a^\dagger] = 1$ , and the Landau length is  $l_B = \sqrt{\frac{\hbar c}{eB}}$ .

The LL Hamiltonian is

$$H^{\text{LL}} = \frac{1}{2m} ((\Pi^x)^2 + (\Pi^y)^2) = \hbar\omega_c \left( a^\dagger a + \frac{1}{2} \right) \quad , \quad (128)$$

where the cyclotron frequency is  $\omega_c = \frac{eB}{mc}$ . The eigenenergies are

$$\epsilon_{k,\nu} = \hbar\omega_c \left( \nu + \frac{1}{2} \right) \quad , \quad k = 1, \dots, N_L \quad . \quad (129)$$

where the integer LL index is  $\nu$ , and  $N_L = \frac{BA}{\Phi_0}$  is the number of states per area  $A$  in each LL.

The guiding center operators are,

$$\begin{aligned} R^x &= x + \frac{l_B^2}{\hbar} \Pi^y \\ R^y &= y - \frac{l_B^2}{\hbar} \Pi^x \quad , \end{aligned} \quad (130)$$

where

$$[R^\alpha, \Pi^\beta] = 0, \quad [R^x, R^y] = -il_B^2 \quad . \quad (131)$$

The polarization operators are

$$\begin{aligned} P^x &= ex = eR^x - e\frac{l_B^2}{\hbar} \Pi^y \quad , \\ P^y &= ey = eR^y + e\frac{l_B^2}{\hbar} \Pi^x \quad . \end{aligned} \quad (132)$$

Since  $\Pi^x, \Pi^y$  change the LL index by  $\pm 1$ , while  $R^\alpha$  connect states within each LL. Hence under degeneracy projection, the  $\Pi$ -operators are projected out, and DPP's are simply proportional to the guiding center operators,

$$\begin{aligned} \tilde{P}^x &= eR^x \quad , \\ \tilde{P}^y &= eR^y \quad . \end{aligned} \quad (133)$$

The DPP Hall conductivity formula (106) yields

$$\begin{aligned} \sigma_{xy}^{\text{dc}} &= -\frac{e^2}{\hbar^2 \mathcal{V}} \sum_{k,\nu} n(\epsilon_{k,\nu}) \text{Im} \langle k, \nu | [R^x, R^y] | k, \nu \rangle \\ &= \frac{eC}{B\mathcal{V}} \sum_{k,\nu} n(\epsilon_{\nu,k}) = \frac{n_e eC}{B} \quad , \end{aligned} \quad (134)$$

where  $n_e(\mu, T, B)$  is the electron density.

While the sum in Eq. (134) includes all occupied states, Eq. (106) shows that the Hall conductivity can be written only in terms of states near the Fermi energy  $\epsilon_F$ .

Where are these current carrying states? On finite systems with OBC, the semiclassical eigenenergies in each LL (which apply for smooth confining potential on the scale of  $l_B$ ), reach the Fermi energy  $\epsilon_F$  at the sample edges. Each LL band contributes one gapless edge mode. The Hall conductivity is precisely given by Eq. (134).

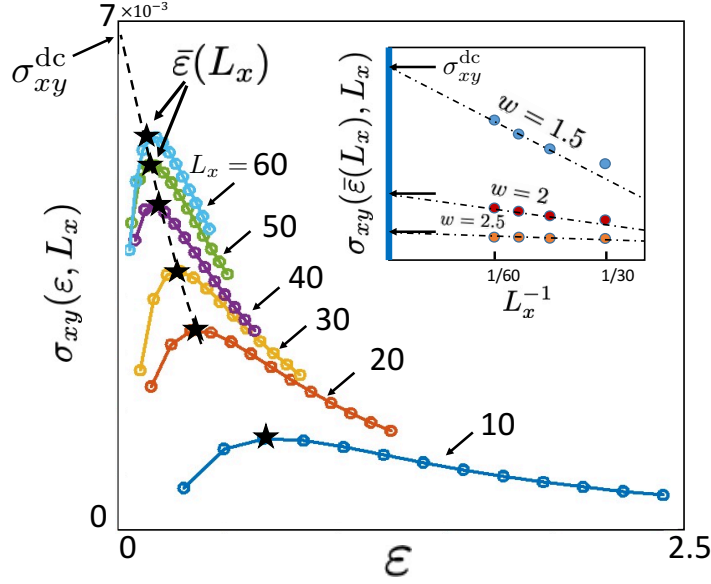


Figure 4: Extrapolation of numerical Hall conductivities of the square lattice Hamiltonian, Eq. (17). Disorder averaged  $\sigma_{xy}$  are plotted versus  $\epsilon$ , for a sequence of linear dimensions  $L_x$ . Stars mark the values of  $\bar{\epsilon}$  as defined in Eq. (136). The disorder strength is fixed at  $w = 3$ . The temperature, Fermi energy, and magnetic field are  $T = 0.3$ ,  $\epsilon_F = -1$  and  $B = 0.025$  respectively. **Inset:** The DC limit  $\sigma_{xy}^{dc}$  (marked by black arrows) for three values of disorder strength.

## 19. DPP Hall conductivity in a disordered metal

In the weak disorder and magnetic field regime proxies such as Chern numbers and Streda formulas do not work, since disorder mixes Landau levels, and the longitudinal conductivity is finite. Since  $\sigma_{xy}$  strongly depends on the scattering lifetime, it is instructive to compare Boltzmann's theory to the Kubo formula by numerically calculating it via the DPP formalism. It also gives us a chance to demonstrate how the DC limit is taken in a metallic gapless system.

In Ref. [63], the weakly disordered square lattice (DSL) Hamiltonian was considered,

$$H^{\text{DSL}} = - \sum_{\langle ij \rangle} \left( e^{-iA_{ij}} c_i^\dagger c_j + \text{h.c.} \right) + \sum_i (w_i - \epsilon_F) c_i^\dagger c_i \quad , \quad (135)$$

where  $w_i \in [-w/2, w/2]$  is a uniformly distributed random number and  $B = \sum_{\square} A_{ij}$  is the magnetic flux per plaquette. Using the DPP formula (104), we compute the disordered averaged curves  $\sigma_{xy}(\epsilon, L)$  for a sequence of linear sizes  $L$ , as shown in Fig. 4.

For each curve we determine  $\bar{\epsilon}(L)$  by

$$\left. \frac{d\sigma_{xy}(\epsilon, L)}{d\epsilon} \right|_{\epsilon=\bar{\epsilon}} = 0 \quad , \quad (136)$$

which is marked by black star in Fig. 4. These values fit the function  $\bar{\epsilon} \simeq 7(L_x)^{-1}$ . This scaling is consistent with level spacings of one dimensional extended states.

The DC conductivity is estimated by graphically extrapolating the sequence,

$$\sigma_{xy}^{\text{dc}} = \lim_{L \rightarrow \infty} \sigma_{xy}(\bar{\epsilon}(L), L) \quad . \quad (137)$$

In the inset of Figure 4, we extrapolate the Hall conductivities at various values of disorder strength  $w$  to their their respective DC limits.

The DPP formula calculation [63] has found  $\sigma_{xy}^{\text{dc}} \sim Bw^{-4}$ , as depicted in Fig. 5. These results are consistent with DB and BE theories (6,13) which predict that  $\sigma_{xy} \propto \omega_c \tau^2$  in the weak magnetic field regime  $\omega_c \tau \ll 1$ . The  $w^{-4}$  scaling is consistent with Fermi's golden rule for the disorder-driven scattering rate, Eq. (24), i.e.  $\tau^{-1} \propto w^2$ .

## 20. Physical consequences of DPP formulas

The first implication of Eqs. (104) is that the Hall conductivities are *on-shell* expressions which is in apparent contrast to the original Kubo formula (94). Furthermore, at low temperatures, the conductivity is dominated by the low energy excitations  $|E_n - E_0| \leq O(T)$ . Conceptual conclusions from the DPP formulas are:

1. A OBC system exhibiting a non-zero Hall-type conductivity possesses quasi-degenerate (gapless) manifolds of eigenstates which are created by the presence of the magnetic field.
2. At low temperatures, since the DPP's involve low energy eigenstates, it is easy to see that  $\alpha_{xy}^{\text{dc}}$  and  $\kappa_{xy}^{\text{dc}}$  vanish as  $T \rightarrow 0$ . It is also simple to verify for phonons and spin-wave models, that the anomalous (i.e.  $a^\dagger a^\dagger, aa$ ) terms are in the current operators.
3. These manifolds are subjected to the *non commutative geometry* generated by the DPP's. That is to say, since

$$\langle [\tilde{P}^\alpha, \tilde{P}^\beta] \rangle \propto i\sigma_{\alpha\beta}^{\text{dc}} . \quad (138)$$

then  $\frac{1}{\sigma_{\alpha\beta}^{\text{dc}}} \tilde{P}^\beta$  acts as a conjugate momentum to  $\tilde{P}^\alpha$ . The DPP's are therefore similar in spirit to the non-commuting guiding center coordinates which act within a quasi-degenerate Landau level in the strong magnetic field limit.

4. In quantum Hall and topological insulator phases, the Hall-current carrying states are supported on the OBC sample edges. For compressible metallic phases, the Hall current is carried on chiral extended states which percolate through the bulk. An explicit description of these states has been used by Chalker and Coddington model [64] to describe the quantum-percolation transition between Hall plateaux.
5. Finally, DPP formula for  $\kappa_{xy}$  proves that thermal Hall currents in insulators [65, 66, 67] are carried by extended chiral modes.

*Numerical advantages.*— The elimination of the higher eigenstates in the DPP formulas at low temperatures allows us to replace  $H(B)$  by its effective Hamiltonian  $H^{\text{eff}}(B)$  renormalized onto the lower energy Hilbert space.  $H^{\text{eff}}(B)$  may be computationally easier to work with than  $H$ .

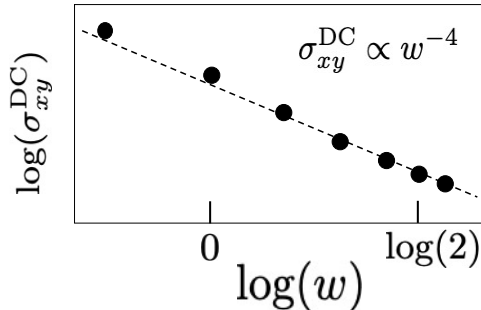


Figure 5: DC extrapolated Hall conductivity for weak magnetic field  $B = 0.03$  and moderate disorder strength  $w$ , at Fermi energy  $\epsilon_F = -1$ . The Hall conductivity scales as  $w^{-4}$  as expected by Drude's theory  $\sigma_{xy} \propto \omega_c \tau^2$ .

## Part V

# Continued fractions of longitudinal conductivities

### 21. Moments expansion

Real longitudinal conductivities (in the  $x$  direction) are given by the real part of Eq. (91),

$$L_{ii}^{xx}(\omega) = \frac{1}{\mathcal{V}} \text{Im} \left( J_i^x \left| \left( \frac{1}{\mathcal{L} - \omega - i\varepsilon} \right) \right| J_i^x \right) = \frac{\pi}{\mathcal{V}} (J^x | \delta_\varepsilon(\mathcal{L} - \omega) | J^x) \quad , \quad i = 1, 2, 3 \quad . \quad (139)$$

where  $\delta_\varepsilon$  is a broadened Dirac  $\delta$ -function of width  $\varepsilon > \mathcal{V}^\dagger$ . Henceforth we suppress  $\varepsilon, \mathbf{q}, \mathcal{V}$  dependence, keeping in mind the eventual correct DC order of limits of Eq. (57). For the moments expansion we define a symmetrized mixed electric+thermal current as

$$J_3^x = (J_1^x + J_2^x)/2 \quad . \quad (140)$$

Thus, the thermoelectric conductivity can be written as a sum of auto-correlation functions,

$$\alpha_{xx}(\omega) = \frac{2}{T} L_{33}^{xx}(\omega) - \frac{1}{2} \sigma_{xx}(\omega) - \frac{1}{2} \kappa_{xx}(\mathbf{q}, \omega) \quad . \quad (141)$$

Henceforth we discuss  $L_{ii}^{xx}(\omega)$  and suppress the currents' label  $i$ .

The moment of order  $2k$  of  $L$  is

$$\begin{aligned} \mu_{2k} &= \int_{-\infty}^{\infty} \frac{d\omega}{\pi} L^{xx}(\omega) \omega^{2k} \\ &= \frac{1}{\mathcal{V}} \int_{-\infty}^{\infty} d\omega (J^x | \delta(\mathcal{L} - \omega) \mathcal{L}^{2k} | J^x) \\ &= \frac{1}{\mathcal{V}} (J^x | \mathcal{L}^{2k} | J^x) \quad . \end{aligned} \quad (142)$$

The  $k = 0$  moment is the CSR,

$$\mu_0 = \frac{1}{\mathcal{V}} (J^x | J^x) = \frac{1}{\mathcal{V}} \text{ImTr}(\rho [P^x, J^x]) \equiv \chi_{\text{csr}} \quad . \quad (143)$$

which uses Eq. (31) to express the susceptibility as a thermodynamic expectation value. All odd moments vanish by antisymmetry of  $mn \rightarrow nm$ ,

$$(J^x | \mathcal{L}^{2k+1} | J^x) = \sum_{mn} W_{mn} (E_m - E_n)^{2k+1} A_{nm}^* A_{nm} = 0 \quad . \quad (144)$$

Moments are thermodynamic expectation values of time-independent operators,

$$\begin{aligned} \mu_{2k} &= \frac{1}{\mathcal{V}} \left( J^x \left| \overbrace{[H_0, [H_0, \dots [H_0, J^x]] \dots]}^{2k} \right. \right) \\ &= \frac{1}{\mathcal{V}} \text{ImTr} \left( \rho [P^x, \overbrace{[H_0, [H_0, \dots [H_0, J^x]] \dots}]^{2k-1} \right) \quad , \end{aligned} \quad (145)$$

where we used Eq. (86) and  $P^x$  is the  $x$ -polarization corresponding to  $J^x$  by Eq. (31).



Moments are coefficients of the short time Taylor series of the real-time conductivity,

$$\begin{aligned} L^{xx}(t) &= \frac{1}{\pi} \int_{-\infty}^{\infty} d\omega L^{xx}(\omega) e^{i\omega t} = \frac{1}{\mathcal{V}} (J^x | e^{i\mathcal{L}t} | J^x) \\ &= \sum_{k=0, \infty} \frac{(-1)^k \mu_{2k}}{(2k)!} t^{2k} . \end{aligned} \quad (146)$$

Unfortunately, a finite set of moments cannot, in general, determine the long time behavior of Eq. (146), and the low frequency behavior of Eq. (139).

The following constraints can be very helpful in guiding us to a viable extrapolation scheme to high orders.

1. Since  $\delta_\varepsilon(\mathcal{L} - \omega)$  is a non-negative hermitian hyperoperator,  $L^{xx}(\omega) \geq 0$  is a non-negative spectral function.
2.  $L^{xx}(\omega) = L^{xx}(-\omega)$ , which therefore permits a finite DC conductivity at  $\omega = 0$ .
3. All the moments  $\mu_{2k}$  are squares of norms  $\|\mathcal{L}^k A\|^2$ , and therefore non negative.
4. By thermodynamic arguments, the real-time conductivities of Eq. (146) should be continuous and differentiable for  $t \in (-\infty, \infty)$ . Also, they are expected to decay (relax) at long times. This ensures the analyticity of  $L^{xx}(z)$  in the upper half plane  $\text{Im}(z) > 0$ .<sup>4</sup> Thus, by (146), the asymptotic growth of the high order moments is bounded by,

$$\lim_{k \rightarrow \infty} \frac{\mu_{2k}}{(2k)!} < \infty . \quad (147)$$

### 21.1. Krylov bases

An orthonormal Krylov basis of hyperstates can be constructed from the current operator. We start with the normalized root (zeroth order) state,

$$|0\rangle \equiv \frac{J}{\sqrt{\langle J|J \rangle}} . \quad (148)$$

( $|\bullet\rangle$ ) denotes normalized hyperstates, in contrast to non normalized hyperstates such as  $|\bullet\rangle$ .)

Higher order Krylov hyperstates are inductively generated by the equations

$$|n+1\rangle = \frac{1}{N_{n+1}} (\mathcal{L}|n\rangle - \Delta_n |n-1\rangle) , \quad N_{n+1} \equiv (\langle n|\mathcal{L}^2|n\rangle - \Delta_n^2)^{\frac{1}{2}} , \quad n = 1, 2, \dots \infty \quad (149)$$

where  $\Delta_n$  is the *recurrent* of order  $n$ , which is equal to the matrix elements of the Liouvillian,

$$\Delta_n = \langle n|\mathcal{L}|n-1\rangle = \langle n-1|\mathcal{L}|n\rangle . \quad (150)$$

In order to evaluate  $\Delta_n$  the following statements are verified:

1. The Liouvillian expectation values vanish in the Krylov basis. By construction of Eq. (149), even (odd) order Krylov hyperstates involve states with even (odd) powers  $\mathcal{L}^n|J\rangle$ . Hence we can expand any Krylov hyperstate as

$$|n\rangle = \sum_{k=0}^{\text{Int}(n/2)} a_{n-2k} \mathcal{L}^{n-2k} |0\rangle . \quad (151)$$

The expectation values of  $\mathcal{L}$  in Krylov hyperstates are,

$$\begin{aligned} \langle n|\mathcal{L}|n\rangle &= \sum_{k,k'=0}^{\text{Int}(n/2)} a_{n-2k} a_{n-2k'} \langle 0|\mathcal{L}^{n-2k} \mathcal{L} \mathcal{L}^{n-2k'} |0\rangle \\ &= \sum_{k,k'=0,n} a_k b_{k'} \langle 0|\mathcal{L}^{2(n-k-k')+1} |0\rangle = 0 , \end{aligned} \quad (152)$$

which follows from Eq. (144).

<sup>4</sup>The only notable exception is in a superconductor, where persistent currents do not decay. For superconductors, the zero frequency conductivity is excluded from  $L^{xx}(\omega)$ .

2. The Krylov basis is orthonormal,

$$\langle m|n \rangle = \langle n|m \rangle = \delta_{nm} \quad , \quad n, m = 0, 1, 2, \dots \infty \quad (153)$$

which is proven by induction using Eq. (149) starting from  $n, m = 0$ .

3. The Liouvillian representation in the Krylov basis is,

$$L_{nm} = \langle n|\mathcal{L}|m \rangle = \delta_{m,n-1}\Delta_n + \delta_{n,m-1}\Delta_{n+1} \quad , \quad (154)$$

$$= \begin{pmatrix} 0 & \Delta_1 & 0 & 0 & 0 & \dots \\ \Delta_1 & 0 & \Delta_2 & 0 & 0 & \dots \\ 0 & \Delta_2 & 0 & \Delta_3 & 0 & \dots \\ 0 & 0 & \Delta_3 & 0 & \Delta_4 & \dots \\ 0 & 0 & 0 & \Delta_4 & 0 & \dots \\ 0 & \vdots & \vdots & \vdots & \vdots & \dots \end{pmatrix}_{nm} \quad n, m = 0, 1, 2, \dots \infty \quad . \quad (155)$$

The matrix  $L_{nm}$  can be regarded as a tight binding hopping Hamiltonian on a half chain, with hopping parameters  $\Delta_n$ .

4. The phases of  $|n\rangle$  can be chosen such that we can gauge all the recurrences  $\Delta_n$  to be real and positive.

$G_{nm}(z)$  is the ‘‘Liouvillian Green function’’,

$$G_{nm}(z) \equiv \langle n|(z - \mathcal{L})^{-1}|m \rangle \quad . \quad (156)$$

Since  $L$  is symmetric, so is  $G_{nm}(z)$ , which is in general complex. On the real axis  $z \rightarrow \omega + i0^+$ ,  $-\text{Im}G_{nm}(\omega + i\epsilon) = -G''_{nm}(\omega)$  is a *spectral function*. It is non-negative and symmetric in  $\omega \rightarrow -\omega$ . The real part of the complex function  $G_{nm}(z)$  can be obtained from the spectral function by the Kramers-Kronig (KK) transform,

$$G'_{nm}(\omega) = \frac{1}{\pi} \int_{-\infty}^{\infty} d\omega' \frac{G''_{nm}(\omega')}{\omega - \omega'} \quad . \quad (157)$$

$G''_{nm}(\omega) = G''_{nm}(-\omega)$ , and by Eq. (157),  $G'_{nm}(0) = 0$ . Non diagonal Green functions  $G_{nm}(0 + i\epsilon)$  can be obtained from the inversion equation  $(GL)_{nm} = \delta_{nm}$ ,

$$\sum_{m \geq 0} G_{nm}(0^+) L_{mn'} = \delta_{nn'} \quad . \quad (158)$$

For example,

$$\begin{aligned} \sum_m G_{0m}(0^+) L_{m1} &= G_{00}\Delta_1 + G_{02}\Delta_2 = 0, \Rightarrow G_{02}(0^+) = iG''_{00} \left( -\frac{\Delta_1}{\Delta_2} \right) \quad , \\ \sum_m G_{0m}(0^+) L_{m4} &= G_{02}(0^+)\Delta_3 + G_{04}(0^+)\Delta_4 = 0 + \Rightarrow G_{04}(0^+) = iG''_{00} \left( -\frac{\Delta_1}{\Delta_2} \right) \left( -\frac{\Delta_3}{\Delta_4} \right) \quad , \\ &\vdots \quad \quad \quad \vdots \quad \quad \quad \end{aligned} \quad (159)$$

and generally,

$$\begin{aligned} G_{0,2k}(0^+) &= G_{2k,0}(0^+) = iG''_{00} R_k \quad , \quad k = 0, 1, 2, \dots \\ R_k &= \prod_{k'=1}^k \left( -\frac{\Delta_{2k'-1}}{\Delta_{2k'}} \right) \quad . \end{aligned} \quad (160)$$

Another important relation is,

$$G_{1,n}(0^+) = \frac{\delta_{n,0}}{\Delta_1} \quad , \quad (161)$$

which is purely real. As a consequence, the matrix elements of the imaginary inverse Liouvillian do not connect to the first Krylov state:

$$\left\langle n \left| \left( \frac{1}{\mathcal{L}} \right)'' \right| 1 \right\rangle = \left\langle 1 \left| \left( \frac{1}{\mathcal{L}} \right)'' \right| n \right\rangle = 0 \quad . \quad (162)$$

This result will prove to be useful in Section 24.

### 21.2. The continued fraction representation

Since  $z - L$  is a tridiagonal matrix, an iterative inversion can be used to invert  $G_{00}$  in Eq. (156), and express it as

$$\begin{aligned} G_{00}(z) &= \frac{1}{z - \Delta_1^2 G_{11}^>(z)} \quad , \\ G_{11}^>(z) &= \frac{1}{z - \Delta_2^2 G_{22}^>(z)} \quad , \\ &\vdots = \quad \vdots \quad , \end{aligned} \quad (163)$$

where  $G_{nn}^>$  is the *termination Green function* on the half-chain with the sites  $m \geq n$ . The sequence of equations (163) comprises an infinite continued fraction (CF),

$$G_{00}(z) \simeq \frac{1}{z - \frac{\Delta_1^2}{z - \frac{\Delta_2^2}{z - \frac{\Delta_3^2}{\ddots}}}} \quad . \quad (164)$$

## 22. From moments to recurrences

The first question that comes to mind is: How do we obtain the recurrences  $\Delta_1, \Delta_2 \dots \Delta_k$ , from a given sequence of moments  $\mu_0, \mu_2 \dots \mu_{2k}$  ?

Eq. (142) and (155) generate a sequence of identities:

$$\begin{aligned} \mu_{2k} &= \mu_0 \langle 0 | (L[\Delta])^{2k} | 0 \rangle \quad . \\ \frac{\mu_2}{\mu_0} &= \Delta_1^2 \quad , \\ \frac{\mu_4}{\mu_0} &= \Delta_1^4 + \Delta_1^2 \Delta_2^2 \quad , \\ \frac{\mu_6}{\mu_0} &= \Delta_1^6 + 2\Delta_1^4 \Delta_2^2 + \Delta_1^2 \Delta_2^4 + \Delta_1^2 \Delta_2^2 \Delta_3^2 \quad , \\ \frac{\mu_8}{\mu_0} &= \Delta_1^8 + 3\Delta_1^6 \Delta_2^2 + 3\Delta_1^4 \Delta_2^4 + \Delta_1^2 \Delta_2^6 + 2\Delta_1^4 \Delta_2^2 \Delta_3^2 + 2\Delta_1^2 \Delta_2^4 \Delta_3^2 + \Delta_1^2 \Delta_2^2 \Delta_3^4 + \Delta_1^2 \Delta_2^2 \Delta_3^2 \Delta_4^2 \quad , \\ &\vdots \quad \quad \quad \vdots \end{aligned} \quad (165)$$

Importantly,  $\mu_{2k}/\mu_0$  depend only on the recurrents  $\Delta_1, \Delta_2 \dots \Delta_k$ . This allows us to solve for the recurrents iteratively, starting at  $k = 1$ . As a result we obtain the algebraic equations,

$$\begin{aligned}
\Delta_1^2 &= \bar{\mu}_2 \quad , \\
\Delta_2^2 &= \frac{\bar{\mu}_4}{\bar{\mu}_2} - \bar{\mu}_2 \quad , \\
\Delta_3^2 &= \frac{\bar{\mu}_4^2 - \bar{\mu}_2 \bar{\mu}_6}{\bar{\mu}_2^3 - \bar{\mu}_2 \bar{\mu}_4} \quad , \\
\Delta_4^2 &= \bar{\mu}_2 \frac{(\bar{\mu}_4^3 + \bar{\mu}_6^2 + \bar{\mu}_2^2 \bar{\mu}_8 - \bar{\mu}_4(2\bar{\mu}_2 \bar{\mu}_6 + \bar{\mu}_8))}{(\bar{\mu}_2^2 - \bar{\mu}_4)(\bar{\mu}_2 \bar{\mu}_6 - \bar{\mu}_4^2)} \quad , \\
&\vdots = \vdots
\end{aligned} \tag{166}$$

In general  $\mu_{2k}$  increase very rapidly (of order  $(2k)!$ ) with  $k$ , while  $\Delta_k$  are much smaller numbers which increase at a much slower rate. The presence of subtractions in Eq. (166) imply that small relative errors in  $\mu_{2k}$  may result in large relative errors in  $\Delta_{k \geq k'}$ <sup>5</sup>

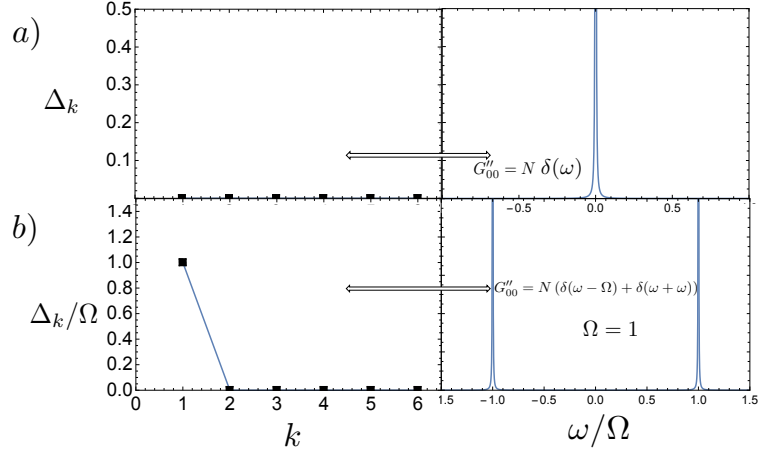


Figure 6: Single mode correlations.

### 22.1. Single Mode Spectra

Let us start with a single sharp mode at zero frequency as shown in Fig. 6(a),

$$-G''_{00}(\omega) = \pi \delta(\omega) \quad . \tag{167}$$

All the recurrents vanish identically, since  $[H, A] = 0$ .

$$\Delta_k^2 = 0 \quad , \quad \forall n \quad . \tag{168}$$

A single mode at finite frequency  $|\Omega| > 0$  is shown in Fig. 6(b). It is described by

$$-G''_{00}(\omega) = \pi (\delta(\omega - \Omega) + \delta(\omega + \Omega)) / 2 \quad . \tag{169}$$

The only non-zero recurrent is  $\Delta_1 = \Omega$ . Physically this occurs when  $J^x$  is an eigen-operator of the Liouvillian

$$\mathcal{L}J^x = \Omega J^x \quad . \tag{170}$$

<sup>5</sup>We thank Snir Gazit for alerting us to this numerical challenge.

and therefore applying  $J^x$  to the Hamiltonian's ground state  $|\Psi_0\rangle$  creates an eigenstate  $J^x|\Psi_0\rangle$  with excitation energy  $\Omega$ .

An approximation which *assumes* a spectral function which approximately is described by a  $\delta$ -function, is the single mode approximation. This approximation was used by Feynman [68] to describe the roton minima in the spectrum of superfluid helium [68], by Girvin, Macdonald and Platzman [69] to describe the magneto-roton excitation of the Fractional Quantum Hall phase, in Refs. [70, 71] to approximate the Haldane gap in a spin-one chain model.

### 23. From recurrences to conductivities

The longitudinal conductivity of Eq. (139) is determined by the zeroth order spectral function,

$$\begin{aligned} L^{xx}(\omega) &= -\mu_0 \lim_{z \rightarrow \omega + i0^+} G''_{00}(z) \\ &= \pi\mu_0 \langle 0 | \delta(\mathcal{L} - \omega) | 0 \rangle \quad , \end{aligned} \quad (171)$$

where  $L[\Delta_n]$  is the infinite tridiagonal matrix of Eq. (155), and  $G_{00}(z)$  is defined as a CF in Eq. (164).

In practice, the calculation of  $\Delta_n$  is limited to a finite sequence. However, truncating the CF at any finite order does not lead to a continuous function, but to a sequence of  $\delta$ -functions. In effect, determining  $G''_{00}$  amounts to inversion of the moments series, which is in general an unsolved problem.

CF however allow us to design extrapolation schemes which may be suitable for certain class of physical problems, which provide additional information about the desired  $G''_{00}$ . For example,  $-G''_{00}(\omega)$  is a positive and symmetric function, whose all its recurrences are finite, non-negative numbers.

Since extrapolation is a tricky art, it is useful to first learn about rigorous results relating high frequency asymptotics of  $G''_{00}$  and high order recurrences.

#### 23.1. Freud's high order asymptotics

For a large class of smooth spectral function  $-G''_{00}(\omega)$  with support on the whole frequency axis <sup>6</sup>, Freud [72] has conjectured an asymptotic relation between the high frequency asymptotic fall-off of the spectral function, and the asymptotic behavior of the high order recurrences  $\Delta_k$  as  $k \rightarrow \infty$ .

This conjecture was proven by Lubinsky, Mhaskar and Saff (LMS) [73], for spectral functions described by

$$-G''_{00}(\omega) = \exp(-Q(\omega)) \quad . \quad (172)$$

The fall-off exponent  $Q$  is assumed to satisfy the following conditions:

1.  $Q(\omega) = Q(-\omega)$ .
2.  $Q'(\omega)$  exists for  $\omega \neq 0$ , and  $\omega Q'(\omega)$  is bounded near the origin as  $\omega \rightarrow 0^+$ . Furthermore,  $Q''$  exists for large enough  $\omega$ .
3. For finite values of  $C > 0, \alpha > 0$  at large enough  $\omega$ ,

$$\begin{aligned} Q'(\omega) &> 0 \quad , \\ \omega^2 |Q''(\omega)| / Q'(\omega) &\leq C \quad , \\ \lim_{\omega \rightarrow \infty} (1 + \omega Q''(\omega) / Q'(\omega)) &= \alpha > 0 \quad . \end{aligned} \quad (173)$$

LMS proved that the corresponding recurrences  $\Delta_n$  for Eq. (172) exhibit the asymptotic behavior,

$$\begin{aligned} \lim_{k \rightarrow \infty} \Delta_k &\sim a_\alpha k^{\frac{1}{\alpha}} \\ a_\alpha &= \frac{1}{2} \left( \frac{\sqrt{\pi} \Gamma\left(\frac{\alpha}{2}\right)}{\Gamma\left(\frac{\alpha+1}{2}\right)} \right)^{\frac{1}{\alpha}} \quad . \end{aligned} \quad (174)$$

<sup>6</sup>We thank Ari Turner for explaining to us the mathematical literature reviewed in this section

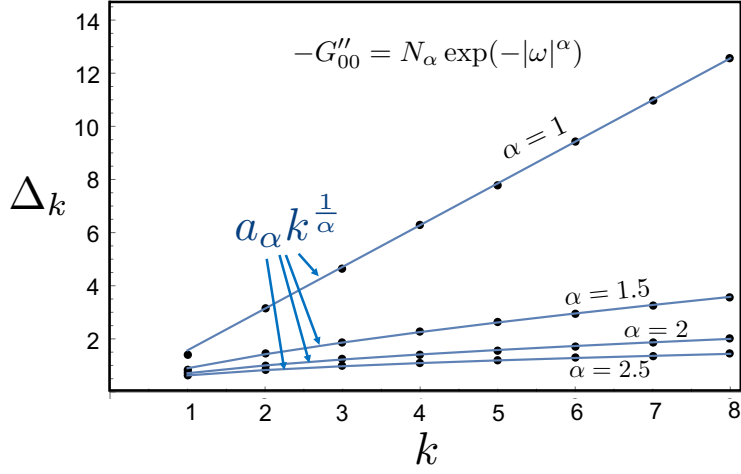


Figure 7: The recurrences of the pure stretched exponentials (black circles), and Freud's asymptotic expression (blue lines) as governed by Eq. (174). The differences between the values are plotted in Fig. 8.

Interestingly, for pure stretched exponential

$$Q(\omega, \alpha) = |\omega|^\alpha, \quad (175)$$

as shown in Figs. 7 and 8, the exact low order recurrences are close but slightly different from the analytic asymptotic values of Eq. (174), except for the pure Gaussian  $\alpha = 2$ , for which Eq. (174) is exact.

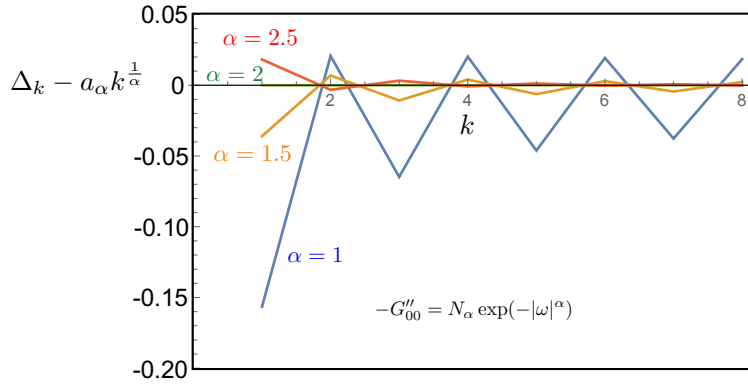


Figure 8: The difference between the true recurrences of the stretched exponential and asymptotic values of Eq. (174), which decrease with the order  $k$ . Note that the asymptotic values are exact only for the Gaussian  $\alpha = 2$ .

In general, since the moments and recurrences are non-negative, by Eqs. (165), the moments grow at least as fast as

$$\mu_{2k} \geq (k!)^{2/\alpha}. \quad (176)$$

Due to assumed continuity of  $G_{00}(t)$  on the real-time axis, by Eq. (147), the moments cannot grow faster than  $\mu_{2n} \leq (2n)!$ .

This implies that for continuous and bounded response functions, the asymptotic power  $\alpha$  of  $Q(\omega)$  is limited to

$$1 \leq \alpha \leq \infty. \quad (177)$$

### 23.2. Termination functions

Assume that we have calculated a finite set of recurrents

$$\{\Delta\}_1^{k_{\max}} = (\Delta_1, \dots, \Delta_{k_{\max}}) \quad . \quad (178)$$

This finite set is not sufficient to describe the continuous function  $G''_{00}(\omega)$ . Extrapolation of recurrents is tantamount to finding an accurate termination function  $\bar{G}_{k_{\max}}^>(z)$  such that,

$$G_{00}(z) \simeq \frac{1}{z - \frac{\Delta_1^2}{z - \frac{\Delta_2^2}{z - \frac{\Delta_{k_{\max}-1}^2}{z - \Delta_{k_{\max}}^2 \bar{G}_{k_{\max}}^>(z; [\alpha])}}} \quad . \quad (179)$$

$\bar{G}_{k_{\max}}^>(z)$  is the normalized CF which contains only the higher order recurrents  $\bar{\Delta}_k, k \geq k_{\max} + 1$ ,

$$\bar{G}_{k_{\max}}^>(z) = \frac{1}{z - \frac{\bar{\Delta}_{k_{\max}+1}^2}{z - \frac{\bar{\Delta}_{k_{\max}+2}^2}{z - \frac{\bar{\Delta}_{k_{\max}+3}^2}{\vdots}}}} \quad . \quad (180)$$

If  $\{\bar{\Delta}\}_k, k = 0, \dots, \infty$  are the known recurrents of a complex variational spectral function  $\bar{G}_{00}(z)$ . The variational recurrents are used to produce the termination function by iteratively inverting the CF of the complex function  $\bar{G}_{00}(z)$ ,

$$\begin{aligned} \bar{G}_{11}^>(z) &= \frac{1}{\bar{\Delta}_1^2} \left( z - \frac{1}{\bar{G}_{00}(z)} \right) \\ &\vdots = \vdots \\ \bar{G}_{k_{\max}}^>(z) &= \frac{1}{\bar{\Delta}_{k_{\max}-1}^2} \left( z - \frac{1}{\bar{G}_{k_{\max}-1}^>(z)} \right) \quad . \end{aligned} \quad (181)$$

We emphasize that or the inversion, both real and imaginary parts of  $\bar{G}_{00}(\omega + i\varepsilon)$  are required, where the real part is obtained by a Kramers-Kronig transformation, Eq. (157), of the imaginary part.

Termination functions can be used to study the effects of low order recurrents on the frequency dependence of  $G''_{00}(\omega)$ .

### 23.3. Low frequency behavior

By LMS theorem, the high order recurrents can determine high frequency decay of a large class of spectral functions. Conversely, low frequency behavior can be deduced in certain cases from the low order recurrents. We first demonstrate the low frequency effects of varying the first recurrent, and then we show the low frequency effects of alternating even-odd deviations of recurrents from their high order asymptotic behavior.

The recurrents of the semicircle spectral function function,

$$-G''_{00}(\omega) = \frac{1}{2\Delta^2} \sqrt{2\Delta^2 - \omega^2} \Theta(2\Delta^2 - \omega^2) \quad (182)$$

are,

$$\bar{\Delta}_k^{\text{sc}} = \Delta \quad , \quad k = 1, 2, \infty \quad . \quad (183)$$

The recurrences of a Gaussian spectral function are,

$$-G''_{00}(\omega) = \sqrt{\pi}e^{-\omega^2} \quad (184)$$

are,

$$\bar{\Delta}_k^{\text{Gauss}} = \sqrt{\frac{k}{2}} \quad , \quad k = 1, 2, \infty \quad . \quad (185)$$

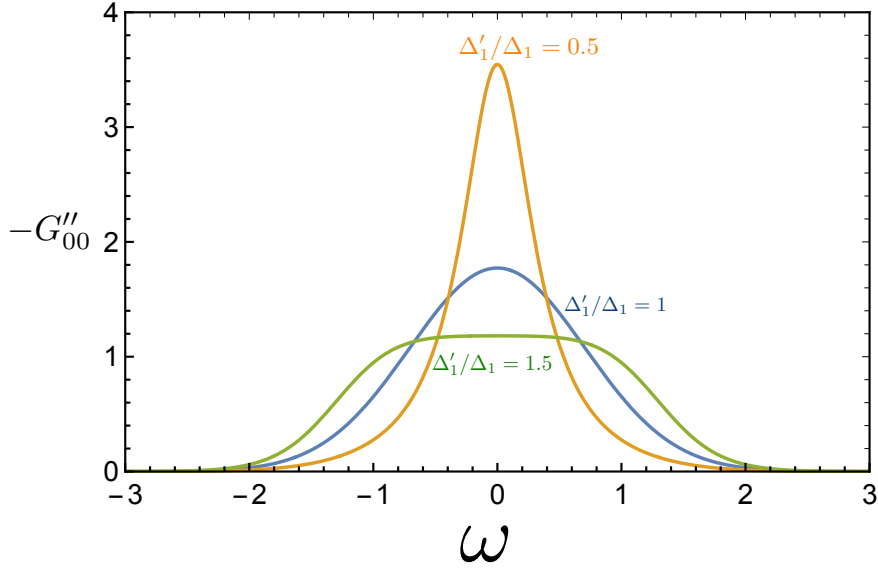


Figure 9: Changing just the first recurrent  $\Delta'_1$  in the Gaussian spectral function.

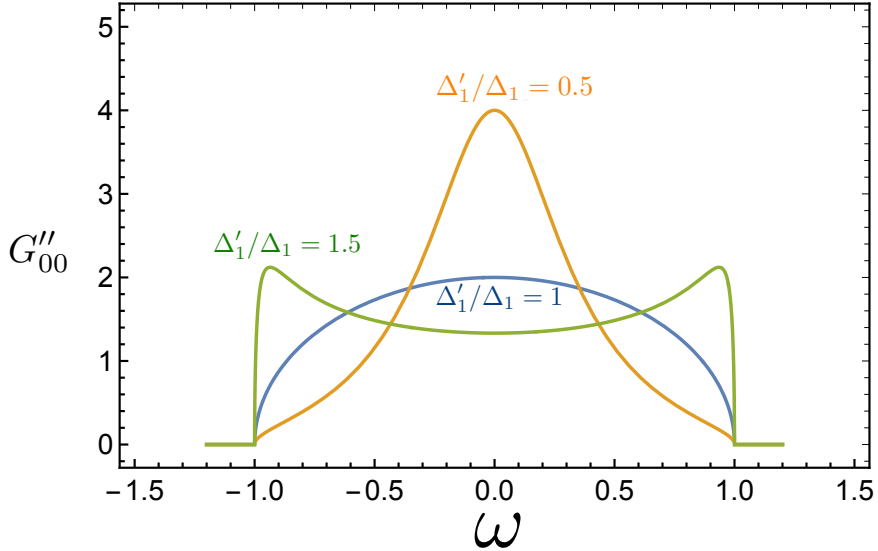


Figure 10: Changing just the first recurrent  $\Delta'_1$  in the semicircle spectral function.

As noted by the memory function approach, in the weak scattering limit, the first order recurrent plays an important role in determining the low frequency conductivity.



The first recurrent  $\Delta_1$  dominates the DC conductivity. This is demonstrated by varying  $\Delta'_1$  in Fig. 9, keeping the higher order recurrences the same. For both the Gaussian in Fig. 9, and the semicircle in Fig. 10, the DC limit of the resulting normalized modified functions vary with  $\Delta'_1/\Delta_1$  as

$$\frac{G''_{00}(0)}{\bar{G}''_{00}(0)} = \frac{(\Delta'_1)^2}{\Delta_1^2} . \quad (186)$$

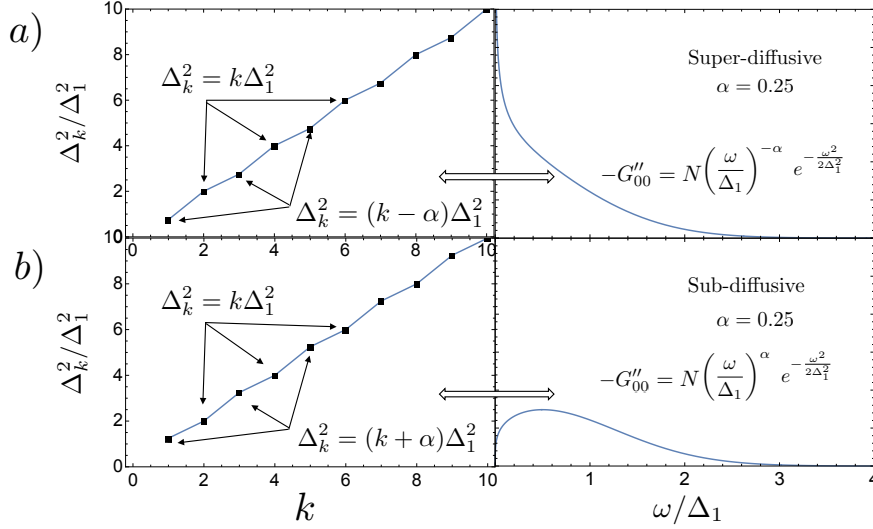


Figure 11: Continued fraction recurrences of PG functions. High frequency Gaussian tail is reflected in the average linear increase of  $\Delta_k^2$ . Low frequency divergence (vanishing) in the super-diffusive (sub-diffusive) functions is signalled in the oscillation of even and odd recurrences starting at the lowest orders.

Stronger modifications of the low frequency behavior is produced by even-odd deviations of the recurrences from the asymptotic form. This is demonstrated by the power-law times Gaussian function (PG), as discussed in detail in Ref. [22],

$$-G''_{\text{PG}}(\omega) = \frac{\sqrt{2\pi}}{\Omega \Gamma\left(\frac{\beta+1}{2}\right)} \left| \frac{\omega}{\Omega} \right|^\beta \exp\left(-\frac{\omega^2}{\Omega^2}\right) . \quad (187)$$

The recurrences of the PG have been evaluated analytically,

$$\left(\Delta_k^{\text{PG}}\right)^2 = \frac{1}{2}(k + \beta) \delta_{k,\text{odd}} + \frac{1}{2}k \delta_{k,\text{even}} \quad (188)$$

and are plotted versus their low order recurrences in Fig. (11). The zero frequency conductivity vanishes or diverges depending on the sign of  $\beta$ . While the relative deviations from the asymptotic  $k^{1/2}$  behavior at large  $k$  decreases, the effects of the low order recurrences are dramatic at low frequencies. A similar effect is seen numerically for power law functions times stretched exponentials at  $\alpha \neq 2$  [22].

#### 23.4. Addition of spectral functions with different frequency scales

The low frequency regime of the response function affects the behavior of the recurrences in a more complicated way than the high frequency asymptotics. For example we consider a sum of two semicircles with different energy scales  $\Omega_2 \ll \Omega_1$

$$G''_{2\text{sc}}(\omega) = G''_{\text{sc}}(\omega; \Omega_1) \pm a_2 G''_{\text{sc}}(\omega; \Omega_2) , \quad (189)$$

where  $G''_{\text{sc}}(\omega; \Omega)$  is given by Eq. (182).  $a_2$  may be positive (for enhanced DC conductivity), or negative, for suppressed DC conductivity. The moments are additive,

$$\mu_{2k}^{2\text{sc}} = \mu_{2k}^{\text{sc}1} \pm a_2 \mu_{2k}^{\text{sc}1} . \quad (190)$$

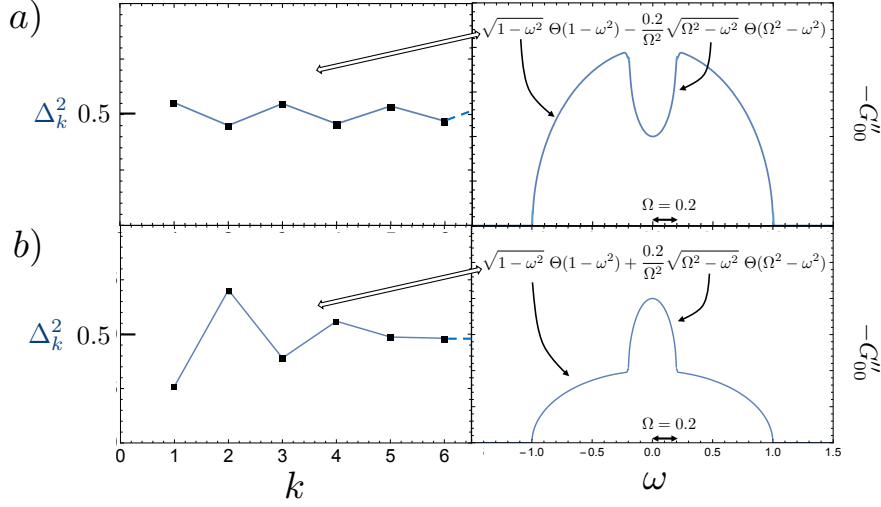


Figure 12: General example of low frequency effects. Top Frames: low frequency suppression of a semicircle function, corresponds to odd order recurrences larger than even orders. Bottom frame: low frequency enhancement corresponds to even order recurrences higher than odd orders. This is qualitatively similar to the effects seen in the recurrences of PGauss functions in Fig. 11

(where we must use  $a_2 < 1$ , since all moments must be non-negative). After hashing the algebraic relations (166), the combined recurrences are highly entangled. The effects of summing two spectral functions are shown in Fig. 12. The addition of two spectral functions results in even-odd oscillations of the recurrences which persist to high orders, although its signature is already observed at low orders.

### 23.5. Variational Extrapolation of Recurrences

Since nested commutators of the Hamiltonian with the current create a factorial growth of number of operators, the computational cost of high order moments and recurrences in many cases increases faster than exponentially.

Here we describe the Variational Extrapolation of Recurrences as a possible scheme which allows for a numerical test of its convergence.

Having computed  $\Delta_1, \dots, \Delta_{n_{\max}}$ , may lead to a reasonable guess for the possible asymptotic behavior at large and low frequencies. We choose a family of analytic variational spectral functions  $\bar{G}''_{00}(\omega; \{\alpha\})$ , which can be parametrized by variational parameters  $\alpha_1, \dots, \alpha_{m_{\text{var}}}$ .

Using Kramers-Kronig relation (157) find the real part of  $\bar{G}_{00}(\omega + i0^+)$ ,

$$\bar{G}'_{00}(\omega; \{\alpha\}) = \frac{1}{\pi} \int_{-\infty}^{\infty} d\omega' \bar{G}''_{00}(\omega'; \{\alpha\}) \quad , \quad (191)$$

and calculate the variational recurrences ( $\bar{\Delta}_1 \dots \bar{\Delta}_{n_{\max}}$ ) from the lowest  $2n_{\max}$  moments of  $\bar{G}''(\omega)$ .

The variational parameters are obtained by minimizing the least squares function with respect to  $\{\alpha\}$ ,

$$\chi^2 = \min_{\{\alpha_1, \dots, \alpha_{m_{\text{var}}}\}} \frac{1}{n_{\max} - n_{\min}} \sum_{n=n_{\min}+1}^{n_{\max}} \left( \frac{\Delta_n - \bar{\Delta}_n(\{\alpha\})}{\Delta_n} \right)^2 \quad . \quad (192)$$

The lower cut-off  $n_{\min} \geq 1$  is chosen to preferentially fit the recurrences of  $\bar{G}_{00}$  to the higher orders of the calculated recurrences. The total number of variational parameters  $m_{\text{var}}$  must be smaller than  $n_{\max} - n_{\min}$  to avoid overfitting.

Inverting Eq. (179) provides  $\bar{G}^>_{n_{\max}, n_{\max}}(z)$  which directly provides the Variational Extrapolation of Recurrences (VER)

approximation for  $G_{00}$  (see Refs. [74, 75])

$$G_{00}^{\text{ver}}(z) \simeq \frac{1}{z - \frac{\Delta_1^2}{z - \frac{\Delta_2^2}{z - \dots \frac{\Delta_{k_{\max}-1}^2}{z - \Delta_{k_{\max}}^2 G_{k_{\max}}^>(z; [\alpha])}}} . \quad (193)$$

The spectral function is given by,

$$\text{Im } G_{00}^{\text{ver}}(\omega + i0^+) \simeq \text{Im} \frac{1}{\omega - \frac{\Delta_1^2}{\omega - \frac{\Delta_2^2}{\omega - \dots \frac{\Delta_{k_{\max}-1}^2}{\omega - \Delta_{k_{\max}}^2 \tilde{G}_{k_{\max}}^>(\omega + i0^+; [\alpha])}}} . \quad (194)$$

Eq. (194) shows that the imaginary part of  $G_{00}$  is due to the complex termination function with  $\text{Im } \tilde{G}_{k_{\max}} \neq 0$ . The quality of the VER can be tested by two criteria: (i) The  $\chi^2$  in (192) should be much less than unity. (ii) Computing some additional recurrences  $\Delta_{k>k_{\max}}$  and comparing them to the extrapolated  $\tilde{\Delta}_k$ .

## Part VI

# Thermodynamic formulas of Hall coefficients

For simplicity, the magnetic field is chosen along the  $z$  axis and  $C_4$  symmetry is assumed in the  $XY$  plane. The Hall-type coefficients are the electric Hall coefficient  $R_H$ , the Nernst Coefficient  $N$ , and the thermal Hall coefficient  $R_{TH}$ :

$$\begin{aligned} R_H &= \frac{1}{(\sigma_{xx}^{dc})^2} \left. \frac{d\sigma_{xy}^{dc}}{dB} \right|_{B=0} , \\ N &= \frac{1}{\sigma_{xx}^{dc}} \left. \frac{d\alpha_{xy}^{dc}}{dB} \right|_{B=0} - R_H \alpha_{xx}^{dc} , \\ R_{TH} &= \frac{1}{(\kappa_{xx}^{dc})^2} \left. \frac{d\kappa_{xy}^{dc}}{dB} \right|_{B=0} . \end{aligned}$$

The coefficients in Eq. (195) exist if we assume that

$$\lim_{B \rightarrow 0} \sigma_{xx} > 0 , \quad \lim_{B \rightarrow 0} \kappa_{xx} > 0 . \quad (195)$$

That is to say, the expressions apply to gapless dissipative phases, and do not apply to superconductor, insulator, or quantum Hall phases. In addition we also assume no spontaneous magnetization at zero magnetic field, which implies no anomalous Hall effect.

Straightforward Kubo formula calculations of Eq. (195) demand determination of both longitudinal and Hall conductivities. The summation formulas [52, 76] derived below, replaces the difficulties of DC Kubo formulas by calculations of thermodynamic coefficients.

### 24. Magnetic Field Expansion of Hall-type Conductivity

The derivative with respect to the magnetic field is very difficult to perform using the Lehmann representation, which requires taking derivatives of current operators, wavefunctions, and eigenenergies.

It is therefore much more convenient to differentiate by parts the DC Hall conductivities as written in Eq. (99),

$$\begin{aligned} \left( \frac{dL_{ij}^{xy}(\varepsilon, V)}{dB} \right)_{B=0} &= \frac{1}{\mathcal{V}} \text{Im} \frac{d}{dB} \text{Tr} \rho \left[ P_i^x - (\tilde{P}_i^x)_\varepsilon, P_j^y - (\tilde{P}_j^y)_\varepsilon \right] \\ &= \cancel{\Xi_{TR}}^0 + \Xi_{\mathcal{L}} . \end{aligned} \quad (196)$$

We assume OBC in order to define uniform polarizations. OBC are also required to continuously vary the magnetic field  $B$  and avoid Dirac's quantization [77].

$\Xi_{TR}$  vanishes under the trace by even time reversal symmetry of  $H_0, \rho, P_i^x, P_j^y$  at  $B = 0$ , and odd symmetry of  $\frac{d\rho}{dB}, \frac{dP_i^x}{dB}, \frac{dP_j^y}{dB}$ .

$$\begin{aligned} \Xi_{TR} &= \frac{1}{\mathcal{V}} \text{Im} \text{Tr} \frac{d\rho}{dB} \left[ P_i^x - \tilde{P}_i^x, P_j^y - \tilde{P}_j^y \right] + \frac{1}{\mathcal{V}} \text{Im} \text{Tr} \rho \left[ (1 - \Theta_\varepsilon) \frac{dP_i^x}{dB}, (1 - \Theta_\varepsilon) P_j^y \right] \\ &\quad + \frac{1}{\mathcal{V}} \text{Im} \text{Tr} \rho \left[ (1 - \Theta_\varepsilon) P_i^x, (1 - \Theta_\varepsilon) \frac{dP_j^y}{dB} \right] = 0 . \end{aligned} \quad (197)$$

The remaining term  $\Xi_{\mathcal{L}}$  is calculated by differentiating the hyper-projector (97) with respect to  $B$ ,

$$\begin{aligned}\frac{d\Theta_{\varepsilon}(B)}{dB} &= \frac{\varepsilon}{\mathcal{L}^2 + \varepsilon^2} (\mathcal{M}\mathcal{L} + \mathcal{L}\mathcal{M}) \frac{\varepsilon}{\mathcal{L}^2 + \varepsilon^2} \\ &= (-i) \frac{\varepsilon}{\mathcal{L}^2 + \varepsilon^2} \mathcal{M} \frac{\varepsilon}{\mathcal{L}^2 + \varepsilon^2} J_i + \frac{\varepsilon}{\mathcal{L}^2 + \varepsilon^2} \mathcal{L}\mathcal{M} \frac{\varepsilon}{\mathcal{L}^2 + \varepsilon^2} .\end{aligned}\quad (198)$$

The hypermagnetization is defined by

$$\mathcal{M} \equiv -\frac{\partial \mathcal{L}}{\partial B} = [M^z, \bullet] , \quad (199)$$

where  $M^z = -\frac{dH_0}{dB}$ .<sup>7</sup>

Thus we obtain,

$$\begin{aligned}\Xi_{\mathcal{L}} &= \frac{1}{\mathcal{V}} \text{ImTr}\rho \left( \left[ P_i^x - (\tilde{P}_i^x)_{\varepsilon}, -\frac{d\Theta_{\varepsilon}}{dB} P_j^y \right] - \left[ P_j^y - (\tilde{P}_j^y)_{\varepsilon}, -\frac{d\Theta_{\varepsilon}}{dB} P_i^x \right] \right) \\ &= \frac{1}{\mathcal{V}} \text{ImTr}\rho \left( \left[ \left( \frac{1}{\mathcal{L}} \right)'_i J_i^x, \frac{\varepsilon}{\mathcal{L}^2 + \varepsilon^2} \mathcal{M}\mathcal{L} \frac{\varepsilon}{\mathcal{L}^2 + \varepsilon^2} P_j^y + i \frac{\varepsilon}{\mathcal{L}^2 + \varepsilon^2} \mathcal{L}\mathcal{M} \frac{\varepsilon}{\mathcal{L}^2 + \varepsilon^2} P_i^y \right] + (J_i^x \leftrightarrow J_j^y) \right) \\ &= -\frac{1}{\mathcal{V}} \text{Im} \left( J_i^x \left| \left( \frac{1}{\mathcal{L}} \right)''_i \mathcal{M} \left( \frac{1}{\mathcal{L}} \right)''_j \right| J_j^y \right) + \Xi_0(J_i^x, J_j^y) - (J_i^x \leftrightarrow J_j^y) .\end{aligned}\quad (200)$$

In the last row of (200), we applied Eq. (86) to reconstruct the OHS current matrix element. The vanishing of  $\Xi_0$  is proven as follows. Using the hermiticity of  $\mathcal{L}$  (80), we can write:

$$\begin{aligned}\Xi_0 &= \frac{i}{\mathcal{V}} \text{Im} \left( J_i^x \left| \left( \frac{1}{\mathcal{L}} \right)''_i \mathcal{L} \mathcal{M} \left( \frac{1}{\mathcal{L}} \right)''_j \right| P_j^y \right) \\ &= \frac{i}{\mathcal{V}} \text{Im} \left( \mathcal{L} \left( \frac{1}{\mathcal{L}} \right)''_i J_i^x \left| \mathcal{M} \left( \frac{1}{\mathcal{L}} \right)''_j \right| P_j^y \right) .\end{aligned}\quad (201)$$

Next, we will prove that,

$$\left( \frac{1}{\mathcal{L}} \right)''_i \mathcal{L} |J_i^{\alpha}\rangle = 0 + \mathcal{O}(\varepsilon) . \quad (202)$$

The inner product of the hyperstate given by Eq. (202) with any Krylov basis hyperstate  $\langle n; J_i^{\alpha} |$  belonging to the same root current is,

$$\begin{aligned}\langle n; J_i^{\alpha} | \left( \frac{1}{\mathcal{L}} \right)''_i \mathcal{L} |J_i^{\alpha}\rangle &= \sqrt{\chi_{\text{csr}}} \langle n; J_i^{\alpha} | \left( \frac{1}{\mathcal{L}} \right)''_i \mathcal{L} |0; J_i^{\alpha}\rangle \\ &= \sqrt{\chi_{\text{csr}}} \Delta_1 \text{Im} G_{n1} = 0 + \mathcal{O}(\varepsilon) ,\end{aligned}\quad (203)$$

since  $G_{n1}$  is purely real, as proven in Eq. (162).

In contrast to Eq. (202), the surviving terms in (200) do not vanish since,

$$\begin{aligned}\langle n; J_i^{\alpha} | \mathcal{L} \left( \frac{1}{\mathcal{L}} \right)''_i |P_i^{\alpha}\rangle &= \langle n; J_i^{\alpha} | \left( \frac{1}{\mathcal{L}} \right)''_i \mathcal{L} |P_i^{\alpha}\rangle \\ &= -i \sqrt{\chi_{\text{csr}}} \langle n; J_i^{\alpha} | \left( \frac{1}{\mathcal{L}} \right)''_i |1; J_i^{\alpha}\rangle \\ &= -i \sqrt{\chi_{\text{csr}}} \text{Im} G_{n,0} = -i \delta_{n,2k} \chi_{\text{csr}} G''_{00} R_k \neq 0 .\end{aligned}\quad (204)$$

<sup>7</sup>Note: Under TR,  $M^z \rightarrow -M^z$ , and the commutators in the response functions reverse their order  $[A, B] \rightarrow [\text{TR}(B), \text{TR}(A)]$ . Therefore the hypermagnetization  $\mathcal{M}$  is even under TR.

where the last identity uses Eq. (160).

Thus we obtain

$$\left( \frac{dL_{ij}^{xy}(\varepsilon, \mathcal{V})}{dB} \right)_{\mathbf{B}=0} = -\frac{2}{\mathcal{V}} \text{Im} \left( J_i^x \left| \left( \frac{1}{\mathcal{L}} \right)'' \right. \mathcal{M} \left( \frac{1}{\mathcal{L}} \right)'' \right. | J_j^y \rangle + \mathcal{O}(\varepsilon) \quad . \quad (205)$$

It is possible to evaluate Eq. (205) by inserting two Krylov bases resolutions of identity,

$$\sum_{n=0}^{\infty} |n; J_i^\alpha\rangle \langle n; J_i^\alpha| = \mathbb{1}_{i\alpha} \quad , \quad (206)$$

where  $\mathbb{1}_\alpha$  is the projector onto OHS subspace spanned by the hyperstates  $\mathcal{L}^k |J_i^\alpha\rangle$  for  $0 \leq k \leq \infty$ . Using the  $C_4$  symmetry, we obtain

$$\begin{aligned} \left( \frac{dL_{ij}^{xy}(\varepsilon, \mathcal{V})}{dB} \right)_{\mathbf{B}=0} &= -\frac{2\chi_{\text{csr}}}{\mathcal{V}} \text{Im} \sum_{nm} \langle 0; J_i^x | \left( \frac{1}{\mathcal{L}} \right)'' | n; J_i^x \rangle \mathcal{M}_{nm}^{ij} \langle m; J_j^y | \left( \frac{1}{\mathcal{L}} \right)'' | 0; J_j^y \rangle \\ &= -\frac{2\chi_{\text{csr}}}{\mathcal{V}} \text{Im} \sum_{nm} G''_{0,n} \mathcal{M}_{nm}^{ij} G''_{m,0} \quad . \end{aligned} \quad (207)$$

where  $\mathcal{M}_{nm}^{ij}$  are the  $z$ -hypermagnetization normalized matrix elements between Krylov hyperstates,

$$\mathcal{M}_{nm}^{ij} = \text{Im} \langle n; J_i^x | \mathcal{M} | m; J_j^y \rangle \quad . \quad (208)$$

By Eq. (160),

$$\text{Im} G_{0,n}^i = \delta_{n,2k} R_k^i \text{Im} G_{00}^i, \quad R_k^i = \prod_{k'=1}^k \left( -\frac{\Delta_{2k'-1}^i}{\Delta_{2k'}^i} \right) \quad , \quad (209)$$

and by Eq. (53),

$$\text{Re} L_{ii}^{xx} = \text{Re} L_{ii}^{yy} = -\chi_{\text{csr}}^i \text{Im} G_{00}^i \quad . \quad (210)$$

Thus the sum over  $n, m$  in Eq. (207) includes only even integers and results in the summation formula,

$$\left( \frac{dL_{ij}^{xy}(\varepsilon, \mathcal{V})}{dB} \right)_{\mathbf{B}=0} = -2 \frac{L_{ii}^{yy}(\varepsilon, \mathcal{V}) L_{jj}^{xx}(\varepsilon, \mathcal{V})}{\sqrt{\chi_{\text{csr}}^i \chi_{\text{csr}}^j}} \sum_{kl} R_k^{(i)} R_l^{(j)} \mathcal{M}_{2k,2l}^{ij} + \mathcal{O}(\varepsilon) \quad . \quad (211)$$

The longitudinal conductivities  $L_{ii}^{xx}(\varepsilon)$  and  $L_{jj}^{yy}(\varepsilon)$  factor out of the sum in Eq. (211). They produce the non-commuting DC limit of  $\varepsilon, 1/\mathcal{V} \rightarrow 0$ .

Thus, (unless longitudinal conductivities vanish, or the currents are completely separable as explained in subsection 29.1), the longitudinal conductivities may be divided out and the Hall-type coefficients in Eqs. (195) can be expressed as a  $\varepsilon$ -independent thermodynamic coefficients.

## 25. Hall Coefficient

In the double summation over the Krylov bases we separate out the  $n = 0, m = 0$  term write the electric Hall coefficient as a sum of two terms,

$$R_{\text{H}} = R_{\text{H}}^{(0)} + R_{\text{H}}^{\text{corr}} \quad , \quad (212)$$

where

$$\begin{aligned}
R_{\text{H}}^{(0)} &= \frac{\chi_{\text{cmc}}}{\chi_{\text{csr}}^2} \quad , \\
\chi_{\text{csr}} &= \lim_{\mathbf{q} \rightarrow 0} \lim_{\mathcal{V} \rightarrow \infty} \frac{\hbar}{\mathcal{V}} (j^x | j^x) \quad , \\
\chi_{\text{cmc}} &= -2 \lim_{\mathbf{q} \rightarrow 0} \lim_{\mathcal{V} \rightarrow \infty} \frac{\hbar}{\mathcal{V}} \text{Im}(j^x | \mathcal{M} | j^y) \quad , \\
R_{\text{H}}^{\text{corr}} &= -\frac{2}{\chi_{\text{csr}}} \sum_{kl} R_k R_l \mathcal{M}_{2k,2l} (1 - \delta_{k,0} \delta_{l,0}) \quad .
\end{aligned} \tag{213}$$

$\chi_{\text{csr}}$  is the zeroth moment of the longitudinal conductivity, which was defined in Section 21. It represents the kinetic energy of the constituent charge carriers. The current-magnetization-current (CMC) susceptibility,  $\chi_{\text{cmc}}$ , measures the effect of the Lorentz force on the currents, as shown below.  $R_{\text{H}}^{(0)}$  reproduces Boltzmann's equation result for energy dependent scattering time [78].

The correction term  $R_{\text{H}}^{\text{corr}}$  involves higher order recurrences and hypermagnetization matrix elements,  $\mathcal{M}_{nm}^{ij}$  defined in (207). The recurrences and Krylov operators involve current non-conservation, caused by disorder, hard core interactions and lattice Umklapp scattering. These terms are increasingly difficult to compute. In order to be allowed to neglect them, they must be estimated to be smaller in magnitude than  $R_{\text{H}}^{\text{corr}}$ . In Section 33 and Section 36, such estimates are obtained by calculation of the lowest order terms for certain lattice models of strongly interacting electrons and hard core bosons.

The current-magnetization-current (CMC) susceptibility,  $\chi_{\text{cmc}}$ , measures the effect of the Lorentz force on the currents, as shown below.  $R_{\text{H}}^{(0)}$  reproduces Boltzmann's equation result for energy dependent scattering time [78].  $R_{\text{H}}^{\text{corr}}$  includes the higher order corrections due to disorder, hard core interactions and lattice Umklapp scattering. For Hard Core Bosons,  $R_{\text{H}}^{\text{corr}}$  will be partially evaluated in subsection 36.4.

### 25.1. Weak scattering limit

For non-interacting band electrons with dispersion  $\epsilon_{\mathbf{k}}$ , the CSR is given by Eq. (15), and the CMC is

$$\chi_{\text{cmc}} = \frac{e^3}{c} \sum_{\mathbf{k}} \left( -\frac{\partial f_{\mathbf{k}}^0}{\partial \epsilon} \right) \left( v_{\mathbf{k}}^y \left( v_{\mathbf{k}}^y \frac{\partial}{\partial k^x} - v_{\mathbf{k}}^x \frac{\partial}{\partial k^y} \right) v_{\mathbf{k}}^x \right) \quad . \tag{214}$$

Thus,  $R_{\text{H}}^{(0)} = \chi_{\text{cmc}} / \chi_{\text{csr}}^2$  recovers Boltzmann equation result (16) for isotropic lifetime.  $R^{\text{corr}} \propto \Delta_1$ , which depends on  $[H, j^x] \neq 0$ . Therefore the correction is relatively suppressed at low disorder.

## 26. Modified Nernst Coefficient

The Modified Nernst Coefficient  $\bar{N}$  for  $C_4$  symmetric Hamiltonians is

$$\bar{N} = \frac{1}{\sigma_{xx}^{\text{dc}} \kappa_{xx}^{\text{dc}}} \frac{d\alpha_{xy}}{dB} = \frac{1}{\kappa_{xx}^{\text{dc}}} (N + R_{\text{H}} \alpha_{xx}) \quad . \tag{215}$$

$\bar{N}$  can be expressed by the summation formula,

$$\bar{N} = \bar{N}^{(0)} + \bar{N}^{\text{corr}} \quad , \tag{216}$$

where

$$\begin{aligned}
\bar{N}^{(0)} &= \frac{\chi_{\text{cmc}}^{\text{th-el}}}{\chi_{\text{csr}} \chi_{\text{csr}}^{\text{th}}} , \\
\chi_{\text{csr}}^{\text{th}} &= \lim_{V \rightarrow \infty} \frac{\hbar}{\mathcal{V}} (J_Q^x | J_Q^x) , \\
\chi_{\text{cmc}}^{\text{th-el}} &= -\frac{2}{V} \text{Im} (J_Q^x | \mathcal{M} | J_Q^y) , \\
\bar{N}_{\text{H}}^{\text{corr}} &= -\frac{2}{\sqrt{\chi_{\text{csr}}^{\text{th}} \chi_{\text{csr}}}} \sum_{kl} R_k^{\text{th}} R_l \mathcal{M}_{2k,2l}^{\text{th-el}} (1 - \delta_{k,0} \delta_{l,0}) , \\
\mathcal{M}_{nm}^{\text{th-el}} &= \text{Im} \langle n; J_Q^x | \mathcal{M} | m; J_Q^y \rangle .
\end{aligned} \tag{217}$$

$\chi_{\text{csr}}^{\text{th}}$  and  $\mathcal{M}_{nm}^{\text{th-el}}$  are the thermal CSR, and thermoelectric hypermagnetization matrix elements respectively.  $\bar{N}$  is therefore expressed as a thermodynamic coefficient similar to  $R_{\text{H}}$ , and  $R_{\text{TH}}$  which follows below.

## 27. Thermal Hall coefficient

The thermal Hall coefficient is,

$$R_{\text{TH}} = R_{\text{TH}}^{(0)} + R_{\text{TH}}^{\text{corr}} , \tag{218}$$

where

$$\begin{aligned}
R_{\text{TH}}^{(0)} &= T \frac{\chi_{\text{cmc}}^{\text{th}}}{(\chi_{\text{csr}}^{\text{th}})^2} , \\
R_{\text{TH}}^{\text{corr}} &= -\frac{2T}{\chi_{\text{csr}}^{\text{th}}} \sum_{kl} R_k^{\text{th}} R_l^{\text{th}} \mathcal{M}_{2k,2l}^{\text{th-th}} (1 - \delta_{k,0} \delta_{l,0}) , \\
\mathcal{M}_{nm}^{\text{th-th}} &= \text{Im} \langle n; J_Q^x | \mathcal{M} | m; J_Q^y \rangle .
\end{aligned} \tag{219}$$

## 28. Calculating the correction terms

The correction terms in Eqs. (213,217,219) depend on recurrences  $\Delta_n, n = 1, 2, \dots$ , which demand calculations of moments  $\chi_{\text{csr}}, \mu_2, \mu_4, \dots$ , and hypermagnetization matrix elements  $\mathcal{M}_{2k,2l}$ . The latter are most conveniently derived from the *non-normalized* magnetization matrix elements

$$\tilde{\mathcal{M}}_{nm} \equiv \text{Im} (\mathcal{L}^n J_i^y | \mathcal{M} | \mathcal{L}^m J_j^x) = -\text{Im} \text{Tr} \rho \left[ \mathcal{L}^{n-1} J_i^y, \mathcal{M} \mathcal{L}^m J_j^x \right] , \tag{220}$$

which are thermodynamic expectation values of nested commutators. For short range Hamiltonians, the commutators include sums over connected clusters of operators which are easier to trace over than calculating two-operator susceptibilities. These clusters can be generated and traced over by symbolic manipulation, as demonstrated in Sections 33 and 36.

$\tilde{\mathcal{M}}_{nm}$  are related to  $\mathcal{M}_{nm}$  of the correction terms by the Gramm-Schmidt matrix  $K$ . This matrix is determined as follows. Applying the resolution of identity with the Krylov basis,

$$\begin{aligned}
\mathcal{L}^k |0\rangle &= \sum_{k' \leq k} |k'\rangle \langle k' | \mathcal{L}^k |0\rangle \\
&\equiv \sum_{k'} K_{k,k'} |k'\rangle .
\end{aligned} \tag{221}$$

The matrix  $K$  is obtained by powers of the tridiagonal Liouvillian matrix (155), which results in polynomials of the recurrences  $\Delta_{k' \leq k}$ ,

$$K_{k',k} [\Delta_1, \dots, \Delta_k] = (L^k)_{k',0}, \quad k' \leq k . \tag{222}$$



Thus we obtain,

$$\mathcal{M}_{n,m} = \sum_{n' \leq n} \sum_{m' \leq m} K_{n,n'}^{-1}[\Delta] K_{m,m'}^{-1}[\Delta] \tilde{\mathcal{M}}_{n',m'}'' \quad . \quad (223)$$

## 29. Optimization of thermodynamic approaches

### 29.1. The Separability problem

The thermodynamic approaches have their limitations. The continued fraction extrapolation can only be performed efficiently if a clear asymptotic power law can be deduced from the dependence of the calculated recurrences on their order. In practice, the fluctuations of the calculated recurrences from an asymptotic power law behavior should decrease monotonically if a reliable termination function is to be found.

Nearly separable currents can significantly slow the convergence of continued fractions and Hall coefficients corrections. For example, the recurrences of a sum of two spectral functions with very different characteristic frequency scales is shown in Fig. 12. We note that the fluctuations about average recurrences do not converge rapidly.

Physically, sums of spectral functions with vastly different frequency scales can be expected for separable currents with different relaxation times. That is to say, if the Hamiltonian and its currents can be written as sum of commuting channels,

$$H = \sum_{r=1}^{N_r} H_r \quad , \quad \mathbf{j} = \sum_r \mathbf{j}_r \quad , \quad [\mathbf{j}_r, H_{r'}] \propto \delta_{rr'} \quad , \quad (224)$$

the resulting conductivities will be sums,

$$\sigma_{\alpha\beta}(\omega) = \sum_r \sigma_{\alpha\beta}^r(\omega) \quad . \quad (225)$$

While their moments are additive,

$$\mu_{2k} = \sum_r \mu_{2k}^r \quad , \quad (226)$$

the recurrences which are obtained by Eqs. (166) are highly entangled functions of the separate  $\mu_{2k}^r$ 's.

Similarly, the Hall coefficient summation formulas are formally correct, but cease to be useful for separable currents. Since the total Hall coefficient is,

$$R_H = \frac{\sum_{r=1}^{N_r} (d\sigma_{xy}^r/dB)}{\left(\sum_{r=1}^{N_r} \sigma_{xx}^r\right)^2} \quad , \quad (227)$$

for multichannel separable currents  $N_r > 1$ , ratios between different conductivities must enter the Hall coefficient, which therefore cannot be captured accurately just by  $R_H^{(0)}$ . For example, Fermi surface electrons with strongly dependent  $\mathbf{k}$ -dependent lifetime  $\tau_{\mathbf{k}}$ . At weak scattering, the currents of different wavevectors are separable. While  $R_H^{(0)}$  of Eq. (213) recovers the single lifetime expression of Eq. 14, it does not agree (within a factor of order unity) with the  $\mathbf{k}$ -dependent lifetime result of Boltzmann's equation in Eq. 13. The difference between  $R_H^{(0)}$  and Boltzmann's result is contained in the higher order correction terms, which are unwieldy.

In conclusion, continued fractions and Hall coefficient summation formulas are best suited for a non-separable current governed by one relaxation timescale. Otherwise, in Hamiltonians which support two or more separable currents with different relaxation timescales, the conductivities of each current should be calculated separately and later assembled in Eq. (227) to obtain the total Hall coefficient.<sup>8</sup>

<sup>8</sup>We thank Steve Kivelson for emphasizing the anisotropic lifetime problem in the Hall coefficient formula.

## 29.2. Renormalized Hamiltonians at low temperatures

Effective Hamiltonians are crucially important for efficient use of thermodynamic approaches to DC transport coefficients. As can be seen from the Lehmann representation of longitudinal conductivities (52), and the DPP formulas of the Hall conductivities (100), the important part of the spectrum and eigenstates resides in an energy window of order  $T$  above the ground state. The Hall coefficient formula, which is derived from Eq. (205), also depends on that part of the spectrum as can be seen from,

$$\left( \frac{dL_{ij}^{xy}(\varepsilon, V)}{dB} \right) = -\pi^2 \frac{2}{\mathcal{V}} \text{Im} \sum_{nmn'} W_{nm} \langle n | J_i^x | m \rangle \langle n' | J_j^y | n \rangle \mathcal{M}_{nmn'}^{n'} \delta_\varepsilon(E_n - E_{m'}) \delta_\varepsilon(E_{n'} - E_n) \quad . \quad (228)$$

where  $\delta_\varepsilon(x) = \varepsilon/(x^2 + \varepsilon^2)$ . Thus, in the DC limit,  $dL_{ij}^{xy}/dB$  is also an *on-shell* expression. It is greatly advantageous to replace the microscopic Hamiltonian  $H^{\text{micro}}$  by an effective Hamiltonian  $H^{\text{eff}}(B)$  which operates in the low energy Hilbert space and reproduces the correct spectrum at  $\{E_n \leq \text{const } T\}$ .

The renormalized currents and magnetization within this reduced Hilbert space are defined by,

$$\begin{aligned} \mathbf{j}_i^{\text{eff}} &= i[H^{\text{eff}}, \mathbf{P}_i^{\text{eff}}] \quad , \\ M^{\text{eff}} &= -\frac{\partial H^{\text{eff}}}{dB} \quad , \end{aligned} \quad (229)$$

where  $\mathbf{P}_i^{\text{eff}}$  are also projected onto the reduced Hilbert space. A consequence of renormalization in certain models is to reduce the magnitude of currents' non-conservation, i.e.

$$\| [H^{\text{eff}}, \mathbf{j}_i^{\text{eff}}] \| \leq \| [H^{\text{micro}}, \mathbf{j}_i] \| \quad . \quad (230)$$

The relative magnitude of the first recurrent depends on this commutator. Since all terms in the Hall coefficient's correction terms  $R_{\text{corr}}$  are proportional to  $\Delta_1$ , this ensures reduction of the relative magnitude  $R_{\text{corr}}/R_{\text{H}}^{(0)}$ .

An simple example of the value of renormalization is demonstrated by comparing the zeroth Hall coefficients of the microscopic Hamiltonian of electrons in a periodic potential, to that of the conduction band effective Hamiltonian. The microscopic Hamiltonian is  $H^{\text{particles}}$  given in Eq. (32). Its magnetization is given by

$$M^z = \frac{1}{2c} \sum_{i=1}^{N_p} \mathbf{x}_i \times \frac{\mathbf{p}_i}{m} \quad . \quad (231)$$

The CSR and CMC are completely independent on the potential terms and hence,

$$\begin{aligned} \chi_{\text{csr}}^{\text{particles}} &= \frac{N_p e^2}{\mathcal{V} m} \\ \chi_{\text{cmc}}^{\text{particles}} &= \frac{N_{\text{tot}} e^3}{\mathcal{V} m^2 c} \\ R_{\text{H}}^{(0), \text{particles}} &= \frac{\mathcal{V}}{N_p e c} \quad . \end{aligned} \quad (232)$$

Where  $N_p$  includes the electrons in *all* the filled bands and core states. The zeroth Hall coefficient must clearly be very far from the full answer, since we know from Boltzmann's equation (16) that  $R_{\text{H}}$  depends only on the filling of the *conduction* band. The correction term is therefore expected to be significant. Indeed, the magnitude of the first recurrent, which is a factor in  $R^{\text{corr}}$  is of order

$$\Delta_1^2 = \frac{1}{\mathcal{V} \chi_{\text{csr}}} \sum_{\mathbf{k}, \mathbf{q}, n, n'} \frac{f_{\mathbf{k}, n} - f_{\mathbf{k}+\mathbf{q}, n'}}{\epsilon_{\mathbf{k}+\mathbf{q}, n} - \epsilon_{\mathbf{k}, n'}} (q^x)^2 |V(\mathbf{q})|^2 \quad , \quad (233)$$

which can be very large for crystal potentials  $|V(\mathbf{q})| \gg |\epsilon_F|$ .

In comparison, if we use the renormalized conduction band Hamiltonian,

$$\begin{aligned} H^{\text{eff}} &= \sum_{\mathbf{k}} \frac{\mathbf{k}^2}{2m^*} c_{\mathbf{k}}^\dagger c_{\mathbf{k}} + \frac{1}{\mathcal{V}} \sum_{\mathbf{k}, \mathbf{k}'} U_{\mathbf{k}\mathbf{k}'}^{\text{dis}} c_{\mathbf{k}}^\dagger c_{\mathbf{k}'} \quad , \\ \mathbf{j}^{\text{eff}} &= \sum_{\mathbf{k}} \frac{\mathbf{k}}{m^*} c_{\mathbf{k}}^\dagger c_{\mathbf{k}} \quad . \end{aligned} \quad (234)$$

where  $U^{\text{dis}} \ll \epsilon_F$  is due to impurities, then

$$\begin{aligned} \chi_{\text{csr}}^{\text{eff}} &= \frac{(e^*)^2 n_{\text{cond}}}{m^*} \quad , \\ \chi_{\text{cmc}}^{\text{eff}} &= \frac{(e^*)^2 n_{\text{cond}}}{(m^*)^2 c} \quad , \\ (R_{\text{H}}^{(0)})^{\text{eff}} &= \frac{1}{n_{\text{cond}} e^* c} \quad . \end{aligned} \quad (235)$$

$n_{\text{cond}}$  is just the density of the partially filled conduction band.  $R_{\text{H}}^{(0)}$  recovers Drude-Boltzmann theory (7), with a small correction term which is suppressed by a factor of  $U^{\text{dis}}/\epsilon_F \ll 1$ .

For dirty semimetals [78], where the interband gap is of the same order as  $U^{\text{dis}}$ , the Hall coefficient can be well approximated by  $R_{\text{H}}^{(0)}$  of the two-band Hamiltonian, including both intraband and interband current matrix elements. The Hall coefficient formula provides a simpler route to the Hall coefficient than the coupled two-band Boltzmann equation [39, 40, 41].

## Part VII

# Numerical algorithms for thermodynamic coefficients

In Parts V and VI, longitudinal conductivities and Hall-type coefficients were expressed in terms of thermodynamic expectation values, for which a host of statistical mechanics algorithms exist. Below, as a preparation for the calculations of high temperature conductivities of strongly correlated lattice models in Parts VIII and IX, we elaborate on the application of high temperature series and stochastic (Monte-Carlo) methods to evaluate the following relevant thermodynamic coefficients:

1. The CSR, as defined by Eq. 143.
2. The conductivity moments  $\mu_{2k}, k = 1, 2, \dots$  as defined by Eq. (145). The recurents can be obtained from themoments by Eq. (166).
3. CMC susceptibilities, which can be written as expectation values,

$$\chi_{\text{cmc}} = 2 \lim_{\mathcal{V} \rightarrow \infty} \frac{\hbar}{\mathcal{V}} \text{ReTr} (\rho [P^x, , [M, J^y]]) \quad , \quad (236)$$

4. The hypermagnetization matrix elements, of Eq. 220.

At low temperatures, the use of variational wavefunctions to compute thermodynamic expectation values has seen enormous progress in recent years.. As examples, we refer the reader to the density matrix renormalization group [4, 5], projected entangled-pair states [6] and tensor networks [7]. For lack of space, these algorithms will not be reviewed here.

### 30. High temperature series

For interacting Hamiltonians, an advantage of thermodynamic expectation values over dynamic (time dependent) correlations, is its amenability to high temperature series expansion. Each term in the series involves traces over powers of the Hamiltonian, which are much less costly than Hamiltonian diagonalization over large lattice sizes.

The expansion works as follows. The density matrix  $\rho = \exp(-\beta H)/Z$  in powers of  $\beta$ ,

$$\begin{aligned}\exp(-\beta H) &= \sum_{n=0}^{\infty} \frac{(-\beta)^n}{n!} H^n \quad , \\ Z(\beta) &= \sum_{n=0}^{\infty} \frac{(-\beta)^n}{n!} \text{Tr} H^n \quad .\end{aligned}\quad (237)$$

For simplicity we restrict the following discussion to Hamiltonians which are sums of traceless bond operators on a bipartite lattice. Such Hamiltonians are used to describe the strongly correlated electrons and bosons models in Parts VIII and IX respectively. Hence, traces over even powers of  $H$  are assumed to vanish.

Expansion of the expectation value of a local operator  $O$  up to fourth order in  $\beta$  yields,

$$\begin{aligned}\langle O \rangle &= \text{Tr}(O) - \beta \text{Tr}(HO) + \frac{\beta^2}{2} \left( \text{Tr}(H^2 O) - \text{Tr}(O) \times \text{Tr}(H^2) \right) \\ &\quad - \frac{\beta^3}{3!} \left( \text{Tr}(H^3 O) - 3 \text{Tr}(HO) \times \text{Tr}(H^2) \right) \\ &\quad + \frac{\beta^4}{4!} \left( \text{Tr}(H^4 O) - 6 \text{Tr}(H^2 O) \times \text{Tr}(H^2) - 4 \text{Tr}(HO) \times \text{Tr}(H^3) - \text{Tr}(O) \times \text{Tr}(H^4) \right) + O(\beta^5) \quad .\end{aligned}\quad (238)$$

The thermodynamic coefficients are obtain by tracing over a lattice large enough to include *at least* all the connected operators in  $H^4$  which share sites with  $O$ .

#### 30.1. Linked clusters theorem

Let's consider a local operator  $O$  with  $\text{Tr} O \neq 0$ , which occupies a cluster of sites  $c_O = \{\mathbf{r}_1, \dots, \mathbf{r}_{n_O}\}$ . The strings of site operators which have sites in  $c_O$  define a connected cluster to  $c_O$ . The trace  $\text{Tr} H^n O$  is a sum of strings of operators which can be factorized as a trace over sites in the cluster  $c_O^k$  which are connected by  $k$  powers of  $H$  to  $c_O$ , and a trace over the rest of the powers of  $H$  as follows:

$$\text{Tr}(H^n O) = \sum_{k=0}^n \frac{n!}{k!(n-k)!} \text{Tr}_{c_O^{(k)}}(H^k O) \times \text{Tr}_{\notin c_O^{(k)}}(H^{n-k}) \quad .\quad (239)$$

A cancellation of all the non-connected clusters  $\notin c_O$  in Eq. (238) occurs between the numerator and the expansion of the partition function at each order in  $\beta^n$ . This leaves us to compute only traces over strings of operators in  $(H^k O)$  which include sites in  $c_O^{(k)}$  (linked clusters of  $H^k O$ ), and traces of  $H^{n-k}$  for  $k = 0, 1 \dots n$  (a.k.a linked cluster theorem). Eq. (238) then reads as

$$\begin{aligned}\langle O \rangle &= \text{Tr}(O) - \beta \text{Tr}_{\in c_O}(HO) + \frac{\beta^2}{2} \left( \text{Tr}_{\in c_O^{(2)}}(H^2 O) - \text{Tr}_{\in c_O^{(2)}} \times \text{Tr}_{\in c_O^{(2)}}(H^2) \right) \\ &\quad - \frac{\beta^3}{3!} \left( \text{Tr}_{\in c_O^{(3)}}(H^3 O) - 3 \text{Tr}_{\in c_O^{(3)}}(HO) \times \text{Tr}_{\in c_O^{(3)}}(H^2) \right) \\ &\quad + \frac{\beta^4}{4!} \left( \text{Tr}_{\in c_O^{(4)}}(H^4 O) - 6 \text{Tr}_{\in c_O^{(4)}}(H^2 O) \times \text{Tr}_{\in c_O^{(4)}}(H^2) - \text{Tr}(O) \times \text{Tr}_{\in c_O^{(4)}}(H^4) \right) + O(\beta^5) \quad .\end{aligned}\quad (240)$$

An example of a calculation of  $\beta^3 \left( \text{Tr}_{\in c_O^{(3)}}(H^3 O) \right)$  is described in Fig. 13. Here,  $H$  is taken as a sum over traceless bond operators  $H_{ij}$  on the square lattice, while  $O_{12}$  is any traceless bond operator.

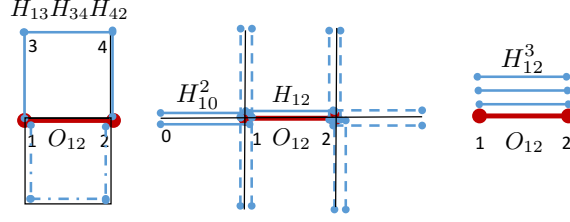


Figure 13: High temperature expansion of a nearest neighbor Hamiltonian on the square lattice. The graphs describe the three types of connected operator products in  $\text{Tr}(H^3 O_{12})_{\epsilon c_O^{(3)}}$  of Eq. (240). The linked cluster  $c_O^{(3)}$  is defined by the lattice of 7 bonds which is shown in the central graph, on which the counter-term  $-3\text{Tr}_{\epsilon c_O^{(3)}}(HO) \times \text{Tr}_{\epsilon c_O^{(3)}}(H^2)$  is also defined.

### 31. Stochastic algorithms

Stochastic sampling of thermodynamic expectation values a.k.a. Quantum Monte Carlo (QMC), have proven to be very efficient in extending high temperature series to lower temperatures. The algorithms described below are particularly tailored for interacting quantum particles on lattices. These are the Determinant QMC (DQMC) for fermions and the Directed Loop Algorithm (DLA) for lattice bosons and spins.

#### 31.1. Determinant Quantum Monte Carlo

In DQMC, the goal is to rewrite the grand-canonical partition function of a given fermionic Hamiltonian as a sum of “statistical weights” over a space of field configurations [79]. To illustrate the method [80], we consider the single band Hubbard model (HM),

$$H^{\text{HM}} = -t \sum_{\langle ij \rangle \sigma} (c_{i\sigma}^\dagger c_{j\sigma} + h.c.) - \mu \sum_{i\sigma} n_{i\sigma} + U \sum_i \left( n_{i\uparrow} - \frac{1}{2} \right) \left( n_{i\downarrow} - \frac{1}{2} \right) . \quad (241)$$

where  $c_{i\sigma}^\dagger$  creates a fermion of spin  $\sigma = \uparrow, \downarrow$  on lattice site  $i$ , and  $n_{i\sigma} = c_{i\sigma}^\dagger c_{i\sigma}$ .  $\mu$  is the chemical potential.

One now divides  $\beta$  into  $L_\tau$  ‘Trotter’ steps, such that  $\beta = \Delta\tau L_\tau$ . The partition function is rewritten as-

$$Z = \text{Tr}(e^{-\beta H}) = \text{Tr}(e^{-\Delta\tau H})^{L_\tau} \approx \text{Tr} \underbrace{(e^{-\Delta\tau K} e^{-\Delta\tau V} e^{-\Delta\tau K} e^{-\Delta\tau V} \dots)}_{L_\tau} , \quad (242)$$

where  $K = -\sum_{\langle ij \rangle \sigma} t_{ij} (c_{i\sigma}^\dagger c_{j\sigma} + h.c.) - \mu \sum_{i\sigma} n_{i\sigma}$  is the kinetic term and  $V = U \sum_i \left( n_i - \frac{1}{2} \right) \left( n_j - \frac{1}{2} \right)$  is the potential term. The second equality is approximate as  $K$  and  $V$  don’t commute. The approximation improves upon increasing  $L_\tau$  (decreasing  $\Delta\tau$ ). To handle the interaction  $V$  term, we employ the discrete Hubbard-Stratonovich (HS) transformation:

$$e^{-U\Delta\tau(n_i - \frac{1}{2})(n_j - \frac{1}{2})} = \frac{1}{2} e^{-\frac{U\Delta\tau}{4}} \sum_s e^{\lambda s(n_i - n_j)} , \quad (243)$$

where  $\cosh \lambda = e^{U\Delta\tau/2}$  and  $s = \pm 1$  is an Ising variable.

The  $e^{-\Delta\tau K}$  terms are bilinear in the fermion operators. For each factor of the  $L_\tau$  terms  $e^{-\Delta\tau V}$ , we introduce N number of HS fields, one for each spatial site, where we have an on-site interaction to decouple. The HS field  $s(i, l)$  therefore has two indices, space  $i$  and imaginary time  $l$ . Now, the  $e^{-\Delta\tau V(l)}$  also become bilinear in the fermion operators. We put an argument  $l$  on the  $V$ -terms to emphasize that while the  $K$ -terms are all identical, the  $V(l)$  contain different HS fields on the different imaginary time slices.

Finally, the trace evaluates to

$$Z = \sum_{s(i,l)} \det M_\uparrow \det M_\downarrow , \quad (244)$$

where  $M_\sigma = I + e^{-k} e^{-v_\sigma(1)} e^{-k} e^{-v_\sigma(2)} \dots e^{-k} e^{-v_\sigma(L_\tau)}$ . Here, the matrix elements of  $k$  are equal to  $\Delta\tau k_{ij}$ .  $v_\sigma(l)$  equals the diagonal matrix, whose elements are  $\lambda s(i, l)$ , obeying  $v_\uparrow(l) = -v_\downarrow(l)$ .  $I$  is the  $N \times N$  identity matrix.

Thus, we get a determinant for each of the two spin species. The quantum partition function has now been re-expressed as a classical Monte Carlo problem. One needs to sum over the possible configurations of the real, classical variables  $s(i, l)$  with the ‘‘Boltzmann weight’’, which is the product of the two fermion determinants. The workhorse of the algorithm is the Green’s function  $G_\sigma$ , which is first initialized as-

$$G_\sigma = [I + e^{-k} e^{-v_\sigma(1)} e^{-k} e^{-v_\sigma(2)} \dots e^{-k} e^{-v_\sigma(L_\tau)}]^{-1} \quad . \quad (245)$$

Next, the HS fields are updated one by one, and the new  $G_\sigma$ ’s are computed. Finally, after completing an entire set of updates on all space-time points of the lattice, measurements are made from these Green’s functions. A couple of simple examples are-

$$\begin{aligned} \langle n_{i\sigma} \rangle &= 1 - [G_\sigma]_{ii} \\ \langle S_i^+ S_j^- \rangle &= -[G_\uparrow]_{ji} [G_\downarrow]_{ij} \quad , \end{aligned} \quad (246)$$

where  $\langle n_{i\sigma} \rangle$  denotes the local spin density at site  $i$  and  $\langle S_i^+ S_j^- \rangle$  expresses (equal-time) spin correlations between sites  $i$  and  $j$ . The algorithm scales in CPU time as  $N^4 L$ . The reason is that re-evaluating the determinant of  $M$  takes  $N^3$  operations, and we must do that  $NL$  times to sweep through all the HS variables. There are tricks to reduce this computational cost to  $N^3 L$ , relying on the sparse nature of the ‘‘difference matrix’’  $dM$ , after updating the HS fields.

Some salient features of DQMC simulations are as follows-

- Measurement of correlation functions with non-zero imaginary time separation is possible, but requires more work. Analytic continuation of such correlations is required to get the dynamical response. That is significantly more difficult and often requires uncontrolled approximations [81].
- The product of matrices required in constructing  $M$  and hence  $G = M^{-1}$  is numerically unstable at low temperatures and strong couplings. Special ‘‘stabilization’’ is required to do the matrix manipulations [82].
- The determinants of the matrices can turn negative. This is the infamous ‘‘fermion sign problem’’ [83, 84, 85]. The sign problem does not occur for certain special cases. For example, if  $U$  is negative (the ‘‘attractive’’ Hubbard model), the individual determinants can go negative, but the matrices are always equal and hence the determinant appears as a perfect square. If  $U > 0$ , but the chemical potential  $\mu = U/2$  (‘‘half-filling’’), it’s also fine. The matrices are not identical in this case, but the determinants are nevertheless related by a positive factor, i.e., they again have the same sign, so their product is always positive.
- Alternate HS transformations are possible [86]. One may couple more symmetrically to the spin, which does not single out the  $z$ -component. Alternatively, one can couple to pair creation operators. So far, all such alternatives give a worse sign problem than the one mentioned here.

A determinant QMC calculation for expectation values of lattice fermions with discrete auxiliary fields can be implemented using the ALF package [87]. The statistical fluctuations can be evaluated by ‘‘Jackknife resampling’’ [88] (a method used for error estimation). The average fermion-induced sign in the QMC sampling is defined as

$$\langle S \rangle = \langle \text{sgn}(\det) \rangle \quad . \quad (247)$$

Empirically, the value of  $\langle S \rangle$  is found to low temperature, reflecting the diminishing effects of exchange processes in fermion world lines. It has been argued to be safe to use the expectation value of  $S$  to normalize the QMC averages, provided  $\langle S \rangle > 0.8$ .

The CMC and CSR susceptibilities are computed by first expressing the operators in terms of fermionic creation and annihilation operators. Since the Boltzmann weights are given by imaginary-time action of free fermions with time dependent fields, the operator expectation values can be factorized as products of Green’s functions (using Wick’s theorem), which can be sampled over configurations of the auxiliary fields. The displayed data in Section 33 is restricted to the regime of  $\langle S \rangle \geq 0.8$ , which for  $U = 8t$  and all doping range is satisfied at  $T \geq t/2 \approx J$ .

### 31.2. Directed Loop Algorithm

The Stochastic Series Expansion [1] (SSE) and QMC world-line and worm algorithms [2, 3] have been found to be very efficient for lattice bosons and spin models [89, 90].

A particular variant of these algorithms is the Directed Loop Algorithm (DLA) [91], which may be formulated along both world-line and SSE approaches. For simplicity, we review the DLA scheme within the SSE method, where the bonds of the Hamiltonian are decomposed as

$$H = - \sum_a \sum_b H_{a,b}, \quad (248)$$

where  $H_{a,b}$  satisfies  $H_{a,b}|\alpha\rangle = |\alpha'\rangle$  for a chosen basis  $\{|\alpha\rangle\}$ . The index  $a$  refers to operator type (either diagonal or off-diagonal in the chosen sites basis), and index  $b$  labels a particular bond position on the lattice.  $H_{0,0}$  denotes the unit operator. Using a Taylor expansion, the partition function is expressed as,

$$Z = \sum_{\alpha} \sum_{S_M} \frac{\beta^n (M-n)!}{M!} \left\langle \alpha \left| \prod_{p=1}^M H_{a_p, b_p} \right| \alpha \right\rangle, \quad (249)$$

where  $M$  is the truncation order of the expansion,  $S_M = [[a_1, b_1], [a_2, b_2], \dots, [a_M, b_M]]$  denotes the operator product and  $n$  is the number of non-[0, 0] elements.  $M$  is adjusted during the equilibration. Typically  $M \sim \beta N$  suffices for most purposes, where  $N$  denotes the number of lattice sites. Next, one defines a state  $|\alpha(p)\rangle$  by

$$\begin{aligned} |\alpha(p)\rangle &\equiv \prod_{i=1}^p H_{a_i, b_i} |\alpha(0)\rangle, \\ |\alpha(p)\rangle &= |\alpha(p)\rangle / (\alpha(p) |\alpha(p)\rangle)^{\frac{1}{2}}. \end{aligned} \quad (250)$$

The periodicity constraint  $|\alpha(M)\rangle = |\alpha(0)\rangle$  needs to be satisfied for a non-vanishing contribution to  $Z$ . The sum is sampled by transitions  $(\alpha, S_M) \rightarrow (\alpha', S'_M)$  satisfying detailed balance.

To concretize the procedure, we consider the anisotropic Heisenberg model in a magnetic field, whose Hamiltonian is-

$$H = \sum_{\langle ij \rangle} J[S_i^x S_j^x + S_i^y S_j^y + \Delta S_i^z S_j^z] - h \sum_i S_i^z. \quad (251)$$

We'll use the standard  $z$ -component basis ( $|\alpha\rangle = |S_1^z S_2^z \dots S_N^z\rangle$ ). The diagonal and off-diagonal bond operators are defined as-

$$\begin{aligned} H_{1,b} &= \epsilon + \Delta/4 - \Delta S_{i(b)}^z S_{j(b)}^z + h_b [S_{i(b)}^z + S_{j(b)}^z] \\ H_{2,b} &= -\frac{1}{2} [S_{i(b)}^+ S_{j(b)}^- + S_{i(b)}^- S_{j(b)}^+] \end{aligned}, \quad (252)$$

where  $i(b), j(b)$  are the sites connected by bond  $b$  and  $h_b$  is the bond field ( $h_b = h/2d$  on a  $d$ -dimensional cubic lattice). The constant  $\epsilon + \Delta/4 + h_b$  is added to the diagonal bond operator to ensure that all its matrix elements are positive. Moreover, on a bipartite lattice, the minus sign in front of the off-diagonal operator is irrelevant, as it can be ‘‘gauged out’’. Storing the operator sequence  $S_M$  and a single state  $|\alpha(p)\rangle$ , diagonal updates of the form  $[0, 0] \leftrightarrow [1, b]$  can be carried out sequentially for  $p = 1, \dots, M$  at all elements  $[a_p, b_p]$  in  $S_M$  with  $a_p = 0, 1$ . The Metropolis acceptance probabilities for these processes may be derived as-

$$\begin{aligned} P([0, 0] \rightarrow [1, b]) &= N_b \beta \langle S_i^z(p) S_j^z(p) | H_{1,b} | S_i^z(p) S_j^z(p) \rangle / (M-n) \\ P([1, b] \rightarrow [0, 0]) &= (M-n+1) / [N_b \beta \langle S_i^z(p) S_j^z(p) | H_{1,b} | S_i^z(p) S_j^z(p) \rangle], \end{aligned} \quad (253)$$

where  $P > 1$  is interpreted as probability one.

We next discuss the ‘‘operator loop’’ updates, which are efficient off-diagonal updates. To formulate these, it is useful to introduce a different representation of the SSE configurations. It is not necessary to store the full states  $|\alpha(p)\rangle$  as

they contain a great deal of redundant information. One can represent the matrix element in Eq. (249) as a linked list of “vertices”. First, we note that the weight of a configuration  $(\alpha, S_M)$  can be written as-

$$W(\alpha, S_M) = \frac{\beta^n (M - n)!}{M!} \prod_{p=1}^n W(p) \quad , \quad (254)$$

where the product is over the  $n$  non-[0, 0] operators in  $S_M$ . The  $W(p)$  are called “bare vertex weights” and are given by-

$$W(p) = \langle S_{i(b_p)}^z(p) S_{j(b_p)}^z(p) | H_{b_p} | S_{i(b_p)}^z(p-1) S_{j(b_p)}^z(p-1) \rangle \quad , \quad (255)$$

where  $H_b = H_{1,b} + H_{2,b}$  is the full bond operator. A vertex represents the spins on bond  $b_p$  before and after the operator has acted. These four spins constitute the legs of the vertex. There are six allowed vertices, with four different vertex weights-

$$\begin{aligned} W_1 &= \langle \downarrow \downarrow | H_b | \downarrow \downarrow \rangle = \epsilon \quad , \\ W_2 &= \langle \downarrow \uparrow | H_b | \downarrow \uparrow \rangle = W_3 = \langle \uparrow \downarrow | H_b | \uparrow \downarrow \rangle = \Delta/2 + h_b + \epsilon \quad , \\ W_4 &= \langle \uparrow \downarrow | H_b | \downarrow \uparrow \rangle = W_5 = \langle \downarrow \uparrow | H_b | \uparrow \downarrow \rangle = 1/2 \quad , \\ W_6 &= \langle \uparrow \uparrow | H_b | \uparrow \uparrow \rangle = \epsilon + 2h_b \quad . \end{aligned} \quad (256)$$

The building of a loop in the linked-vertex representation consists of a series of steps. The starting point of a loop is chosen at random. One creates two link-discontinuities (worm “head” and “tail”) here and propagates the head, keeping the tail fixed. The head enters a vertex at one leg (the entry leg) and an exit leg is chosen according to probabilities that depend on the entry leg and the spin states on all the legs. The entrance to the following vertex is given by the link from the chosen exit leg. The spins at all visited legs are flipped, except in the case of a “bounce”, where the exit is the same as the entrance leg, and only the direction of movement is reversed. When the head and tail meet each other, the loop closes, and a configuration contributing to  $Z$  is generated. Measurements of diagonal operators (like the magnetization  $\langle S^z \rangle$ ) are done over these class of configurations. The statistics obtained from the worm propagation moves (while the loop is open) corresponding to a fixed space-time separation of the worm head and tail directly provide an estimate for the two-point off-diagonal correlation functions (like  $\langle S_i^+(\tau) S_j^-(0) \rangle$ ).

The probabilities for the different exit legs, given the type of the vertex and an entrance leg, are chosen such that detailed balance is satisfied. This leads to the directed-loop equations. These equations underdetermine the required probabilities, and additional considerations (like minimizing the number of bounces) are required to constrain them. For brevity, we refrain from providing a detailed discussion of this issue here and point to the references mentioned above [89, 92]. The relation between the SSE and world-line approaches is explained in Ref. [93]. The algorithm becomes slightly more complicated if longer range interactions are included in the Hamiltonian [94].

As a concrete implementation of the DLA within a world-line scheme, we used the DSQSS package [95]. In Fig. 14, we show a toy example of a worm update in this scheme. One starts with the Heisenberg model ( $H = \vec{S}_1 \cdot \vec{S}_2$ ) of two spins on a bond (in a full lattice model with nearest neighbour interactions, it’s enough to consider this for simplicity, since one can always decompose the total Hamiltonian into a sum of nearest neighbour bond operators). The imaginary time axis is periodic, with  $\tau = 0$  and  $\tau = \beta$  identified. The blue arrows exhibit the starting ( $\tau = 0$ ) spin configuration. One first distributes the “vertices” on various nearest neighbor bonds, with *a priori* weights consistent with the temperature and Hamiltonian matrix elements in the  $S^z$  basis (within SSE, these are given by Eq. 254).

As depicted in Fig. 14, in each configuration, the solid (dashed) black vertical lines denote the propagation of up (down) spins in imaginary time. There are both “off-diagonal” (red) and “diagonal” (brown) vertices, which either flip the entering spins or not, respectively.

The worm update is depicted in five consecutive steps, whose sequence is marked by solid black arrows. A pair of “worm heads” (open and filled black ovals) are introduced at a randomly chosen space-time point. This represents the insertion of an off-diagonal operator in the Ising basis (such as  $S^x$ ). Thereafter, the filled oval (called the “tail”) is kept fixed while the other (called “head”) propagates vertically, with periodic boundary condition in the vertical direction, until it encounters a vertex. Each vertex has two entry and two exit points (also called “legs”). Depending on the “entry leg” and the “leg probabilities” satisfying directed loop equations, the worm head may travel horizontally (instead of



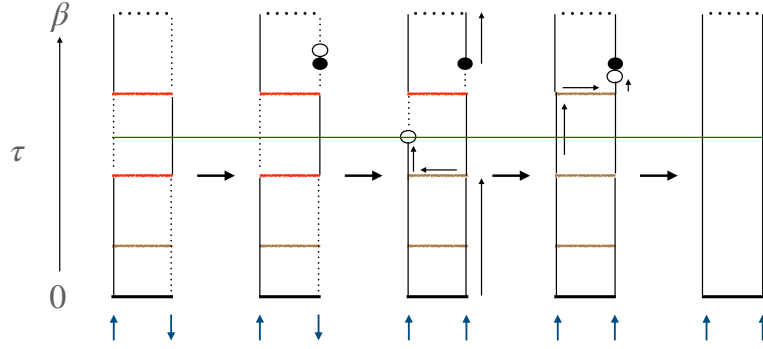


Figure 14: The propagation of a worm within DLA for the  $H = \vec{S}_1 \cdot \vec{S}_2$  model. The vertical axis represents the imaginary-time axis running from 0 to  $\beta$ , with  $\tau = 0$  and  $\tau = \beta$  identified. The short blue arrows at the bottom denote the starting ( $\tau = 0$ ) spin states. The brown (red) horizontal bars depict the “diagonal”(“off-diagonal”) Hamiltonian vertices. Solid and dashed vertical lines stand for the propagation of up and down spins respectively. The worm ‘head’ and ‘tail’ are represented by open and filled ovals. Once the worm head propagates, it flips the spins on the go and also may (or may not) change the vertex type it encounters. Moreover, the worm can move from site to site through these vertices, as shown in the third diagram of the sequence. The worm movement is shown by black arrows. Finally, once the worm head and tail meet each other, they annihilate and a new vertex configuration needs to be generated. The number of times the worm head crosses the green line contributes as counts for the  $\langle S_1^+(\tau)S_2^-(\tau) \rangle$  correlation function.

vertically), and may also change the vertex type. It always flips the spins on the legs it goes through. Finally, the propagation terminates when the head meets the tail. The green horizontal arrow in Fig. 14 denotes an imaginary time slice. The fact that this line is crossed by the worm head once during its propagation, contributes an integer count to the expectation value of  $\langle S_1^+(\tau)S_2^-(\tau) \rangle$ .

## Part VIII

# Strongly Correlated Electrons

### 32. The Hubbard Model

Electrons in a tight binding bandstructure, with strong local interactions can be minimally described by the HM [96, 97], as defined by Eq. (241).

For historical reasons, the electron filling in the HM is often measured by the “hole concentration” relative to half filling, i.e.  $x = \langle n_i^h \rangle$ , as defined by  $n_i^h = 1 - \sum_{s=\uparrow,\downarrow} n_{is}$ .

For  $U = 0$  the HM reduces to the non-interacting tight binding model  $H^{\text{SL}}$  of Eq. (17). As shown in Section 25.1,  $R_{\text{H}}^{(0)}$  is given by the isotropic scattering time solution of Boltzmann’s equation which is depicted in Fig. 2.

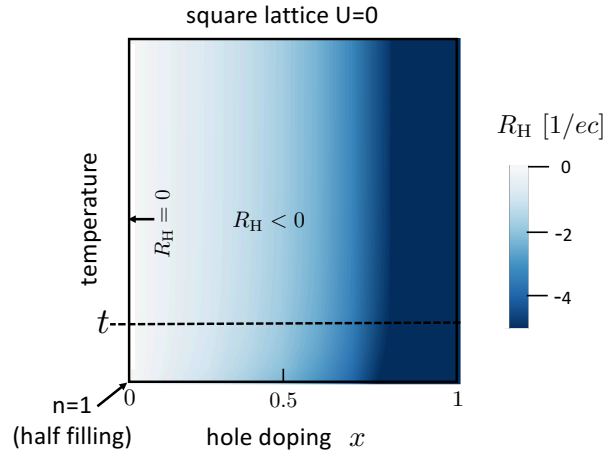


Figure 15: Hall coefficient of weakly disordered ( $U = 0$ ) square lattice.  $R_{\text{H}}^{\text{SL}}$  given by Eq. (16). The strongest prediction of Boltzmann theory for this model is that  $R_{\text{H}} < 0$  for  $0 < x < 1$ , and does not diverge anywhere except at  $x \rightarrow 1$ .

The Hall coefficient temperature-doping map of the nn SL model, is depicted in Fig. 15. We note that the Hall sign is negative for all  $x > 0$ , and vanishes half filling  $x_{\text{sign}} = 0$ . This Hall map will be contrasted with the Hall map in the  $U \gg t$  regime.

### 33. The t-J Model

In the strong interacting regime of  $U \gg t$ , the electronic correlations of the HM differ dramatically from the predictions of the weakly interacting model on the SL. This is true especially near half filling  $x = 0$ , where a charge gap of order  $U$  appears between the singly occupied spin and hole configurations, and configurations which contain doubly occupied sites. At zero temperature  $T \ll U$ , the half filled HM describes a Mott insulator, which orders antiferromagnetically. Away from half filling, the ground state phase diagram is still under debate, with variational studies indicating possible charge and spin density wave order, and/or  $d$ -wave superconducting order [6, 24, 97].

As argued in subsection 29.2, at temperatures  $T \ll U$ , the thermodynamic approaches converge much better after the HM Hamiltonian is renormalized onto its lower energy Gutzwiller-projected (GP) subspace of no-double-occupancies.

There, for  $U \gg t$ , the HM maps onto the t-J model (tJM) [71, 98], which to second leading order in  $t/U$ ,

$$\begin{aligned}
H^{\text{JM}} &= \mathcal{P}_{\text{GP}}(H^t + H^J + H^J) \mathcal{P}_{\text{GP}} + \mathcal{O}(t^3/U^2) \quad , \\
H^t &= -t \sum_{\langle ij \rangle} K_{ij}^+ \quad , \\
H^J &= J \sum_{\langle ij \rangle} \mathbf{s}_i \cdot \mathbf{s}_j (1 - n_i^h)(1 - n_j^h) \quad , \\
H^J &= -\frac{J}{4} \sum_{\langle ij \rangle \langle jk \rangle} (K_{ik}^+ - 2\Sigma_{ik}^+ \cdot \mathbf{s}_j)(1 - n_j^h) \quad .
\end{aligned} \tag{257}$$

The GP bond operators are

$$\begin{aligned}
K_{ij}^\pm &\equiv \sum_s \tilde{c}_{is}^\dagger \tilde{c}_{js} \pm \tilde{c}_{js}^\dagger \tilde{c}_{is} \quad , \\
\Sigma_{ij}^\pm &\equiv \sum_{ss'} \tilde{c}_{is}^\dagger \vec{\sigma}_{ss'} \tilde{c}_{js'} \pm \tilde{c}_{js}^\dagger \vec{\sigma}_{ss'} \tilde{c}_{is'} \quad ,
\end{aligned} \tag{258}$$

where  $\tilde{c}_{is}^\dagger \equiv c_{is}^\dagger(1 - n_{i,-s})$ .  $K^+$  ( $K^-$ ) describes the bond kinetic energy (current) and  $\Sigma^\pm$  describes the spin-dependent hopping.  $J = 4t^2/U$  is Anderson's antiferromagnetic superexchange energy.

### 33.1. Linear Resistivity slope

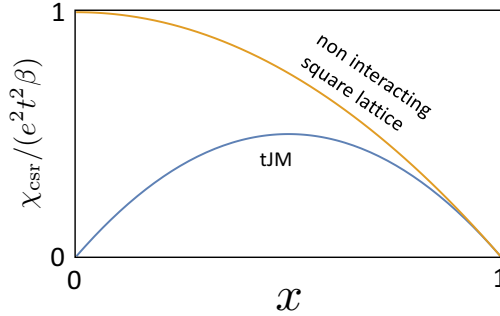


Figure 16: Doping dependent CSRs at intermediate temperatures  $t < T \ll U$ . In contrast to the non-interacting case, the CSR of the tJM vanishes toward the Mott phase as  $x \rightarrow 0$ . This results in an interaction induced divergence of  $R_H$  and the resistivity slope.

$H^t$ , (the “t-model”), dominates the metallic charge transport at  $U \gg T \gg J$ . The doping dependence of the CSR of the  $H^t$  was calculated by Jaklic and Prelovsek [99] and Perepelitsky *et al.* [100] up to order  $\beta^3$ :

$$\chi_{\text{csr}} = 2\beta e^2 t^2 x(1-x) + \frac{\beta^3 e^2 t^4}{6} x(1-x)(-9 + 2x + x^2) + \mathcal{O}(\beta^5 t^6) \quad . \tag{259}$$

As depicted in Fig. 16, the CSR vanishes toward  $x \rightarrow 0$  as a consequence of the GP. It is also suppressed relative to the non-interacting limit even far from half filling. Vanishing of the CSR produces a divergence of the Hall coefficient by Eq. (309).

The high temperature limit of the first two conductivity recurrences of  $H^t$  are

$$\Delta_1^2 = t^2(3 - 2x - x^2) \quad , \quad \Delta_2^2 = t^2 \frac{24(1+x)}{3+x} \quad , \tag{260}$$

which are shown as functions of doping  $x$  in Fig. 17.  $\Delta_1^2$  was calculated by Jak *et al.* [99].  $\Delta_2^2$  was calculated by Khait *et al.* in Ref. [23].

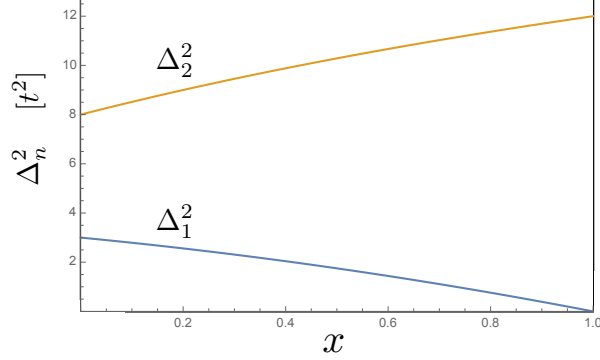


Figure 17: The first two recurrents of  $H^t$  at order  $\beta^0$  as a function of hole doping  $x$ .

The DC conductivity as a CF is,

$$\sigma_{xx}(\omega) = -\beta\chi_{\text{csr}} \lim_{\varepsilon \rightarrow 0} \text{Im} \frac{1}{i\varepsilon - \frac{\Delta_1^2}{i\varepsilon - \Delta_2 G_{22}^>(i\varepsilon)}} . \quad (261)$$

$\Delta_1$  and  $\Delta_2$ , can be extrapolated to evaluate  $\text{Im}G_{22}^>$  by semicircle termination (SCT), Eq. (183)),

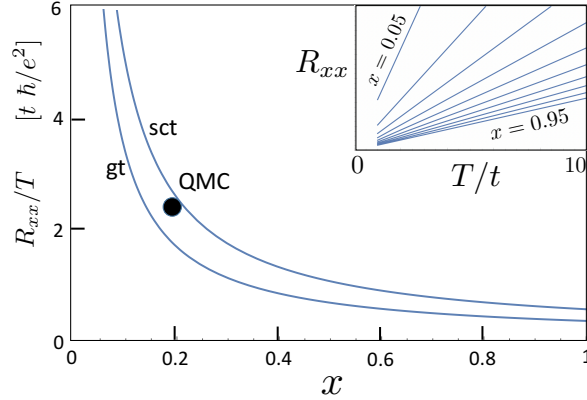


Figure 18: High temperature resistivity slopes of  $H^t$ . sct and gt denote two different continued fraction extrapolation schemes (see text). Inset depicts  $R_{xx}(T)$  for gt approximation. The solid circle marks the Quantum Monte Carlo result for the  $U=8t$  HM, reported in Fig. S3 of Ref. [101].

$$(\bar{\Delta}_n^{\text{sct}})^2 \Rightarrow \Delta_2^2 , \quad n = 2, 3, \dots \infty , \quad (262)$$

and by Gaussian termination (GT), Eq. (185)),

$$(\bar{\Delta}_n^{\text{gt}})^2 \Rightarrow \frac{1}{2}n\Delta_2^2 , \quad n = 2, 3, \dots \infty . \quad (263)$$

In Fig. 18, the high temperature DC resistivity slopes of  $H^t$  are plotted for both termination approximations. We see that the slopes diverge toward the Mott limit, as expected by the suppression of the CSR depicted in Fig. 16. Interestingly, the resistivity is finite at high temperatures even in the dilute electron density limit  $x \rightarrow 1$ . The slopes of Fig. 18 are in qualitative agreement with the HM calculation in Ref. [101].

Note: Perepelitsky *et al.* [100] had evaluated the high temperature resistivity slope of the large  $U/t$  HM in the high dimensional lattice (large- $d$ ) limit as,

$$\begin{aligned} R_{xx}^{d \rightarrow \infty}(x, T) &\approx \frac{1}{x} R_0(x=1, T) \quad , \\ R_0(x=1, T) &\propto \frac{T}{t} \quad . \end{aligned} \quad (264)$$

In the large  $d$  limit, vertex corrections to the conductivity bubble can be neglected [100]. As  $x \rightarrow 1$ , the vanishing compressibility effectively cancels the diverging effective scattering time. This conclusion agrees with the CF extrapolation of Ref. [23] at  $d = 2$ ,

$$R_{xx}^{d=2} = \frac{T}{te^2} \frac{2}{\sqrt{\pi}} \frac{\Delta_1^2}{\chi_{\text{CSR}} \Delta_2} \propto \frac{T}{xt} \quad , \quad (265)$$

where the  $x$ -dependence is given by Eqs. (259) and (260). In the CF, the ratio  $\Delta_2/\Delta_1^2$  is interpreted as the effective scattering time, which diverges as  $x \rightarrow 1$ . The resistivity slopes therefore saturate at  $x \rightarrow 1$  as depicted in Fig. 18.

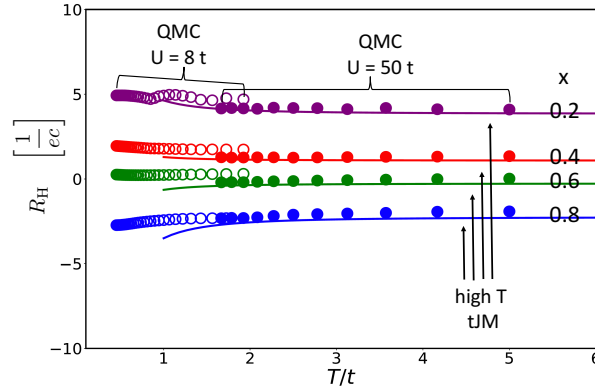


Figure 19: Hall coefficient  $R_H^{(0)}$  in the intermediate temperature regime  $J \leq T \ll U$  from Ref. [23]. Lines depict the asymptotic high temperature values for the  $t$ -model Eq. (267), which are calculated by the high temperature series expansion reviewed in Section 30. The solid and open circles are obtained by DQMC (see Section 31.1) using Boltzmann weights of the HM. The different values of  $U/t$  are used to cover different temperature regimes. The DQMC results are shown in regimes of negligible fermion sign error. We note that the high temperature expansion agrees with the DQMC data down to  $T \simeq 2t$ , and the DQMC data shows quite weak temperature dependence down to  $T \simeq J$ .

### 33.2. Hall map for large $U/t$

$R_H$  of the  $t$ -model was calculated in Ref. [23] by Eq. (213), using the high temperature series described in Section 30. The doping dependent CMC was determined up to order  $(\beta t)^4$ ,

$$\begin{aligned} \chi'_{\text{cmc}} &= \frac{\beta^2 t^4 e^3}{2c} x(1-x)(-5 + 10x + 3x^2) \\ &+ \frac{\beta^4 t^6 e^3}{16c} x(1-x)(45 - 136x + 50x^2 + 48x^3 - 71x^4) \quad . \end{aligned} \quad (266)$$

The zeroth Hall coefficient was determined up to second order in  $\beta t$ ,

$$R_H^{t,(0)} = \frac{1}{ec} \left( \frac{-5 + 10x + 3x^2}{8x(1-x)} \right) + \left( (\beta t)^2 \frac{-45 - 53x + 145x^2 + 225x^3}{192x} \right) \quad . \quad (267)$$

The calculation of  $R_H^{t,(0)}$  was extended down to the intermediate temperature (IT) regime:  $J \leq T \ll U$ , by DQMC which is reviewed in Section 31.1. The weights are given by the HM, which at large  $U/t$  effectively includes the

effects of the spin interactions  $H^J$  in the tJM. The DQMC data is plotted in Fig. 19. The analytic high temperature series curves of Eq. (267) are depicted by solid lines. The DQMC was performed using Boltzmann weights of the strongly interacting HM on the square lattice. Typical feasible system sizes are chosen between  $8 \times 8$  and  $12 \times 12$  lattice sites, where we found little size dependence of our results. This indicates a short correlation length in the studied temperature regime. The imaginary time step was chosen to render the Trotter errors to be insignificant. The number of Monte Carlo sweeps was generally  $\sim 10^5$ .

The DQMC data shown in Fig. 19 was included for temperatures and doping concentrations where the average fermion-induced sign of the Boltzmann weights  $\langle S \rangle$  (see Eq. (247)), is higher than 0.8. Ref. [23] also showed that  $\langle S \rangle$  decreases or large values of  $U/t$ , and at intermediate doping concentrations, while it approaches unity at high temperatures and for  $x \rightarrow 1$  and  $x \rightarrow 0$ .

In the extremely high temperatures regime  $T \gg U$ , the tJM is not valid. One can use the unprojected HM of Eq. (241) since the suppression of double occupancies in the HM diminishes since the Boltzmann weights become weakly dependent of  $U$ .  $R_H^{(0)}$  is then simply given by the high temperature limit of the non-interacting SL, i.e.,

$$\begin{aligned} \chi_{\text{csr}}^{\text{HM}} &\sim \beta e^2 t^2 n(2-n) \quad , \quad \chi_{\text{cmc}}^{\text{HM}} \sim \beta^2 \frac{e^3}{c} t^4 n(2-n)(1-n) \quad , \\ R_H^{(0)} &= \frac{2(1-n)}{n(2-n)ec} + O(\beta U)^2 \simeq R_H^{\text{SL}} \quad , \end{aligned} \quad (268)$$

where  $n = 1 - x$  is the electron density.

Interestingly, at lower temperatures, which lie within the applicability of the tJM, the recovery of the  $U \simeq 0$  behavior at high temperatures is heralded by the effects of  $H^J$  in the tJM (257).  $H^J$  become important in the CMC susceptibility, by adding to the currents and magnetizations next neighbor hopping terms,

$$\begin{aligned} j_{ijk}^{\prime\alpha} &= -ieJ(1-n_j^h) \left( K_{ik;\alpha}^- - 2\Sigma_{ik;\alpha}^- \cdot \mathbf{s}_j \right) \\ M' &= \frac{1}{2c} \sum_{(ij)\langle jk \rangle} (x_i j_{ijk}^{\prime y} - y_i j_{ijk}^{\prime x}) \quad . \end{aligned} \quad (269)$$

Since  $J \ll t$ , these terms are unimportant for the CSR. However, for the CMC they contribute one less power of  $\beta H$  than those  $\chi_{\text{cmc}}^t$ , since they encircle a magnetic flux with one less Hamiltonian bond. Hence they become dominant at temperatures of order  $T \simeq U$ ,

$$\chi_{\text{cmc}}^{J'} = \frac{\beta J e^3}{2} x(1-x)(1+2x-3x^2) \quad . \quad (270)$$

We note that  $\chi_{\text{cmc}}^{J'}$  has the opposite sign to  $\chi_{\text{cmc}}^t$ , and  $H^J$  yields the contribution to  $R_H^{(0)}$  of,

$$\Delta R_H^{J'} = \frac{4T}{ecU} \left( \frac{1+2x-3x^2}{8x(1-x)} \right) \quad . \quad (271)$$

Therefore, as  $x \rightarrow 0$  and  $T \rightarrow U$ ,  $\Delta R_H^{J'}$  reduces the positive Hall coefficient divergence, and the doping levels of the Hall sign reversal. Its effect is observed in the upper blueish regions of Fig. 1.

### 33.3. Hall coefficient corrections

We calculate the correction term up to second order

$$R_H^{\text{corr}(2)} = \frac{1}{\chi_{\text{csr}}} \left( \left( \frac{\Delta_1}{\Delta_2} \right)^2 \mathcal{M}_{2,2} - \left( \frac{\Delta_1}{\Delta_2} \right) (\mathcal{M}_{2,0} + \mathcal{M}_{0,2}) \right) \quad . \quad (272)$$

The three hypermagnetization matrix elements  $\mathcal{M}_{02}, \mathcal{M}_{20}, \mathcal{M}_{22}$  were evaluated numerically.

The calculation of  $M_{2,2}''$  to leading order in  $(\beta t)$  involved traces over up to  $10^5$  operator clusters.

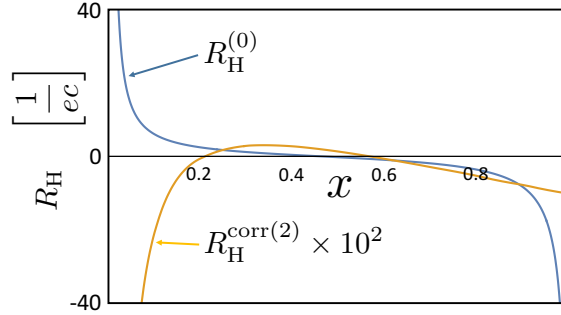


Figure 20: Comparison of the the leading order high temperature Hall coefficient of  $t$ -model, defined in Eq. (267) (blue line), with its second order correction term (orange line, multiplied by 100 for visibility) defined in Eq. (272). The ratio of magnitudes vanishes at  $x \rightarrow 1$ , and approaches 0.06 at  $x \rightarrow 0$ .

In Fig. 20, we plot the final result for  $R_H^{\text{corr}(2)}$  for all doping concentrations. We see that in comparison  $R_H^{(0)}$ , the its quantitative effect is negligible, and maximized toward  $x \rightarrow 0$  by

$$\lim_{x \rightarrow 0} |R_H^{\text{corr}(2)} / R_H^{(0)}| \rightarrow 6\% \quad . \quad (273)$$

Based on the high temperature ( $\mathcal{O}(\beta t)^0$ ) result in Eq. (273), and the weak temperature dependence found for  $R_H^{(0)}$  shown in Fig. 19, we may assume that the correction term remains negligible throughout the IT regime. We note that we have not calculated  $R_H^{\text{corr}}$  for the HM at  $T \geq U$ .

### 33.4. Numerical calculation Krylov operators and hypermagnetization matrix elements

The high temperature moments  $\mu_2, \mu_4$  which yield the recurrences  $\Delta_1, \Delta_2$ , and the hypermagnetization matrix elements  $\tilde{\mathcal{M}}_{02}, \tilde{\mathcal{M}}_{20}, \tilde{\mathcal{M}}_{22}$  defined in Section 28, were evaluated numerically by symbolic manipulation.

The operator  $\mathcal{L}^n j_i^\alpha$  is expanded in terms of products of site operators  $O_{i_1}(\mathbf{r}_1) \cdot O_{i_2}(\mathbf{r}_2) \cdot \dots \cdot O_{i_N}(\mathbf{r}_N)$  with real coefficients that are stored separately. Each application of the Liouvillian or the hypermagnetization changes the hyperstate after multiplying the operators site-by-site using the tJM multiplication Table 1 of the 8 GP fermions and spin operators. One keeps track of the overall order of the fermion operators  $\tilde{c}_i, \tilde{c}_j^\dagger$ , and the negative signs produced when reordering the contributions to the same final hyperstate from different multiplication paths.

|                                | $\tilde{c}_\uparrow^\dagger$   | $\tilde{c}_\downarrow^\dagger$ | $\tilde{c}_\uparrow$ | $\tilde{c}_\downarrow$ | $n_\uparrow$         | $n_\downarrow$         | $\tilde{s}^+$          | $\tilde{s}^-$        |
|--------------------------------|--------------------------------|--------------------------------|----------------------|------------------------|----------------------|------------------------|------------------------|----------------------|
| $\tilde{c}_\uparrow^\dagger$   | 0                              | 0                              | $n_\uparrow$         | $\tilde{s}^+$          | 0                    | 0                      | 0                      | 0                    |
| $\tilde{c}_\downarrow^\dagger$ | 0                              | 0                              | $\tilde{s}^-$        | $n_\downarrow$         | 0                    | 0                      | 0                      | 0                    |
| $\tilde{c}_\uparrow$           | $n_h$                          | 0                              | 0                    | 0                      | $\tilde{c}_\uparrow$ | 0                      | $\tilde{c}_\downarrow$ | 0                    |
| $\tilde{c}_\downarrow$         | 0                              | $n_h$                          | 0                    | 0                      | 0                    | $\tilde{c}_\downarrow$ | 0                      | $\tilde{c}_\uparrow$ |
| $n_\uparrow$                   | $\tilde{c}_\uparrow^\dagger$   | 0                              | 0                    | 0                      | $n_\uparrow$         | 0                      | $\tilde{s}^+$          | 0                    |
| $n_\downarrow$                 | 0                              | $\tilde{c}_\downarrow^\dagger$ | 0                    | 0                      | 0                    | $n_\downarrow$         | 0                      | $\tilde{s}^-$        |
| $\tilde{s}^+$                  | 0                              | $\tilde{c}_\uparrow^\dagger$   | 0                    | 0                      | 0                    | $\tilde{s}^+$          | 0                      | $n_\uparrow$         |
| $\tilde{s}^-$                  | $\tilde{c}_\downarrow^\dagger$ | 0                              | 0                    | 0                      | $\tilde{s}^-$        | 0                      | $n_\downarrow$         | 0                    |

Table 1: Multiplication table of GP operators in the tJM. The entry  $O_{i,j} = O_i \cdot O_j$ , where  $i$  and  $j$  are row and column respectively, and  $\tilde{s}^\alpha = s^\alpha(1 - n^h)$ ,  $n_{\uparrow,\downarrow} = (1 - n^h)(\frac{1}{2} \pm \tilde{s}^\alpha)$ .

When evaluating the final traces to obtain the moments or matrix elements, most operators vanish unless they only contain unit operators and density operators  $n_\gamma$ .

### 34. Discussion

Sign reversal of the Hall coefficient at low doping has been previously obtained by dynamical mean field theory (DMFT) [102, 103], QMC [104, 105] and determinant QMC [106]. These methods have found evidence of hole pockets in the momentum dependent occupation, which is qualitatively consistent with our results at low doping. Refs. [107, 108, 109] calculate (within DMFT) the Hall conductivity of the Hubbard model at strong magnetic fields. They found that the Hall sign is reversed relative to band theory, near half filling. These effects were attributed to the Chern numbers of the non-interacting Hofstadter's butterfly bands of the square lattice. It is interesting that these sign changes which were predicted at strong fields, (as measured in strongly correlated flat bands Moiré systems [110]), are qualitatively similar to the Hall sign we obtain in the weak field limit.

Here however, we find that the sign reversal occurs already at  $x \leq 0.45$ , which may come as a surprise vis-a-vis the widely used band theoretical approaches at much lower doping. The reason is simply related to the spin and charge entangled commutation relations of GP current operators of the tJM,

$$[K_{12}^-, K_{23}^-] = K_{13}^- \left( \frac{1 + n_2^h}{2} \right) + \Sigma_{13}^- \cdot \mathbf{s}_2 (1 - n_2^h) \quad , \quad (274)$$

which affects the hole density dependence of the CMC, and determines the doping concentration of the sign reversal. Since the hole density operators have coefficients of order unity, it is natural that the sign change occurs at a fraction with a denominator not much larger than unity. The important lesson we can learn from this is that the effects of GP reach far into the high doping and temperature regimes.

Previous QMC calculations of  $R_H^{(0)}$  for the HM [104, 111] have used our Eq. (213), and neglected  $R_H^{\text{corr}}$ . They have also reported a positive Hall sign near half filling (but no apparent divergence) for the square lattice model. However in the regime of  $U/t \simeq 16$ ,  $R^{\text{corr}} \propto \| [H, j^x] \| \sim U/t$ , is expected to dominate over  $R_H^{(0)}$ , and hence cannot be ignored.

The difference between  $R_H^{(0)}$ (HM) [111] and  $R_H^{(0)}$ (tJM) of Eq. (267), can be explained by the fact that  $R^{\text{corr}}(\text{tJM}) \ll R^{\text{corr}}(\text{HM})$  in the IT regime.

We can compare  $R_H^{(0)}$  of Eq. (267) to the infinite frequency Hall coefficient of the t-model calculated at leading order in  $\beta$  by Shastry, Shriman and Singh [112],

$$R_H^* = \frac{d}{dB} \lim_{\beta \rightarrow 0, \omega \rightarrow \infty} \rho_{xy}(\omega) = \frac{1}{ec} \left( -\frac{1}{4x} + \frac{1}{1-x} - \frac{3}{4} \right) \quad . \quad (275)$$

$R_H^*$  changes sign at  $x = 1/3$  and diverges as  $1/(4x)$  toward the Mott limit. While Eq. (267) changes sign at  $x = 0.4415$  and diverges as  $5/(8x)$  at small  $x$ . Still, the qualitative similarity we find between the infinite and zero frequencies is surprising, but we cannot infer any general relations from this coincidence. We note that  $R_H^*$  may be relevant to the optical Kerr effect [113].

In summary, the calculation of the DC Hall coefficient as a function of hole doping in the IT regime appears to be well controlled. We can learn from it that the Mott insulator phase affects the charge carriers in the nearby metallic phase. This has theoretical implication to any possible ordered phases at lower temperatures, such as superconductivity and/or other orders [4, 24, 25, 114]. The superconducting order parameter should consist of GP holes, with spin entangled commutation relations (274), rather than quasiparticles near the non-interacting Fermi surface. The GP also governs the relation between superfluid stiffness (which is bounded by the CSR), and the electron density [115]. It affects the moving vortex charge and the Hall sign in the flux flow regime [116, 117].



## Part IX

# Strongly Correlated Bosons

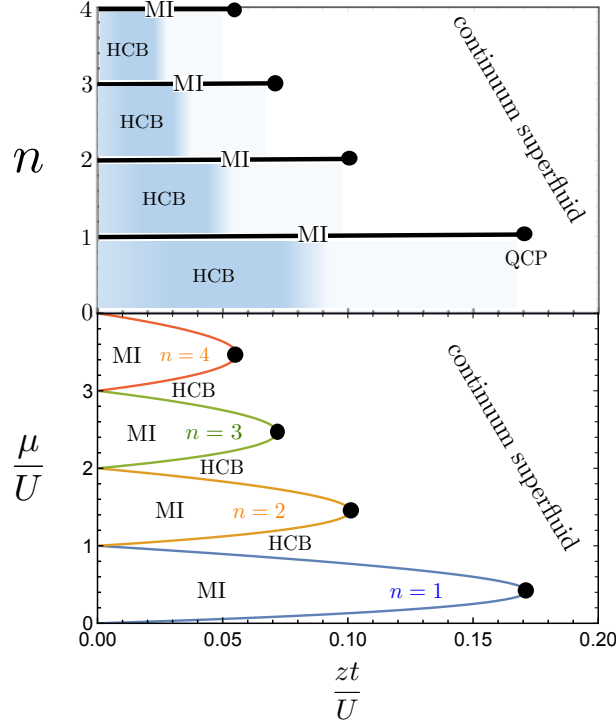


Figure 21:  $T = 0$  phase diagram of the Bose Hubbard Model, Eq. (276). At weak interactions  $U/zt \rightarrow 0$ , the lattice periodicity is unimportant, and the bosons condense into a continuum superfluid ground whose excitations are governed by the Gross-Pitaevskii field theory (277). The quantum critical points (marked by black disks), denote second order transitions into gapped Mott insulators of integer fillings  $n$ . Sandwiched between the Mott insulator phases, at fractional average densities, the Hamiltonian renormalizes into Hard Core Bosons (HCB) model Eq. (291), whose boson occupations are constrained to fluctuate between two consecutive integers.

### 35. The Bose Hubbard model

The Bose Hubbard model (BHM) is a minimal model of interacting lattice bosons,

$$H^{\text{BHM}} = -t \sum_{\langle ij \rangle} (e^{-iqA_{ij}/c} a_i^\dagger a_j + e^{iqA_{ij}/c} a_j^\dagger a_i) + U \sum_i n_i^2 - \mu \sum_i n_i \quad . \quad (276)$$

$t$  is the hopping rate and  $U$  is the local repulsive interaction,  $q$  is the boson charge, and  $c$  is the speed of light. The lattice constant is unity.  $a_i^\dagger$  creates a boson on lattice site  $i$ , and  $n = a_i^\dagger a_i$  is the boson occupation.  $A_{ij} = \int_{\mathbf{x}_i}^{\mathbf{x}_j} d\mathbf{x} \cdot \mathbf{A}$ , where  $\mathbf{A}$  is the electromagnetic vector potential.

$H^{\text{BHM}}$  can be realized by cold bosonic atoms trapped in an optical lattice, where  $\mathbf{A}$  can be implemented by light induced artificial gauge fields [118].

The BHM also describe a Josephson junction array where the BCS pairing gap in each grain is larger than the Josephson coupling  $t$ .  $U$  would be the inverse capacitance of each grain.

The BHM has a well known phase diagram [119] which is shown in Fig. 21.

### 35.1. Weak interactions

We note that for weak interactions,  $t/U \rightarrow \infty$ , the bosons condense into the  $\mathbf{k} \simeq 0$  eigenstates with effective dispersion  $\omega_{\mathbf{k}} \simeq \frac{\hbar^2 \mathbf{k}^2}{2m^*}$ . The low energy theory is therefore effectively a Galilean symmetric continuum theory described by the Gross-Pitaevskii (GP) action [120],

$$S^{\text{GP}} = \int dt d^d x \left( i\psi^* \dot{\psi} - \frac{1}{2m^*} |\nabla - i\frac{q}{c} \mathbf{A}\psi|^2 + U|\psi|^4 - \mu|\psi|^2 \right) , \quad (277)$$

where  $\psi(\mathbf{x}_i)$  is a complex coherent-state field which represents the lattice boson operator  $a_i$ . For dimension  $d > 2$ ,  $S^{\text{GP}}$  describes a superconductor at low temperatures, and a charged bosons gas above a finite transition temperature. In the presence of impurities, the metallic conductivity tensor is described by Drude theory Eq. (6) with scattering rate which vanishes with impurity concentration. Therefore by (7), the Hall coefficient is equal to the Galilean symmetric result,

$$R_{\text{H}}^{\text{GP}} = \frac{1}{nqc} , \quad (278)$$

where  $n$  is the boson density. No Hall sign change is expected as a function of density or temperature in the weak interactions regime.

### 35.2. Strong interaction

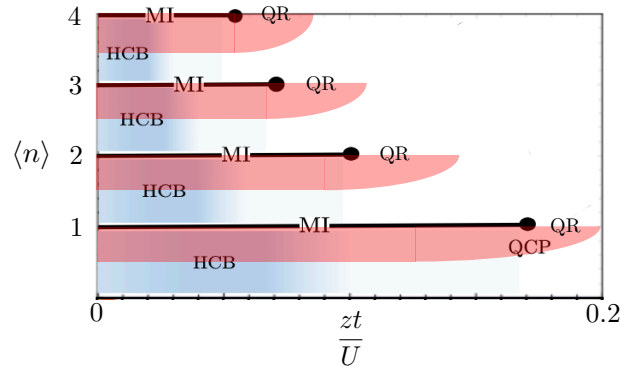


Figure 22: Hall signs (for  $q > 0$ ) for the BHM phase diagram as calculated by the ground state Chern number Eq. (67) [121, 122]. Red regions are negative, and blue and white regions are positive. QR and HCB regions denote the effective strong interaction models (281) and (291) respectively. The BHM ground state Chern number sign agrees with that of  $R_{\text{H}}$  at high temperatures.

Fig. 22 depicts the BHM ground state Chern number (Eq. (67)) as calculated by Huber and Lindner [121] in the strong interaction regime. We note the red regions of Hall sign reversal at strong interactions. While at zero temperature the ground state is a gapless superfluid with zero Hall resistivity, and the Chern calculation should not apply (see Section 13). Nevertheless, we find that the Hall sign agrees with the Hall coefficient sign in the corresponding metallic phases at higher temperature, as described below.

For strong interactions,  $t/U < 1$  there are Mott insulator lobes in which the boson filling is locked into an integer  $\langle n_i \rangle = m = 0, 1, 2, \dots$ . The mean field boundaries  $\mu_{\text{cr}}(U, m)$  for the Mott lobe  $m$ , is given by the implicit equation [123],

$$zt \left( \frac{m+1}{Um - \mu} - \frac{m+1}{Um - \mu} \right) = 1 , \quad (279)$$

which also determines the location of the Quantum Critical Points (QCP)  $(\mu_{\text{cr}}(m), U_{\text{cr}}(m))$ , by the equation  $\left( \frac{\partial \mu}{\partial U} \right)^{-1} = 0$ .

Near the QCP at density  $\bar{n}$ , the BHM maps onto an O(2) quantum field theory [124], described by a complex field  $\psi(\mathbf{x}_i) \propto \langle b_i \rangle$ . In a dimensionless scaled form [125] the O(2) action is,

$$S^{O(2)} = \frac{1}{g} \int \int d^{d+1}x \sum_{\mu=1, d+1} |(\partial_\mu - i\frac{q}{c}A_\mu)\psi|^2 + \frac{m_0}{8} (|\psi|^2 - 2)^2 \quad . \quad (280)$$

$x_{d+1}$  is the imaginary time coordinate,  $A_{d+1} = c\mu/q$ . The coupling constant  $g \propto U/t$  determines ground state. In  $d \geq 2$ ,  $g < g_c$ , the field theory describes a superconductor, and for  $g > g_c$  it is a Mott insulator.  $g_c$  is the QCP.  $m_0$  is the bare Higgs (amplitude mode) mass. The low energy Higgs mass and the superfluid stiffness vanish at the QCP.

In order to obtain operator expression for the currents and magnetization, which are necessary for the CMC and CSR susceptibilities, the BHM near the QCP can be renormalized onto an effective Quantum Rotators (QR) Hamiltonian [123],

$$H^{\text{QR}} = \sum_i \frac{q^2}{2C} (n_i - \chi_c \mu)^2 - J^{\text{eff}} (n_i - \bar{n}) \sum_{\langle ij \rangle} \cos(\phi_i - \phi_j - \frac{q}{c}A_{ij}) \quad , \quad (281)$$

where

$$[n_i, \phi_j] = -i\delta_{ij} \quad . \quad (282)$$

$H^{\text{QR}}$  physically describes a Josephson junction array, whose grain capacitance and Josephson couplings are related to the BHM parameters,

$$C \simeq \frac{1}{U} \\ J^{\text{eff}} \simeq 2dt \quad . \quad (283)$$

Near the QCP,  $J^{\text{eff}}$  is renormalized down to the low energy superfluid stiffness  $\rho_s$ , as given by the CSR,

$$\chi_{\text{csr}} = q^2 (j^x | j^x) = q^2 \rho_s(\bar{n}) \quad . \quad (284)$$

$\rho_s$  vanishes at the QCP as  $(g_c - g)^{\nu}$ , where  $\nu$  is the  $d+1$  dimensional correlation length exponent of the O(2) model [18].  $\rho_s$  also depends on the electron density  $n$ . Expanding the density fluctuations about the integer Mott density  $\bar{n}$  in the path integral, we obtain the operator,

$$\rho_s[n_i] = \rho_s(\bar{n}) + \sum_i \frac{d\rho_s(\bar{n})}{d\bar{n}} (n_i - \bar{n}) \quad . \quad (285)$$

Thus, the renormalized current and magnetization operators involve both phase and density operators

$$j^\alpha(\mathbf{x}_i) = \frac{q \sum_i \rho_s[n_i] \nabla^\alpha \phi(\mathbf{x}_i) + \text{h.c.}}{2} \\ m(\mathbf{x}_i) = \frac{\frac{q}{2c} \rho_s[n_i] (x_i j^y - y_i j^x) + \text{h.c.}}{2} \quad . \quad (286)$$

The CMC can be calculated using the canonical commutations in Eq. (282):

$$\chi_{\text{cmc}} = \frac{2}{\mathcal{V}} (j^y, [M^z, j^x]) = \frac{q}{\mathcal{V}} \left( j^y, x \partial_x \left( \frac{d\rho_s}{dn} \right) j^y \right) = \frac{q^3}{c} \rho_s \frac{d\rho_s}{d\bar{n}} \quad , \quad (287)$$

which according to Eq. (309):

$$R_{\text{H}}^{(0)} = \frac{\chi_{\text{cmc}}}{\chi_{\text{csr}}^2} = \frac{1}{qc} \frac{d \log \rho_s}{d\bar{n}} \quad , \quad (288)$$

which qualitatively agrees with similar expressions found for the reactive Hall constant near a Mott insulator [126], and for the Hall coefficient of a two leg Luttinger-liquid [127].  $R^{\text{corr}}$  may be assumed to be small near the QCP since it depends on current relaxation which scales with the ratio of lattice constant to the longer correlation length.

Since the Mott densities  $\bar{n}$  minimize  $\rho_s[\bar{n}]$ , The Hall coefficient vanishes at extrema of  $\rho_s(n)$ . Near the QCP,  $R_{\text{H}}/q$  changes from negative to positive at the Mott density  $\bar{n} = 1, 2, \dots$ , since the superfluid stiffness vanishes at the QCP. The switch from  $R_{\text{H}}/q > 0$  (given by Eq. (278) at low densities) to  $R_{\text{H}}/q < 0$  is expected around midpoint between two Mott lobes. This behavior is captured by the Hard Core Bosons model below.

### 36. Hard Core Bosons on the square lattice

Between consecutive Mott lobes, at temperatures below  $T \ll |\mu_{\text{cr}}(n) - \mu_{\text{cr}}(n+1)|$ , there is a superfluid phase with constrained density fluctuations.

These fluctuations can be described by the renormalizing the BHM onto the projected space between two Mott lobes,  $n_i \in (m, m+1)$ . The projected charge fluctuations are described hard core bosons (HCB) operators,

$$\begin{aligned} \tilde{a}_i, \tilde{a}_i^\dagger, \quad (\tilde{a})^2 = (\tilde{a}^\dagger)^2 = 0, \\ 0 \leq \tilde{n}_i \leq 1. \end{aligned} \quad (289)$$

These operators are faithfully represented by SU(2) spin-half operators,

$$\tilde{a}_i^\dagger \rightarrow S_i^+, \quad \tilde{n}_i - \frac{1}{2} \rightarrow S_i^z, \quad \mathbf{S}^2 = \frac{3}{4}. \quad (290)$$

which can be used to represent the HCB hamiltonian by the gauged quantum XY model of spin half,

$$H^{\text{HCB}} = -t \left( \sum_{\langle ij \rangle} e^{-i\frac{q}{c}A_{ij}} S_i^+ S_j^- + h.c. \right) - \mu \sum_i S_i^z, \quad (291)$$

where  $\mu, t$ , which depend on  $U/t, m$  are renormalized from the corresponding BHM values. The HCB charge polarizations, currents and magnetization operators are respectively represented by,

$$\begin{aligned} \mathbf{P} &= q \sum_i \mathbf{x}_i S_i^z, \quad \mathbf{j} = i[H, \mathbf{P}] = \sum_{\langle ij \rangle} \mathbf{j}_{ij}, \\ j_{ij}^\alpha &= -iqt(S_i^+ S_j^- - S_i^- S_j^+)(x_j^\alpha - x_i^\alpha), \\ M &= \frac{1}{4c} \sum_{\langle ij \rangle} (\mathbf{x}_i + \mathbf{x}_j) \times \mathbf{j}_{ij}. \end{aligned} \quad (292)$$

Here  $\mathbf{r}_i$  denotes the position of site  $i$ . For the square lattice, the density dependent BKT transition temperature for HCB on the square lattice has been evaluated by QMC: [128, 129, 130]

$$T_{\text{BKT}}(n) \simeq 2.8tn(1-n). \quad (293)$$

#### 36.1. Superconducting phase

HCB on the square lattice exhibit long range superfluid order below the Berezinskii, Kosterlitz and Thouless [131, 132] transition (BKT) transition temperature  $T - \text{BKT}$ . At  $T \geq 0$  the two dimensional superfluid stiffness  $\rho_s$  in the classical (large  $S$  approximation) is,

$$\rho_s \equiv q^{-2} \frac{d^2 F^{\text{cl}}(T, n)}{(dA_x)^2} \Big|_{A=0} > 0, \quad (294)$$

which yields a maximum at half filling,

$$\rho_s^{\text{cl}}(0, n) = 2tn(1-n). \quad (295)$$

Quantum corrections to  $\rho_s^{\text{cl}}(0, \frac{1}{2})$  enhance it by about 7% [133, 134].

The zero temperature AC longitudinal conductivity at half filling  $n = \frac{1}{2}$ , is evaluated by computing the conductivity moments  $\mu_0, \dots, \mu_{12}$  in Eq. (145) by ED. The resulting 6 recurrences  $\Delta_1, \dots, \Delta_6$  are depicted in Fig. 23(a). The large odd > even oscillations of the recurrences indicates that the conductivity is suppressed at low frequencies. In fact, the continuous form of  $\sigma_{xx}(\omega)$ , shown in Fig. 23(a), exhibits a threshold at around  $\omega = 5t$ . This threshold behavior is supported by an ED calculation for the Kubo formula on a  $4 \times 4$  lattice.

$$\sigma_{xx}(A, \varepsilon) = \frac{1}{A} \sum_{n>0} |\langle \Psi_0 | j^x | \Psi_n \rangle|^2 \frac{\varepsilon}{(E_n - E_0 - \omega)^2 + \varepsilon^2}. \quad (296)$$

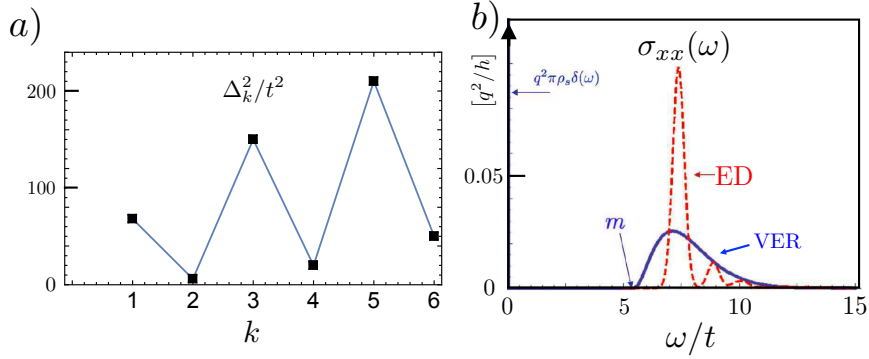


Figure 23: Dynamical conductivity  $\sigma_{xx}(\omega)$  of HCB in the superfluid phase. a) 6 ground state recurrences, computed by ED on  $4 \times 4$  lattice. Even-Odd alternation of the recurrences indicates a strong suppression of  $\sigma_{xx}$  at low frequencies. b)  $\rho_s$  is the zero temperature superconducting stiffness. Blue line: Conductivity by continued fraction extrapolation by Variation extrapolation of recurrences. Red line: Exact Diagonalization calculation of Kubo formula. The apparent threshold energy  $m$  is interpreted as Higgs-amplitude mode's mass.

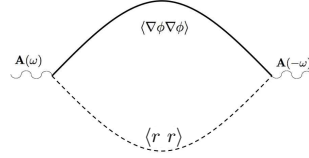


Figure 24: Dynamical conductivity of the Relativistic Gross Pitaevskii model Eq. (297), at zero temperature in the superconducting phase at weak coupling.  $r$  is the amplitude/Higgs mode with mass  $m$ , and  $\phi$  the massless Goldstone mode. The conductivity exhibits a threshold at  $\omega = m$  as shown in Eq. (299).

We note that this threshold feature is not expected by BCS theory in a single band, weak coupling superconductor without disorder. By Mattis and Bardeen [135], such a threshold would appear at  $2\Delta$ , where  $\Delta$  is the pairing gap only if there is sufficient disorder. For HCB model (291)  $\Delta = \infty$ , and there is no disorder!

This threshold was argued to be the Higgs-amplitude mode of the particle-hole symmetric Relativistic Gross-Pitaevskii (RGP) theory [18, 125] with Euclidean action,

$$S^{\text{RGP}} = \frac{1}{2g} \int_{\Lambda} d^{2+1}x \left[ \left| (\nabla - i\frac{q}{c}\mathbf{A})\vec{\Phi} \right|^2 + \frac{m_0^2}{4} (|\vec{\Phi}|^2 - 1)^2 \right]. \quad (297)$$

Here,  $\vec{\Phi}$  is the two component rotator field, defined at wavevectors below the cut-off  $\Lambda$ . The imaginary time component is  $x_3 = c\tau$ , where  $c = \sqrt{\rho_s/\chi}$ ,  $\rho_s \sim t$  is the microscopic stiffness, and  $\chi \sim \frac{1}{v}$  is the local compressibility.  $g$  is the quantum parameter, which drives a quantum phase transition [123] into a bosonic Mott insulator as it grows toward  $g \rightarrow g_c$ .

At weak coupling and zero temperature,  $\vec{\Phi}(\mathbf{x}) = \vec{\Phi}_0$ , and the conductivity is evaluated by fluctuations of the amplitude  $r$  and phase  $\phi$ ,

$$\vec{\Phi} = \Phi_0(1+r)\hat{\mathbf{r}} + \phi\hat{\mathbf{z}} \times \hat{\mathbf{r}}. \quad (298)$$

At lowest order in  $g^0$ , the bubble diagram in Fig. 24 yields a threshold AC conductivity given by [125],

$$\sigma_{xx}^{\text{RGP}}(\omega) \sim \omega^5 \Theta(\omega^2 - m^2), \quad (299)$$

where  $m$  is the mass-gap of the amplitude field  $r$ .  $m(g) \sim |g - g_c|^\nu$  is the analogue of the Higgs particle mass, which vanishes at the critical point with the three dimensional XY model's correlation length exponent  $\nu \simeq 0.671$ .

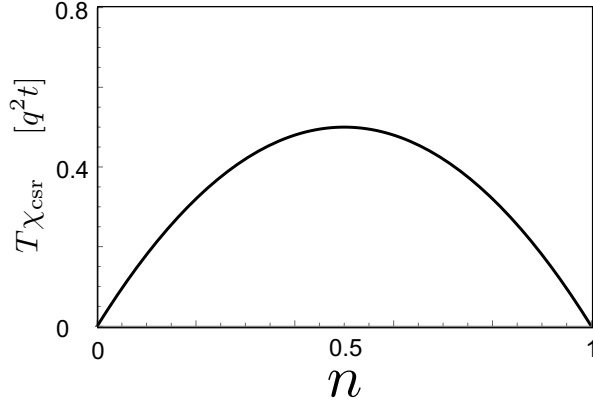


Figure 25: CSR of HCB at order,  $O(\beta)$ , as give by Eq. (300).

### 36.2. Metallic phase: longitudinal conductivity

The longitudinal conductivity was evaluated for the metallic phase of  $H^{\text{HCB}}$  on the square lattice, at  $T > T_{\text{BKT}}$  In Refs. [74, 136]. The CF expansion is extrapolated following the Variational Extrapolation of Recurrents [75] as described in subsection 23.5.

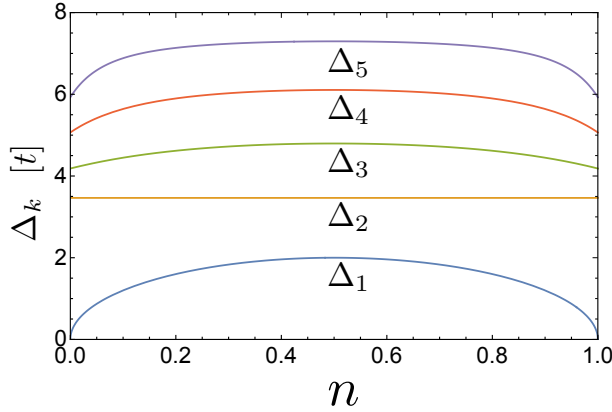


Figure 26: Density dependence of the five lowest recurrents. The cancellation of the density dependence of  $\Delta_1(n)$  and  $\chi_{\text{csr}}(n)$  leads to the weak density dependence of the linear resistivity slopes.

The leading orders CSR is,

$$\chi_{\text{csr}} = 2q^2\beta t^2 n(1-n) + O(\beta t)^3 \quad . \quad (300)$$

$\mu_{2k}, k = 0, \dots, 5$  were also evaluated to leading order in  $\beta t$ , which yields recurrents of order  $O(\beta^0)$ . In Fig. 26, the recurrents are plotted for densities  $0 < n < 1$ .

According to (174) and Fig. 7, the termination function appears to be well fit by the stretched exponential form i.e.

$$\begin{aligned} \tilde{G}_{00}''(\omega, \alpha) &= N_\alpha \exp\left(-\left|\frac{\omega}{\Omega_\alpha}\right|^\alpha\right) \quad , \\ \tilde{G}_{00}'(\omega, \alpha) &= \frac{1}{\pi} \text{PV} \int_{-\infty}^{\infty} d\omega' \frac{\tilde{G}_{00}''(\omega, \alpha)}{\omega - \omega'} \quad , \end{aligned} \quad (301)$$

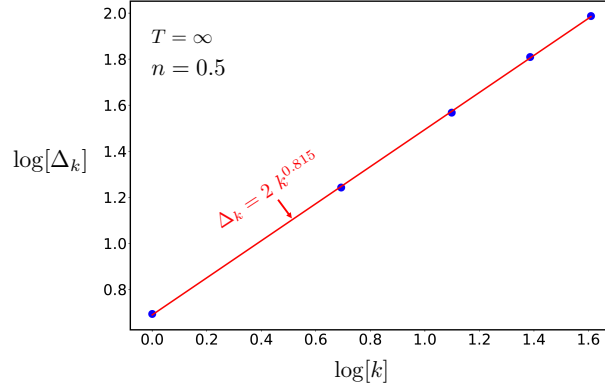


Figure 27: Order dependence of HCB recurrences (in units of  $t$ ) at half filling, and infinite temperature

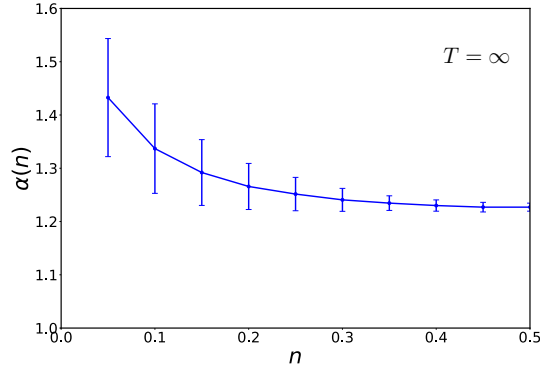


Figure 28: The fit exponent  $\alpha$  as a function of HCB filling  $n$ , which determines the termination function  $G_2^>$  of the AC conductivity. Error bars describe the mean square deviations for the power law fits of  $\Delta_k \sim k^\alpha$ ,  $k = 2, \dots, 5$ .

where the normalization

$$N_\alpha = \frac{\pi\alpha}{2\Omega_\alpha \Gamma\left(\frac{1}{\alpha}\right)} \quad (302)$$

ensures that  $\int d\omega \bar{G}_{00}''(\omega, \alpha) = \pi$ .

The  $S^z \rightarrow -S^z$  symmetry of the HCB hamiltonian leads to  $\sigma_{xx}(n) = \sigma_{xx}(1-n)$ . For  $n \neq 0.5$ ,  $\Delta_1$  is an outlier of the power law line, since it vanishes as  $n \rightarrow 0, 1$ . The higher recurrences are fit by

$$\bar{\Delta}_k = \Omega_\alpha a_\alpha k^{\alpha(n)} \quad , \quad k = 2, \dots \quad (303)$$

where  $\alpha(n)$  is obtained by least square fit in Fig. 28. The error bars increase away from half filling. We find that fluctuations of the recurrences about Eq. (303) induces large uncertainty in the extrapolated  $\sigma_{xx}(\omega)$ . Hence the use of Eq. (303) to the regime  $0.35 \leq n \leq 0.5$ .

The high temperature dynamical conductivities are plotted in Fig. 29. Since the first two recurrences are,

$$\Delta_1^2 = 16n(1-n)t^2 \quad , \quad \Delta_2^2 = 12t^2 \quad . \quad (304)$$

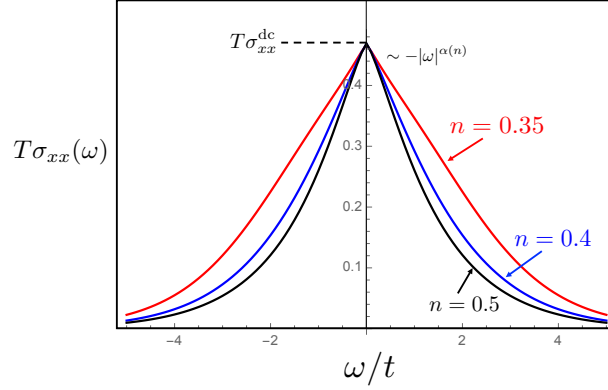


Figure 29: HCB dynamical conductivity at high temperatures. The DC value of  $T\sigma_{xx}(0)$  is independent of boson density  $n$ , while the width of the conductivity increases away from half filling. The singularity at zero frequency depends on  $\alpha$  as determined by Fig. 28.

The conductivity is proportional to the density independent ratio,

$$\sigma_{xx} \propto \frac{\chi_{\text{csr}}(n)\Delta_2}{\Delta_1^2(n)} . \quad (305)$$

Eq. (305) is interpreted as the ratio of kinetic energy ( $\chi_{\text{csr}}(n)$ ) to scattering rate ( $\Delta_1^2(n)/\Delta_2$ ), which have a similar density dependence. Hence, since  $\alpha$  changes very little ( $\sim 1\%$  in the range  $n \in (0.35, 0.5)$ ), the linear resistivity slope in this regime is very weakly density dependent, and given by

$$R_{xx}^{\text{dc}} \simeq 0.33 \frac{T}{t} R_Q \quad , \quad R_Q \equiv \frac{h}{q^2} . \quad (306)$$

The CF extrapolation also yields a singular frequency dependence at low frequencies, as shown in Fig. (29),

$$\frac{\sigma_{xx}(\omega) - \sigma_{xx}^{\text{dc}}}{\sigma_{xx}^{\text{dc}}} \sim - \left| \frac{\omega}{\Omega_\alpha} \right|^\alpha . \quad (307)$$

The sharp zero frequency cusp is consistent with Mukerjee, Oganessian, and Huse [137], (MOH) who found a similar singularity in the high temperature conductivity of a one dimensional non-integrable fermion model, and predicted similar behavior in higher dimensional models.

The high temperature linear temperature slope of the HCB resistivity can be connected to the superconducting transition at  $T_{\text{BKT}} \simeq 0.7t$ . Halperin and Nelson (HN) [138] described the superconducting fluctuation region just  $T_{\text{BKT}}$ , where the resistivity rises as

$$\begin{aligned} R_{\alpha\beta}^{\text{HN}} &\simeq 2.7 R_{\alpha\beta}^{\text{n}}(T) \left( \frac{\xi_+}{\xi_c} \right)^{-2} \\ &= 2.7 R_{\alpha\beta}^{\text{n}}(T) \exp \left( -2b \left( \frac{T_{\text{BKT}}}{T - T_{\text{BKT}}} \right)^{\frac{1}{2}} \right) . \end{aligned} \quad (308)$$

$\xi_+$  is the BKT correlation length, and  $\xi_c$  is of the order of the HCB lattice constant and  $b \simeq 1$ . For the HCB model, the “normal state” resistivity  $R_{xx}^{\text{n}}(T)$  is obtained from our Eq. (306). We use these values to plot the crossovers from HN theory Eq. (308) to higher temperatures as dashed lines in Fig. 30.

### 36.3. Metallic phase: Hall coefficient

The zeroth term,

$$R_{\text{H}}^{(0)} = \frac{\chi_{\text{cmc}}}{\chi_{\text{csr}}^2} . \quad (309)$$



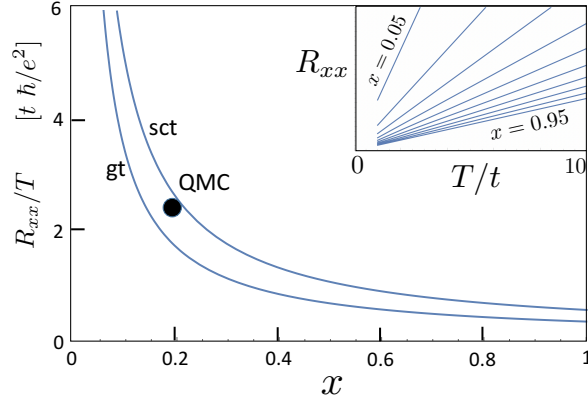


Figure 30: Resistivity versus temperature of HCB at half filling. The high temperature linear slope of Eq. (306) (solid line) is matched toward the superconducting transition temperature  $T - \text{BKT}$  using Halperin and Nelson's (HN) free vortices theory, Eq. (308) (Dashed line).

is calculated by the high temperature expansion of the CSR, Eq. (300) and the CMC susceptibility, as prescribed in Section 30. The leading order in  $\beta$  evaluated in Ref. 291 is

$$\begin{aligned}\chi_{\text{cmc}} &= \frac{2}{c} q^3 t^2 \text{Tr}(\rho(\beta, n)(S_1^+ S_3^- + S_1^- S_3^+) S_2^z) \\ &= \frac{1}{c} \beta^2 q^3 t^4 (1 - 2n)(1 - (2n - 1)^2) \quad .\end{aligned}\quad (310)$$

One observes that  $\chi_{\text{csr}}$  ( $\chi_{\text{cmc}}$ ) is “particle-hole” symmetric (antisymmetric) under  $n \rightarrow 1 - n$ . The zeroth Hall coefficient expanded to second order in  $\beta$  [136] is

$$R_{\text{H}}^{(0)} = \frac{1}{qc} \left( \frac{2n - 1}{n(n - 1)} + \frac{2}{3} (\beta t)^2 \left( n - \frac{1}{2} \right) \right) \quad .\quad (311)$$

Notably at low density, the Hall coefficient recovers the continuum Galilean invariant result  $R_{\text{H}}^{(0)} \rightarrow (nqc)^{-1}$ . Near half-filling,  $R_{\text{H}} \sim -8(n - \frac{1}{2})/(qc)$ , reflecting the effects of lattice Umklapp and hard core scattering.

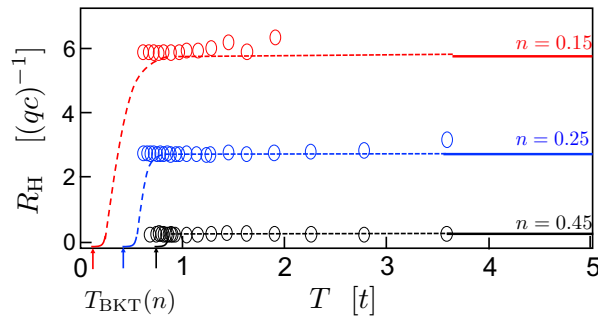


Figure 31: Metallic Hall coefficient  $R_{\text{H}}^{(0)}$  of HCB, from Ref. [136]. High temperature asymptotes are depicted by solid lines, and lower temperature QMC calculations are plotted with circles. Dashed lines interpolate between  $R_{\text{H}}^{(0)}(T)$  and vortex fluctuations theory [138] near the superfluid transition at  $T_{\text{BKT}}(n)$ .

Eq. (311) was extended to lower temperatures numerically [136] by a path-integral based QMC for bosonic lattice models using the DSQSS package [95], with a DLA algorithm [91]. The method is reviewed Section 31.2.

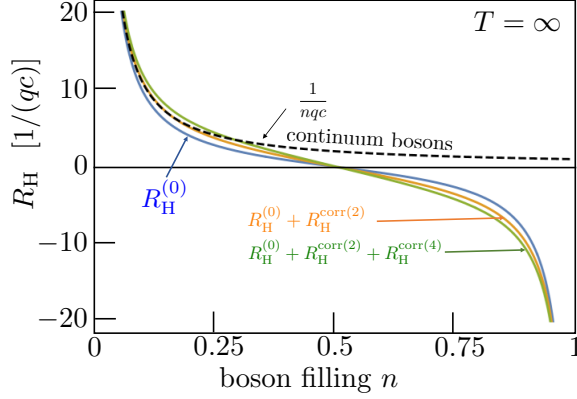


Figure 32: Density dependent Hall coefficient  $R_H(n)$  of HCB on a square lattice at high temperature from Ref. [136].  $R_H^{(0)}$  and  $R_H^{\text{corr}}$  are defined in Eqs. (309) and (312). Monotonous convergence of the corrections up to fourth order are shown by the yellow and green curves. The Hall sign change at half filling is a consequence of the the hard core interactions and the lattice effects on the bosons.

We used the equal-time ( $\tau_1 - \tau_2 = 0$ ) correlation function results for evaluating the static expectation values. For two-body operators (e.g. as needed for the CSR), one can directly use this result, for nearest-neighbour separation. For the CMC, we had to ‘re-weight’ the measurements of the DSQSS code (which can only measure two-point correlation functions) to account for the additional  $S^z$  operator at the nearest neighbour location. Since the algorithm is explicitly formulated in the  $S^z$  basis, the lattice configuration of these values are easily accessed at each imaginary time slice. Hence, a simple modification of the correlation function measurement part of the source code sufficed for our purpose. For acceptable statistical error, we used  $24 \times 24$  size lattices, which were sufficient for converging expectation values at temperatures higher than the expected superfluid transition. The number of Monte Carlo sweeps was  $\sim 10^6$ . In Fig. 31, the solid lines are the analytical results of Eq. (311), while the QMC data are depicted by open circles. We see that the Hall coefficients above the HN regime, rapidly saturate to their high temperature limit.

#### 36.4. Hall coefficient corrections

In general,  $R^{\text{corr}}$  can be a cumbersome calculation. The relative simplicity of the HCB Hamiltonian permits a feasible computation of  $R^{\text{corr}}$  up to fourth Krylov order. The calculated correction [136] is the truncated sum,

$$\begin{aligned}
 R_H^{\text{corr}(4)} &= \frac{1}{\chi_{\text{csr}}} \sum_{i,j=0}^4 R_i R_j (1 - \delta_{i,0} \delta_{j,0}) \mathcal{M}_{2i,2j} \\
 \mathcal{M}_{2i,2j} &= \text{Im} \left( \langle 2i; y | \mathcal{M} | 2j; x \rangle - \langle 2i; x | \mathcal{M} | 2j; y \rangle \right) , \\
 R_{i>1} &= \prod_{r=1}^i \left( -\frac{\Delta_{2r-1}}{\Delta_{2r}} \right) , \quad R_0 = 1 .
 \end{aligned} \tag{312}$$

The high temperature hypermagnetization matrix elements  $\mathcal{M}_{2i,2j}$  are calculated as described in Section 28.  $\tilde{\mathcal{M}}_{44}$  required numerical evaluation of the traces of over  $\sim 10^7$  operator products, using a multiplication table similar to the calculations described in Section Section 33.4. The density dependent high temperature Hall coefficient is depicted in Fig. 32.

We see that these corrections do not qualitatively change the zeroth term’s behavior especially near the densities  $n = 0, 1, \frac{1}{2}$ , although they converge slower around intermediate densities  $n = 0.25, 0.75$ . Since the Hall coefficient is finite for any metal, the summation over higher order corrections must converge. Thus,  $R_H^{(0)}$  appears to be qualitatively correct at high temperatures. At lower temperatures  $R_H^{(0)}$ , as evaluated by QMC in Fig. 31, appears to be blind to the onset of long range superconducting phase correlations and vortices, as described by HN theory. Therefore toward  $T \rightarrow T_{\text{BKT}}$ , the correction term is expected to grow relative to  $R_H^{(0)}$  and cancel it completely at  $T_{\text{BKT}}$ .

### 37. Discussion

From the calculations shown above, one concludes that near half filling, the ‘weakly interacting continuum bosons’ description fails for HCB. The quantum mechanical effects of lattice periodicity and constraints of no-double occupancies play a crucial role in the transport coefficients.

We note that metallic phases of HCB and the tJM electrons share their proximity to Mott insulators. As shown in Part VIII, the Hall sign of the tJM also diverges toward the Mott phase, and reverses its sign relative to that predicted by models of weak interactions.

## Part X

# Summary and Future Directions

This report reviews recent theoretical advances in quantum transport theory with particular emphasis on application to strongly interacting, gapless phases of matter. The DPP formulas for DC Hall-type conductivities can reduce the computational cost of Kubo formulas in the Lehmann representation. They also help clarify conceptual dilemmas about the role of gapless eigenstates in carrying the Hall currents on OBC, and the ultimate irrelevancy of the magnetization subtractions in thermal Hall conductivities. The DPP formulas generalize the Berry curvature expressions derived in Section 17, for clean non interacting models. This may help us understand the interplay between Berry curvatures and effects of boundaries and disorder [58] within the Kubo formula framework, without appealing to semiclassical approximations.

A significant fraction of this report is devoted to thermodynamic approaches which include continued fractions for AC conductivities, and thermodynamic summation formulas for the electric, thermoelectric and thermal Hall coefficients. These approaches converge better by first renormalizing the Hamiltonian down to the temperature scale of interest, and calculating conductivities which do not consist of separable contributions.

As examples, continued fractions and Hall coefficient summation formulas are applied to basic models of interacting lattice fermions and bosons: the Hubbard, t-J, and HCB Hamiltonians. Conductivities of strongly interacting models are contrasted with their weakly interacting limits in order to illuminate the qualitative effects of strong interactions.

In future studies, thermodynamic approaches can take advantage of reliable variational ground states, e.g. DMRG [4], to obtain low temperature dynamical correlations in other strongly correlated lattice models of spins, fermions and bosons. For example: thermal Hall coefficient formula of strongly frustrated magnetic insulators [65], the Hall conductivity of Heavy fermion metals [139], and nearly ferroelectric material  $\text{SrTiO}_4$  [140], conductivities of interacting flat band multilayers of graphene [141] and transition metal dichalcogenides [142, 143].

Experimental measurements of conductivities of cold fermionic and bosonic atoms trapped in optical lattices with artificial gauge fields [144] could test the accuracy of thermodynamic calculations. On the mathematical side, further understanding of the relation between low order recurrences and the low frequency behavior of conductivities would be very worthwhile.

### 38. Acknowledgements

We thank Gil Refael for his encouragement to write the Report. We are indebted to Netanel Lindner, Snir Gazit, Ilia Khait, Noga Bashan, Abhisek Samanta and Ari Turner, whose results are reviewed in this Report. We are grateful for critical comments by Steve Kivelson, Steve Simon, Bruno Uchoa, and Daniel Arovas, which improved the readability of the manuscript. A.A. acknowledges the Israel Science Foundation (ISF) Grant No. 2081/20. This Report was written in part at the Aspen Center for Physics, which is supported by National Science Foundation grant PHY-2210452, and at the Kavli Institute for Theoretical Physics (KITP) supported in part by Grant Nos. NSF PHY-1748958, NSF PHY-1748958 and NSF PHY-2309135.

### References

- [1] A. W. Sandvik, Stochastic series expansion method with operator-loop update, *Physical Review B* 59 (22) (1999) R14157.
- [2] N. Prokof'ev, B. Svistunov, I. Tupitsyn, "worm" algorithm in quantum monte carlo simulations, *Physics Letters A* 238 (4) (1998) 253–257. doi:[https://doi.org/10.1016/S0375-9601\(97\)00957-2](https://doi.org/10.1016/S0375-9601(97)00957-2). URL <https://www.sciencedirect.com/science/article/pii/S0375960197009572>
- [3] N. Prokof'ev, B. Svistunov, Worm algorithms for classical statistical models, *Phys. Rev. Lett.* 87 (2001) 160601. doi:10.1103/PhysRevLett.87.160601. URL <https://link.aps.org/doi/10.1103/PhysRevLett.87.160601>
- [4] S. R. White, Density matrix formulation for quantum renormalization groups, *Phys. Rev. Lett.* 69 (1992) 2863–2866. doi:10.1103/PhysRevLett.69.2863. URL <https://link.aps.org/doi/10.1103/PhysRevLett.69.2863>

- [5] U. Schollwöck, The density-matrix renormalization group in the age of matrix product states, *Annals of Physics* 326 (1) (2011) 96 – 192, January 2011 Special Issue. doi:<http://dx.doi.org/10.1016/j.aop.2010.09.012>. URL <http://www.sciencedirect.com/science/article/pii/S0003491610001752>
- [6] P. Corboz, S. R. White, G. Vidal, M. Troyer, Stripes in the two-dimensional t-j model with infinite projected entangled-pair states, *Physical Review B* 84 (4) (2011) 041108.
- [7] M. Fishman, S. White, E. Stoudenmire, The itensor software library for tensor network calculations, *SciPost Physics Codebases* (2022) 004.
- [8] W. Kohn, J. Luttinger, Quantum theory of electrical transport phenomena, *Physical Review* 108 (3) (1957) 590.
- [9] J. Ziman, *Electrons and phonons: the theory of transport phenomena in solids*, Oxford university press, 1960.
- [10] G. Mahan, *Many-Particle Physics, Physics of Solids and Liquids*, Springer, 2000. URL <https://books.google.co.il/books?id=xzSgZ4-yyMEC>
- [11] M. E. Cage, K. Klitzing, A. Chang, F. Duncan, M. Haldane, R. B. Laughlin, A. Pruisken, D. Thouless, *The quantum Hall effect*, Springer Science & Business Media, 2012.
- [12] B. A. Bernevig, *Topological Insulators and Topological Superconductors*, Princeton University Press, Princeton, 2013 [cited 2024-02-20]. doi:doi:10.1515/9781400846733. URL <https://doi.org/10.1515/9781400846733>
- [13] D. J. Thouless, M. Kohmoto, M. P. Nightingale, M. den Nijs, Quantized hall conductance in a two-dimensional periodic potential, *Phys. Rev. Lett.* 49 (1982) 405–408. doi:10.1103/PhysRevLett.49.405. URL <https://link.aps.org/doi/10.1103/PhysRevLett.49.405>
- [14] J. E. Avron, R. Seiler, Quantization of the hall conductance for general, multiparticle schrödinger hamiltonians, *Physical review letters* 54 (4) (1985) 259.
- [15] P. Streda, L. Smrcka, Thermodynamic derivation of the hall current and the thermopower in quantising magnetic field, *Journal of Physics C: Solid State Physics* 16 (24) (1983) L895. URL <http://stacks.iop.org/0022-3719/16/i=24/a=005>
- [16] V. Emery, S. Kivelson, Superconductivity in bad metals, *Physical Review Letters* 74 (16) (1995) 3253.
- [17] R. Kubo, Statistical-Mechanical Theory of Irreversible Processes. I. General Theory and Simple Applications to Magnetic and Conduction Problems, *Journal of the Physical Society of Japan* 12 (6) (1957) 570–586. arXiv:<https://doi.org/10.1143/JPSJ.12.570>, doi:10.1143/JPSJ.12.570. URL <https://doi.org/10.1143/JPSJ.12.570>
- [18] S. Gazit, D. Podolsky, A. Auerbach, D. P. Arovas, Dynamics and conductivity near quantum criticality, *Phys. Rev. B* 88 (2013) 235108. doi:10.1103/PhysRevB.88.235108. URL <https://link.aps.org/doi/10.1103/PhysRevB.88.235108>
- [19] N. R. Cooper, B. I. Halperin, I. M. Ruzin, Thermoelectric response of an interacting two-dimensional electron gas in a quantizing magnetic field, *Phys. Rev. B* 55 (1997) 2344–2359. doi:10.1103/PhysRevB.55.2344. URL <https://link.aps.org/doi/10.1103/PhysRevB.55.2344>
- [20] T. Qin, Q. Niu, J. Shi, Energy magnetization and the thermal hall effect, *Physical review letters* 107 (23) (2011) 236601.
- [21] N. H. Lindner, A. Auerbach, Conductivity of hard core bosons: A paradigm of a bad metal, *Physical Review B* 81 (5) (2010) 054512.
- [22] V. Viswanath, G. Müller, *The recursion method: application to many body dynamics*, Vol. 23, Springer Science & Business Media, 1994.
- [23] I. Khait, S. Bhattacharyya, A. Samanta, A. Auerbach, Hall anomalies of the doped Mott insulator, *npj Quantum Materials* 8 (1) (2023) 75.
- [24] S. Sorella, The phase diagram of the Hubbard model by Variational Auxiliary Field quantum Monte Carlo, Preprint at: <https://arxiv.org/abs/2101.07045> (2021). doi:10.48550/ARXIV.2101.07045. URL <https://arxiv.org/abs/2101.07045>
- [25] A. Dorneich, M. Troyer, Accessing the dynamics of large many-particle systems using the stochastic series expansion, *Phys. Rev. E* 64 (2001) 066701. doi:10.1103/PhysRevE.64.066701. URL <https://link.aps.org/doi/10.1103/PhysRevE.64.066701>
- [26] N. W. Ashcroft, N. D. Mermin, *Solid state physics*, Cengage Learning, 2022.
- [27] S. M. Girvin, K. Yang, *Modern condensed matter physics*, Cambridge University Press, 2019.
- [28] M.-C. Chang, Q. Niu, Berry phase, hyperorbits, and the hofstadter spectrum: Semiclassical dynamics in magnetic bloch bands, *Phys. Rev. B* 53 (1996) 7010–7023. doi:10.1103/PhysRevB.53.7010. URL <https://link.aps.org/doi/10.1103/PhysRevB.53.7010>
- [29] H. Mori, Transport, collective motion, and brownian motion, *Progress of theoretical physics* 33 (3) (1965) 423–455.
- [30] R. Zwanzig, *Nonequilibrium statistical mechanics*, Oxford university press, 2001.
- [31] N. Das, P. Bhalla, N. Singh, Memory function approach to correlated electron transport: A comprehensive review, *International Journal of Modern Physics B* 30 (23) (2016) 1630015. arXiv:<https://doi.org/10.1142/S0217979216300152>, doi:10.1142/S0217979216300152. URL <https://doi.org/10.1142/S0217979216300152>
- [32] W. Götze, P. Wölfle, Homogeneous dynamical conductivity of simple metals, *Physical Review B* 6 (4) (1972) 1226.
- [33] P. W. Anderson, Absence of diffusion in certain random lattices, *Phys. Rev.* 109 (1958) 1492–1505. doi:10.1103/PhysRev.109.1492. URL <https://link.aps.org/doi/10.1103/PhysRev.109.1492>
- [34] E. Abrahams, P. Anderson, D. Licciardello, T. Ramakrishnan, Scaling theory of localization: Absence of quantum diffusion in two dimensions, *Physical Review Letters* 42 (10) (1979) 673.
- [35] E. Abrahams, *50 years of Anderson Localization*, Vol. 24, world scientific, 2010.
- [36] E. Akkermans, G. Montambaux, *Mesoscopic physics of electrons and photons*, Cambridge university press, 2007.
- [37] A. Ioffe, A. Regel, Non-crystalline, amorphous, and liquid electronic semiconductors, *Progress in semiconductors* (1960) 237–291.
- [38] K. T. N. E. Hussey, H. Takagi, Universality of the mott-ioffe-regel limit in metals, *Philosophical Magazine* 84 (27) (2004) 2847–2864. arXiv:<https://doi.org/10.1080/14786430410001716944>, doi:10.1080/14786430410001716944.

- URL <https://doi.org/10.1080/14786430410001716944>
- [39] P. B. Allen, B. Chakraborty, Infrared and dc conductivity in metals with strong scattering: Nonclassical behavior from a generalized boltzmann equation containing band-mixing effects, *Phys. Rev. B* 23 (1981) 4815–4827. doi:10.1103/PhysRevB.23.4815.  
URL <https://link.aps.org/doi/10.1103/PhysRevB.23.4815>
- [40] A. Sekine, D. Culcer, A. H. MacDonald, Quantum kinetic theory of the chiral anomaly, *Phys. Rev. B* 96 (2017) 235134. doi:10.1103/PhysRevB.96.235134.  
URL <https://link.aps.org/doi/10.1103/PhysRevB.96.235134>
- [41] C. H. Wong, Y. Tserkovnyak, Quantum kinetic equation in phase-space textured multiband systems, *Phys. Rev. B* 84 (2011) 115209. doi:10.1103/PhysRevB.84.115209.  
URL <https://link.aps.org/doi/10.1103/PhysRevB.84.115209>
- [42] J. M. Luttinger, Theory of thermal transport coefficients, *Phys. Rev.* 135 (1964) A1505–A1514. doi:10.1103/PhysRev.135.A1505.  
URL <https://link.aps.org/doi/10.1103/PhysRev.135.A1505>
- [43] B. S. Shastry, Sum rule for thermal conductivity and dynamical thermal transport coefficients in condensed matter, *Physical Review B* 73 (8) (2006) 085117.
- [44] T. Qin, J. Zhou, J. Shi, Berry curvature and the phonon hall effect, *Physical Review B* 86 (10) (2012) 104305.
- [45] H. Katsura, N. Nagaosa, P. A. Lee, Theory of the thermal hall effect in quantum magnets, *Physical review letters* 104 (6) (2010) 066403.
- [46] S. H. Simon, M. S. Rudner, Contrasting lattice geometry dependent versus independent quantities: Ramifications for berry curvature, energy gaps, and dynamics, *Phys. Rev. B* 102 (2020) 165148. doi:10.1103/PhysRevB.102.165148.  
URL <https://link.aps.org/doi/10.1103/PhysRevB.102.165148>
- [47] L. Onsager, Reciprocal relations in irreversible processes. i., *Phys. Rev.* 37 (1931) 405–426. doi:10.1103/PhysRev.37.405.  
URL <https://link.aps.org/doi/10.1103/PhysRev.37.405>
- [48] L. Onsager, Reciprocal relations in irreversible processes. ii., *Phys. Rev.* 38 (1931) 2265–2279. doi:10.1103/PhysRev.38.2265.  
URL <https://link.aps.org/doi/10.1103/PhysRev.38.2265>
- [49] Q. Niu, D. J. Thouless, Y.-S. Wu, Quantized hall conductance as a topological invariant, *Physical Review B* 31 (6) (1985) 3372.
- [50] K. Kudo, H. Watanabe, T. Kariyado, Y. Hatsugai, Many-body chern number without integration, *Physical review letters* 122 (14) (2019) 146601.
- [51] F. D. M. Haldane, Model for a quantum hall effect without landau levels: Condensed-matter realization of the “parity anomaly”, *Physical review letters* 61 (18) (1988) 2015.
- [52] A. Auerbach, Equilibrium formulae for transverse magnetotransport of strongly correlated metals, *Physical Review B* 99 (11) (2019) 115115.
- [53] A. Yacoby, H. Hess, T. Fulton, L. Pfeiffer, K. West, Electrical imaging of the quantum hall state, *Solid state communications* 111 (1) (1999) 1–13.
- [54] D. Xiao, Y. Yao, Z. Fang, Q. Niu, Berry-phase effect in anomalous thermoelectric transport, *Phys. Rev. Lett.* 97 (2006) 026603. doi:10.1103/PhysRevLett.97.026603.  
URL <https://link.aps.org/doi/10.1103/PhysRevLett.97.026603>
- [55] R. Matsumoto, S. Murakami, Rotational motion of magnons and the thermal hall effect, *Phys. Rev. B* 84 (2011) 184406. doi:10.1103/PhysRevB.84.184406.  
URL <https://link.aps.org/doi/10.1103/PhysRevB.84.184406>
- [56] G. Sundaram, Q. Niu, Wave-packet dynamics in slowly perturbed crystals: Gradient corrections and berry-phase effects, *Phys. Rev. B* 59 (1999) 14915–14925. doi:10.1103/PhysRevB.59.14915.  
URL <https://link.aps.org/doi/10.1103/PhysRevB.59.14915>
- [57] T. Jungwirth, Q. Niu, A. MacDonald, Anomalous hall effect in ferromagnetic semiconductors, *Physical review letters* 88 (20) (2002) 207208.
- [58] N. Sinitsyn, Q. Niu, J. Sinova, K. Nomura, Disorder effects in the anomalous hall effect induced by berry curvature, *Physical Review B* 72 (4) (2005) 045346.
- [59] M. P. Marder, *Condensed matter physics*, John Wiley & Sons, 2010.
- [60] J.-i. Inoue, G. E. W. Bauer, L. W. Molenkamp, Suppression of the persistent spin hall current by defect scattering, *Phys. Rev. B* 70 (2004) 041303. doi:10.1103/PhysRevB.70.041303.  
URL <https://link.aps.org/doi/10.1103/PhysRevB.70.041303>
- [61] K. Nomura, J. Sinova, T. Jungwirth, Q. Niu, A. MacDonald, Nonvanishing spin hall currents in disordered spin-orbit coupling systems, *Physical Review B* 71 (4) (2005) 041304.
- [62] A. Shytov, E. Mishchenko, H.-A. Engel, B. Halperin, Small-angle impurity scattering and the spin hall conductivity in two-dimensional semiconductor systems, *Physical Review B* 73 (7) (2006) 075316.
- [63] N. Bashan, A. Auerbach, Degeneracy-projected polarization formulas for hall-type conductivities, *Physical Review Letters* 128 (3) (2022) 036601.
- [64] J. Chalker, P. Coddington, Percolation, quantum tunnelling and the integer hall effect, *Journal of Physics C: Solid State Physics* 21 (14) (1988) 2665.
- [65] Y. Kasahara, K. Sugii, T. Ohnishi, M. Shimozaawa, M. Yamashita, N. Kurita, H. Tanaka, J. Nasu, Y. Motome, T. Shibauchi, Y. Matsuda, Unusual thermal hall effect in a kitaev spin liquid candidate  $\alpha$ -rucl<sub>3</sub>, *Phys. Rev. Lett.* 120 (2018) 217205. doi:10.1103/PhysRevLett.120.217205.  
URL <https://link.aps.org/doi/10.1103/PhysRevLett.120.217205>
- [66] X. Li, B. Fauqué, Z. Zhu, K. Behnia, Phonon thermal Hall effect in strontium titanate, *Physical review letters* 124 (10) (2020) 105901.
- [67] G. Grissonnanche, S. Thériault, A. Gourgout, M. E. Boulanger, E. Lefrançois, A. Ataci, F. Laliberté, M. Dion, J. S. Zhou, S. Pyon, T. Takayama, H. Takagi, N. Doiron-Leyraud, L. Taillefer, Chiral phonons in the pseudogap phase of cuprates, *Nature Physics* 16 (11) (2020) 1108–1111. doi:10.1038/s41567-020-0965-y.  
URL <https://doi.org/10.1038/s41567-020-0965-y>
- [68] R. P. Feynman, Atomic theory of the two-fluid model of liquid helium, *Physical Review* 94 (2) (1954) 262.

- [69] S. M. Girvin, A. H. MacDonald, P. M. Platzman, Magneto-roton theory of collective excitations in the fractional quantum hall effect, *Phys. Rev. B* 33 (1986) 2481–2494. doi:10.1103/PhysRevB.33.2481.  
URL <https://link.aps.org/doi/10.1103/PhysRevB.33.2481>
- [70] D. P. Arovas, A. Auerbach, F. Haldane, Extended heisenberg models of antiferromagnetism: Analogies to the fractional quantum hall effect, *Physical review letters* 60 (6) (1988) 531.
- [71] A. Auerbach, *Interacting electrons and quantum magnetism*, Springer Science & Business Media, 2012.
- [72] G. Freud, On the coefficients in the recursion formulae of orthogonal polynomials, in: *Proceedings of the Royal Irish Academy. Section A: Mathematical and Physical Sciences*, JSTOR, 1976, pp. 1–6.
- [73] D. Lubinsky, H. Mhaskar, E. Saff, A proof of freud’s conjecture for exponential weights, *Constructive Approximation* 4 (1988) 65–83.
- [74] N. H. Lindner, A. Auerbach, Conductivity of hard core bosons: A paradigm of a bad metal, *Physical Review B* 81 (5) (2010) 054512.
- [75] I. Khait, S. Gazit, N. Y. Yao, A. Auerbach, Spin transport of weakly disordered Heisenberg chain at infinite temperature, *Physical Review B* 93 (22) (2016) 224205.
- [76] A. Auerbach, Hall number of strongly correlated metals, *Physical Review Letters* 121 (6) (2018) 066601.
- [77] N. Lindner, A. Auerbach, D. P. Arovas, Vortex dynamics and hall conductivity of hard-core bosons, *Physical Review B* 82 (13) (2010) 134510.
- [78] A. Samanta, D. P. Arovas, A. Auerbach, Hall coefficient of semimetals, *Physical Review Letters* 126 (7) (2021) 076603.
- [79] R. Blankenbecler, D. J. Scalapino, R. L. Sugar, Monte carlo calculations of coupled boson-fermion systems. i, *Phys. Rev. D* 24 (1981) 2278–2286. doi:10.1103/PhysRevD.24.2278.  
URL <https://link.aps.org/doi/10.1103/PhysRevD.24.2278>
- [80] R. T. Scalettar, How to write a determinant qmc code (2010).  
URL <https://scalettar.physics.ucdavis.edu/michigan/howto1.pdf>
- [81] H. Shao, A. W. Sandvik, Progress on stochastic analytic continuation of quantum Monte Carlo data, *Physics Reports* 1003 (2023) 1–88. doi:https://doi.org/10.1016/j.physrep.2022.11.002.  
URL <https://www.sciencedirect.com/science/article/pii/S0370157322003921>
- [82] C. Bauer, Fast and stable determinant quantum Monte Carlo, *SciPost Phys. Core* 2 (2020) 011. doi:10.21468/SciPostPhysCore.2.2.011.  
URL <https://scipost.org/10.21468/SciPostPhysCore.2.2.011>
- [83] R. Mondaini, S. Tarat, R. T. Scalettar, Quantum critical points and the sign problem, *Science* 375 (6579) (2022) 418–424.
- [84] R. Mondaini, S. Tarat, R. T. Scalettar, Universality and critical exponents of the fermion sign problem, *Phys. Rev. B* 107 (2023) 245144. doi:10.1103/PhysRevB.107.245144.  
URL <https://link.aps.org/doi/10.1103/PhysRevB.107.245144>
- [85] S. Isakov, M. I. Katsnelson, A. I. Lichtenstein, Perturbative solution of fermionic sign problem in quantum monte carlo computations, *npj Computational Materials* 10 (1) (2024) 36. doi:10.1038/s41524-024-01221-w.  
URL <https://doi.org/10.1038/s41524-024-01221-w>
- [86] S. Karakuzu, B. Cohen-Stead, C. D. Batista, S. Johnston, K. Barros, Flexible class of exact hubbard-stratonovich transformations, *Phys. Rev. E* 107 (2023) 055301. doi:10.1103/PhysRevE.107.055301.  
URL <https://link.aps.org/doi/10.1103/PhysRevE.107.055301>
- [87] F. F. Assaad, M. Bercx, F. Goth, A. Götz, J. S. Hofmann, E. Huffman, Z. Liu, F. P. Toldin, J. S. E. Portela, J. Schwab, The ALF (Algorithms for Lattice Fermions) project release 2.0. Documentation for the auxiliary-field quantum Monte Carlo code, *SciPost Phys. Codebases* (2022) 1doi:10.21468/SciPostPhysCodeb.1.  
URL <https://scipost.org/10.21468/SciPostPhysCodeb.1>
- [88] B. Efron, Discussion: Jackknife, bootstrap and other resampling methods in regression analysis, *The Annals of Statistics* 14 (4) (1986) 1301–1304.  
URL <http://www.jstor.org/stable/2241457>
- [89] A. W. Sandvik, O. F. Syljuåsen, The Directed-Loop Algorithm, *AIP Conference Proceedings* 690 (1) (2003) 299–308. arXiv:https://pubs.aip.org/aip/acp/article-pdf/690/1/299/11550991/299\1\online.pdf, doi:10.1063/1.1632141.  
URL <https://doi.org/10.1063/1.1632141>
- [90] M. Boninsegni, N. V. Prokof’ev, B. V. Svistunov, Worm algorithm and diagrammatic monte carlo: A new approach to continuous-space path integral monte carlo simulations, *Phys. Rev. E* 74 (2006) 036701. doi:10.1103/PhysRevE.74.036701.  
URL <https://link.aps.org/doi/10.1103/PhysRevE.74.036701>
- [91] O. F. Syljuåsen, A. W. Sandvik, Quantum Monte Carlo with directed loops, *Phys. Rev. E* 66 (2002) 046701. doi:10.1103/PhysRevE.66.046701.  
URL <https://link.aps.org/doi/10.1103/PhysRevE.66.046701>
- [92] A. W. Sandvik, Stochastic series expansion method with operator-loop update, *Phys. Rev. B* 59 (1999) R14157–R14160. doi:10.1103/PhysRevB.59.R14157.  
URL <https://link.aps.org/doi/10.1103/PhysRevB.59.R14157>
- [93] A. W. Sandvik, Computational Studies of Quantum Spin Systems, *AIP Conference Proceedings* 1297 (1) (2010) 135–338. arXiv:https://pubs.aip.org/aip/acp/article-pdf/1297/1/135/11407753/135\1\online.pdf, doi:10.1063/1.3518900.  
URL <https://doi.org/10.1063/1.3518900>
- [94] A. W. Sandvik, Stochastic series expansion method for quantum ising models with arbitrary interactions, *Phys. Rev. E* 68 (2003) 056701. doi:10.1103/PhysRevE.68.056701.  
URL <https://link.aps.org/doi/10.1103/PhysRevE.68.056701>
- [95] Y. Motoyama, K. Yoshimi, A. Masaki-Kato, T. Kato, N. Kawashima, Dsqss: Discrete space quantum systems solver, *Computer Physics Communications* 264 (2021) 107944. doi:https://doi.org/10.1016/j.cpc.2021.107944.  
URL <https://www.sciencedirect.com/science/article/pii/S0010465521000692>

- [96] J. Hubbard, Electron correlations in narrow energy bands, Proc. R. Soc. Lond. (1963). doi:10.1103/PhysRevLett.111.036401.  
URL <http://doi.org/10.1098/rspa.1963.0204>
- [97] D. P. Arovas, E. Berg, S. A. Kivelson, S. Raghu, The hubbard model, Annual Review of Condensed Matter Physics 13 (1) (2022) 239–274. arXiv:<https://doi.org/10.1146/annurev-conmatphys-031620-102024>, doi:10.1146/annurev-conmatphys-031620-102024.  
URL <https://doi.org/10.1146/annurev-conmatphys-031620-102024>
- [98] J. Spałek, Effect of pair hopping and magnitude of intra-atomic interaction on exchange-mediated superconductivity, Phys. Rev. B 37 (1988) 533–536. doi:10.1103/PhysRevB.37.533.  
URL <https://link.aps.org/doi/10.1103/PhysRevB.37.533>
- [99] J. Jaklič, P. Prelovšek, Charge dynamics in the planar t-J model, Physical Review B 52 (9) (1995) 6903.
- [100] E. Perepelitsky, A. Galatas, J. Mravlje, E. Khatami, B. S. Shastry, A. Georges, et al., Transport and optical conductivity in the Hubbard model: A high-temperature expansion perspective, Physical Review B 94 (23) (2016) 235115.
- [101] E. W. Huang, R. Sheppard, B. Moritz, T. P. Devereaux, Strange metallicity in the doped hubbard model, Science 366 (6468) (2019) 987–990. arXiv:<https://www.science.org/doi/pdf/10.1126/science.aau7063>, doi:10.1126/science.aau7063.  
URL <https://www.science.org/doi/abs/10.1126/science.aau7063>
- [102] W. Xu, K. Haule, G. Kotliar, Hidden Fermi Liquid, Scattering Rate Saturation, and Nernst Effect: A Dynamical Mean-Field Theory Perspective, Phys. Rev. Lett. 111 (2013) 036401. doi:10.1103/PhysRevLett.111.036401.  
URL <https://link.aps.org/doi/10.1103/PhysRevLett.111.036401>
- [103] E. Z. Kuchinskii, N. A. Kuleeva, D. I. Khomskii, M. V. Sadovskii, Hall effect in a doped mott insulator: Dmft approximation, JETP Letters 115 (7) (2022) 402–405.
- [104] W. O. Wang, J. K. Ding, B. Moritz, Y. Schattner, E. W. Huang, T. P. Devereaux, Numerical approaches for calculating the low-field dc Hall coefficient of the doped Hubbard model, Phys. Rev. Research 3 (2021) 033033. doi:10.1103/PhysRevResearch.3.033033.  
URL <https://link.aps.org/doi/10.1103/PhysRevResearch.3.033033>
- [105] Imaginary time QMC conductivities require analytic continuation, which is limited to frequencies higher than temperature (see Appendix B in [18]). The DC conductivities are often deduced by proxies to the analytical continuation [104].
- [106] W. Wu, M. S. Scheurer, S. Chatterjee, S. Sachdev, A. Georges, M. Ferrero, Pseudogap and fermi-surface topology in the two-dimensional hubbard model, Phys. Rev. X 8 (2018) 021048. doi:10.1103/PhysRevX.8.021048.  
URL <https://link.aps.org/doi/10.1103/PhysRevX.8.021048>
- [107] A. A. Markov, G. Rohringer, A. N. Rubtsov, Robustness of the topological quantization of the Hall conductivity for correlated lattice electrons at finite temperatures, Phys. Rev. B 100 (2019) 115102. doi:10.1103/PhysRevB.100.115102.  
URL <https://link.aps.org/doi/10.1103/PhysRevB.100.115102>
- [108] J. Vučićević, R. Žitko, Electrical conductivity in the Hubbard model: Orbital effects of magnetic field, Phys. Rev. B 104 (2021) 205101. doi:10.1103/PhysRevB.104.205101.  
URL <https://link.aps.org/doi/10.1103/PhysRevB.104.205101>
- [109] Y. Shi, J. Schirmer, L.-Q. Chen, Hall coefficient and resistivity in the doped bilayer hubbard model, Preprint at: <https://arxiv.org/abs/2308.03862> (2023).
- [110] R. Krishna Kumar, X. Chen, G. Auton, A. Mishchenko, D. A. Bandurin, S. V. Morozov, Y. Cao, E. Khestanova, M. Ben Shalom, A. Kretinin, et al., High-temperature quantum oscillations caused by recurring Bloch states in graphene superlattices, Science 357 (6347) (2017) 181–184.
- [111] W. O. Wang, J. K. Ding, B. Moritz, E. W. Huang, T. P. Devereaux, Dc hall coefficient of the strongly correlated hubbard model, npj Quantum Materials 5 (1) (2020) 51.
- [112] B. Shastry, B. Shraiman, R. Singh, Faraday rotation and the hall constant in strongly correlated fermi systems, Physical review letters 70 (13) (1993) 2004.
- [113] P. Hosur, A. Kapitulnik, S. A. Kivelson, J. Orenstein, S. Raghu, W. Cho, A. Fried, Erratum: Kerr effect as evidence of gyrotropic order in the cuprates [Phys. Rev. B 87, 115116 (2013)], Phys. Rev. B 91 (2015) 039908. doi:10.1103/PhysRevB.91.039908.  
URL <https://link.aps.org/doi/10.1103/PhysRevB.91.039908>
- [114] P. W. Anderson, The Resonating Valence Bond State in LaCuO and Superconductivity, Science 235 (4793) (1987) 1196–1198. arXiv:<https://www.science.org/doi/pdf/10.1126/science.235.4793.1196>, doi:10.1126/science.235.4793.1196.  
URL <https://www.science.org/doi/abs/10.1126/science.235.4793.1196>
- [115] Y. J. Uemura, G. M. Luke, B. J. Sternlieb, J. H. Brewer, J. F. Carolan, W. N. Hardy, R. Kadono, J. R. Kempton, R. F. Kiefl, S. R. Kreitzman, P. Mulhern, T. M. Riseman, D. L. Williams, B. X. Yang, S. Uchida, H. Takagi, J. Gopalakrishnan, A. W. Sleight, M. A. Subramanian, C. L. Chien, M. Z. Cieplak, G. Xiao, V. Y. Lee, B. W. Statt, C. E. Stronach, W. J. Kossler, X. H. Yu, Universal Correlations between  $T_c$  and  $\frac{n_s}{m^*}$  (Carrier Density over Effective Mass) in High- $T_c$  Cuprate Superconductors, Phys. Rev. Lett. 62 (1989) 2317–2320. doi:10.1103/PhysRevLett.62.2317.  
URL <https://link.aps.org/doi/10.1103/PhysRevLett.62.2317>
- [116] S. Y. F. Zhao, N. Poccia, M. G. Panetta, C. Yu, J. W. Johnson, H. Yoo, R. Zhong, G. D. Gu, K. Watanabe, T. Taniguchi, S. V. Postolova, V. M. Vinokur, P. Kim, Sign-Reversing Hall Effect in Atomically Thin High-Temperature  $\text{Bi}_{2.1}\text{Sr}_{1.9}\text{CaCu}_{2.0}\text{O}_{8+\delta}$  Superconductors, Phys. Rev. Lett. 122 (2019) 247001. doi:10.1103/PhysRevLett.122.247001.  
URL <https://link.aps.org/doi/10.1103/PhysRevLett.122.247001>
- [117] A. Auerbach, D. P. Arovas, Hall anomaly and moving vortex charge in layered superconductors, SciPost Phys. 8 (2020) 061. doi:10.21468/SciPostPhys.8.4.061.  
URL <https://scipost.org/10.21468/SciPostPhys.8.4.061>
- [118] Y. J. Lin, R. L. Compton, K. Jiménez-García, J. V. Porto, I. B. Spielman, Synthetic magnetic fields for ultracold neutral atoms, Nature 462 (7273) (2009) 628–632. doi:10.1038/nature08609.  
URL <https://doi.org/10.1038/nature08609>



- [119] R. T. Scalettar, G. G. Batrouni, G. T. Zimanyi, Localization in interacting, disordered, bose systems, *Physical review letters* 66 (24) (1991) 3144.
- [120] L. Pitaevskii, S. Stringari, *Bose-Einstein condensation and superfluidity*, Vol. 164, Oxford University Press, 2016.
- [121] S. D. Huber, N. H. Lindner, Topological transitions for lattice bosons in a magnetic field, *Proceedings of the National Academy of Sciences* 108 (50) (2011) 19925–19930.
- [122] N. H. Lindner, A. Auerbach, D. P. Arovas, Vortex quantum dynamics of two dimensional lattice bosons, *Physical review letters* 102 (7) (2009) 070403.
- [123] S. Sachdev, *Quantum phase transitions*, second ed. Edition, Cambridge University Press, Cambridge, 2011.
- [124] M. P. Fisher, P. B. Weichman, G. Grinstein, D. S. Fisher, Boson localization and the superfluid-insulator transition, *Physical Review B* 40 (1) (1989) 546.
- [125] D. Podolsky, A. Auerbach, D. P. Arovas, Visibility of the amplitude (higgs) mode in condensed matter, *Physical Review B* 84 (17) (2011) 174522.
- [126] X. Zotos, F. Naef, M. Long, P. Prelovšek, *Drude Weight, Integrable Systems and the Reactive Hall Constant*, Springer Netherlands, Dordrecht, 2001, pp. 273–282.
- [127] R. Citro, T. Giamarchi, E. Orignac, Hall response in interacting bosonic and fermionic ladders (2024). [arXiv:2404.16973](https://arxiv.org/abs/2404.16973).
- [128] H.-Q. Ding, M. Makivic, Kosterlitz-thouless transition in the two-dimensional quantum xy model, *Physical Review B* 42 (10) (1990) 6827.
- [129] H.-Q. Ding, Phase transition and thermodynamics of quantum xy model in two dimensions, *Phys. Rev. B* 45 (1992) 230–242. doi: 10.1103/PhysRevB.45.230.  
URL <https://link.aps.org/doi/10.1103/PhysRevB.45.230>
- [130] K. Harada, N. Kawashima, Universal jump in the helicity modulus of the two-dimensional quantum xy model, *Phys. Rev. B* 55 (1997) R11949–R11952. doi:10.1103/PhysRevB.55.R11949.  
URL <https://link.aps.org/doi/10.1103/PhysRevB.55.R11949>
- [131] V. Berezinskii, Destruction of long-range order in one-dimensional and two-dimensional systems having a continuous symmetry group i. classical systems, *Sov. Phys. JETP* 32 (3) (1971) 493–500.
- [132] J. M. Kosterlitz, D. J. Thouless, Ordering, metastability and phase transitions in two-dimensional systems, *Journal of Physics C: Solid State Physics* 6 (7) (1973) 1181.
- [133] A. W. Sandvik, C. J. Hamer, Ground-state parameters, finite-size scaling, and low-temperature properties of the two-dimensional  $s=1/2$  xy model, *Physical Review B* 60 (9) (1999) 6588.
- [134] K. Bernardet, G. Batrouni, J.-L. Meunier, G. Schmid, M. Troyer, A. Dorneich, Analytical and numerical study of hardcore bosons in two dimensions, *Physical Review B* 65 (10) (2002) 104519.
- [135] D. C. Mattis, J. Bardeen, Theory of the anomalous skin effect in normal and superconducting metals, *Physical Review* 111 (2) (1958) 412.
- [136] S. Bhattacharyya, A. De, S. Gazit, A. Auerbach, Metallic transport of hard core bosons, [arXiv:2309.14479](https://arxiv.org/abs/2309.14479) (2023). [arXiv:2309.14479](https://arxiv.org/abs/2309.14479).
- [137] S. Mukerjee, V. Oganesyan, D. Huse, Statistical theory of transport by strongly interacting lattice fermions, *Physical Review B* 73 (3) (2006) 035113.
- [138] B. Halperin, D. R. Nelson, Resistive transition in superconducting films, *Journal of low temperature physics* 36 (1979) 599–616.
- [139] N. Maksimovic, D. H. Eilbott, T. Cookmeyer, F. Wan, J. Ruzs, V. Nagarajan, S. C. Haley, E. Maniv, A. Gong, S. Faubel, I. M. Hayes, A. Bangura, J. Singleton, J. C. Palmstrom, L. Winter, R. McDonald, S. Jang, P. Ai, Y. Lin, S. Ciocys, J. Gobbo, Y. Werman, P. M. Oppeneer, E. Altman, A. Lanzara, J. G. Analytis, Evidence for a delocalization quantum phase transition without symmetry breaking in CeCoIn, *Science* 375 (6576) (2022) 76–81. [arXiv:https://www.science.org/doi/pdf/10.1126/science.aaz4566](https://www.science.org/doi/pdf/10.1126/science.aaz4566), doi:10.1126/science.aaz4566.
- [140] X. Li, B. Fauqué, Z. Zhu, K. Behnia, Phonon thermal Hall effect in strontium titanate, *Physical review letters* 124 (10) (2020) 105901.
- [141] E. Y. Andrei, A. H. MacDonald, Graphene bilayers with a twist, *Nature Materials* 19 (12) (2020) 1265–1275. doi:10.1038/s41563-020-00840-0.  
URL <https://doi.org/10.1038/s41563-020-00840-0>
- [142] M. M. Scherer, D. M. Kennes, L. Classen, Chiral superconductivity with enhanced quantized Hall responses in moiré transition metal dichalcogenides, *npj Quantum Materials* 7 (1) (2022) 100. doi:10.1038/s41535-022-00504-z.  
URL <https://doi.org/10.1038/s41535-022-00504-z>
- [143] J. Pizarro, S. Adler, K. Zantout, T. Mertz, P. Barone, R. Valentí, G. Sangiovanni, T. O. Wehling, Deconfinement of Mott localized electrons into topological and spin-orbit-coupled Dirac fermions, *npj Quantum Materials* 5 (1) (2020) 79. doi:10.1038/s41535-020-00277-3.  
URL <https://doi.org/10.1038/s41535-020-00277-3>
- [144] P. T. Brown, D. Mitra, E. Guardado-Sanchez, R. Nourafkan, A. Reymbaut, C.-D. Hébert, S. Bergeron, A.-M. Tremblay, J. Kokalj, D. A. Huse, et al., Bad metallic transport in a cold atom Fermi-Hubbard system, *Science* 363 (6425) (2019) 379–382.